UNIVERSITETET
I OSLO

Master thesis

Automatic Deviance Detection in the Human Auditory Cortex and Temporoparietal Junction

An intracranial electrophysiology study on automatic auditory deviance detection and its neural signatures in the human brain

Sara Kruge Nossen

Submitted as master's thesis at the Department of Psychology, University of Oslo

Spring 2023

Faculty of Social Sciences

Acknowledgments

First, I want to thank my supervisors Dr Alejandro Omar Blenkmann and Professor Anne-Kristin Solbakk for their patience, continued support, and guidance during the long voyage that ended up being this master's thesis. Specifically, I want to thank Dr Alejandro Blenkmann for trusting me with his data, for sharing his ideas, and for supervising me with the data analysis and writing of the manuscript. I want to thank Professor Anne-Kristin Solbakk for her alertness and unconditional positive regard during the writing and final editing of the manuscript. I feel privileged to have had the both of you as my supervisors. Next, I want to thank Rahul Omprakash Agrawal for his technical finesse and assistance with accessing data, software, and university buildings. Lastly, I would like to give special thanks to the staff at Nevroklinikken at Oslo University Hospital Rikshospitalet, and to the participants for their contribution and their patience during the data collection!

Summary

Author: Sara Kruge Nossen

Title: Auditory Deviance Detection

Supervisor: Alejandro Omar Blenkmann. **Co-supervisor:** Anne-Kristin Solbakk

Author statement: Dr Blenkmann designed the experiments and collected the data, as part of the research project "Oscillatory mechanisms supporting human cognition". The research question and hypotheses were developed in collaboration between supervisors and the author. The author preprocessed the data, performed the analyses, and wrote this master thesis.

Abstract: The goal of this thesis was to investigate the neural signatures of auditory deviance detection in the human brain. Two experiments were conducted to investigate the distribution of tonotopy and processing of statistically regular and irregular acoustic stimuli in the human brain via intracranial recordings. Data were from three adult patients implanted with intracranial depth electrodes due to clinical reasons along the latero-medial axis of Heschl's gyrus, superior temporal gyrus (STG), and the temporoparietal junction (TPJ) of the right hemisphere. The first experiment was a tonotopic mapping task that demonstrated large inter-individual spatial distribution of tonotopy in Heschl's gyrus and STG, and in the medial part of the electrodes implanted in the right TPJ. The second task, a passive repetition auditory oddball task, showed that auditory deviants representing unexpected violations to sounds presented within a regular pattern, significantly increased the magnitudes of broadband high-frequency activity (70 to 150 Hertz) compared to the same sound in an expected task condition. The significant enhancement in broadband high-frequency activity was prominent in non-primary auditory cortical fields corresponding to the STG and the TPJ. Altogether, the results confirm previous studies showing that the brain detects violations to auditory regularities automatically when attention is directed towards an irrelevant task. Moreover, the results provide evidence that cortical areas in non-primary auditory cortex, such as STG and TPJ, rather than Heschl's gyrus, are involved in automatic auditory deviance detection.

Table of Contents

Acknowledgments ii
Summary iii
Table of Contents iv
1 Introduction 1
Research question and hypotheses 3
1.0 Outline 4
1.1 Intracranial Electroencephalography 4
1.1.1 Subdural and intracerebral electroencephalographic recordings 4
1.1.2 The iEEG signal as an electrophysiological correlate of cognitive processing 5
1.2 The human auditory cortex as a processing hierarchy 6
1.2.1 An overview of the subcortical processing stages 6
1.2.2 Auditory processing in the human primary auditory cortex 7
1.2.3 Auditory processing in the human non-primary auditory cortex 9
1.3 Auditory deviance detection in the human auditory cortex 10
1.3.1 The mismatch negativity and other neural correlates of auditory irregularity 10
1.3.2 Hierarchical predictive processing perspectives on auditory deviance detection 13
1.3.3 Intracranial evidence for auditory deviance detection in the human brain 13
1.4. Introduction to the empirical study and its research questions and hypotheses 15
2 Methods 17
2.1 Ethical considerations 17
2.2 Study participants 17
2.3 Procedures 17
2.3.1 Stimuli and experimental design 18
2.4 Data acquisition 20
2.4.1 Imaging data acquisition. 20
2.4.2 Stereotaxic electroencephalography recordings 20
2.4.3 Stimuli presentation 21
2.5 Data preprocessing 21
2.5.1 Electrode localization 21
2.5.2 The SEEG signal 22
2.6 Data analysis 23
2.6.1 High-frequency broadband activity 23
2.6.2 Response onset latency and peak latency of high-frequency activity 24
3 Results 26

3.1 Determination of anatomical localization of implanted electrodes 26
3.1.1 Anatomical localization of electrodes based on neuroimaging 26
3.1.2 Analysis of event-related potential waveforms during the tonotopic mapping task 28
3.1.3 High-frequency activity during the tonotopic mapping task 29
3.2 Effects of violations to auditory regularities on neural activity 33
3.2.1 Localization of polarity inversions to deviant tones in the event-related potentials 33
3.2.2 Violations to auditory regularity increase high-frequency activity 34
3.2.3 Spatial discrepancy in the temporal effects of deviance on high-frequency activity 38
4 Discussion 39
4.1 Inter-individual variability in distributed tonotopy 39
4.2 Violations to acoustic regularity during a passive oddball task 42
4.2.1 Automatic deviance detection in primary versus non-primary auditory cortex 42
4.2.2 Spatial disparity in the temporal effects of auditory deviants on neuronal responses 45
4.2.3 The loci of the neural generators 46
4.3 Limitations and future directions 46
5 Conclusions 50
5.1 Tonotopy in the human auditory cortex 50
5.2 Automatic deviance detection in the human auditory cortex 50
Literature 51
Appendix 70
Tonotopic mapping task 70
Figure X.1.1 SUB1: HFA Responses During Tonotopic Mapping Task 70
Figure X.1.2 SUB2: HFA Responses During Tonotopic Mapping Task 71
Figure X.1.3 SUB2: ERP Responses from TPJ During Tonotopic Mapping Task 72
Figure X.1.4 SUB3: HFA Responses During Tonotopic Mapping Task 73
Figure X.1.5 SUB3: ERP Responses from the TPJ During Tonotopic Mapping Task 74
Oddball task: ERPs 75
Figure X.2.1 SUB1: ERP Responses to Repetition Deviants and Standard Control Tones 75
Figure X.2.2 SUB1: ERP Responses to Alternation Deviants and Standard Control Tones 76
Figure X.2.3 SUB2: ERP Responses to Repetition Deviants and Standard Control Tones 77
Figure X.2.4 SUB2: ERP Responses to Alternation Deviants and Standard Control Tones 78
Figure X.2.5 SUB3: ERP Responses to Repetition Deviants AA and Standard Controls 79
Figure X.2.6 SUB3: ERP Responses to Repetition Deviants BB and Standard Controls 81
Figure X.2.7 SUB3: ERP Responses to Alternation Deviants AB and Control Tones 83
Figure X.2.8 SUB3: ERP Responses to Alternation Deviants BA and Control Tones 84
Oddball task: HFAs 85
Figure X.3.1 SUB1: HFA Responses to Alternation Deviants and Standards 85

Figure X.3.2 SUB1: HFA Responses to Repetition Deviants and Standards..... 86
Figure X.3.3 SUB2: HFA Responses to Alternation Deviants and Standards..... 87
Figure X.3.4 SUB2: HFA Responses to Repetition Deviants and Standards..... 88
Figure X.3.5 SUB3: HFA Responses to Alternation Deviants and Standards..... 89
Figure X.3.6 SUB3: HFA Responses to Repetition Deviants and Standards..... 90
Table X.1 Electrode Contact Number and Anatomical Location..... 92

1 Introduction

As listeners, unexpected sounds often capture our attention, but subtle changes in a stream of regular sounds can escape our notice. Encoding of auditory regularity refers to how the brain extracts statistical regularities from the auditory context (Escera et al., 2014). Extracting information from statistical regularities, and using it to form predictions about upcoming events, provides an evolutionary advantage by allowing organisms to adapt their behavior to the current context. This type of statistical learning based on auditory regularities can be investigated by its inverse – how the brain processes stimuli that deviate from the expected regular pattern of sounds, referred to as auditory deviance detection. A key distinction between experimental paradigms used for investigating how the processing of deviants manifests as brain signals is whether they require the participants to selectively attend to the stimuli (i.e., active paradigms) or something unrelated to the sounds and their structure (i.e., passive paradigms). Findings derived from passive paradigms are of specific interest in automatic regularity encoding because they imply that our brains track and extract task-irrelevant patterns from its surroundings while we are engaging in other tasks (Edwards et al., 2005; Fuhrer et al., 2021). Automatic auditory deviance detection therefore represents a crucial function for survival by facilitating behavioral adaptation to changes in the environment before we are consciously aware of such changes.

One of the most investigated neural correlates of auditory deviance detection is the mismatch negativity (MMN; Näätänen et al., 1978). This event-related potential (ERP) is derived from the differential electroencephalography (EEG) signal between auditory rare and frequent stimuli during an oddball task (Näätänen et al., 2007). Because the MMN and other indices of deviance can be elicited irrespective of whether attention is directed towards the stimuli or towards an irrelevant task (e.g., reading a book; Näätänen et al., 2012), they may function as an automatic mechanism for change detection (Näätänen et al., 2007). In addition, studies show that the MMN can be elicited from more complex expectancy violations such as abstract (non-sensory) rules of stimulus presentation order (Winkler, 2007). Thus, the MMN may reflect aspects of higher-order cognitive processing such as auditory regularity encoding (Näätänen et al., 2007; Winkler, 2007). Moreover, studies comparing clinical and non-clinical groups have reported that aspects of the MMN and other indices of deviance detection differ between various neurodevelopmental and neuropsychiatric disorders, including schizophrenia (Näätänen et al., 2012), auditory processing deficits (Gu & Bi, 2020), attention deficit hyperactivity disorder, and autism spectrum disorders (Gonzalez-Gadea et al., 2015).

However, the neural underpinnings of the MMN and what neural mechanisms such differences between clinical groups reflect, remain largely unknown.

A challenge when investigating the neural substrates of auditory deviance detection is to define its neural generators. Converging evidence from neuroimaging studies such as magnetoencephalography (MEG) and source imaging in EEG, proposes that the neural generators of the intracerebral voltages that comprise the MMN to physical deviance or change detection, are found bilaterally in the superior temporal gyrus (STG) and the right frontal cortex (Näätänen et al., 2007; Paavilainen, 2013). However, the specific neural locus may depend on task instructions and what physical stimulus features represent the deviance (Escara et al., 2014), thus emphasizing the importance of high signal-to-noise ratio of spatiotemporal resolution to pin-point differences between neighboring cortical fields. Furthermore, emerging findings indicate that auditory regularity encoding and deviance detection occur at various stages in the auditory system, rendering questions about how underlying neural processes at these stages relate to the MMN (Escera et al., 2014; Escera, 2017; Paavilainen, 2013). The hierarchical predictive processing framework proposes that sensory processing involves an interaction between processing levels within a predictive hierarchy (Friston, 2010; Walsh et al., 2020). In short, this framework postulates that higher-level predictions about the external world and upcoming stimuli are backpropagated to areas lower in the hierarchy, and only information that diverges from these predictions is feedforwarded in the processing hierarchy (Walsh et al., 2020). Thus, from a hierarchical predictive processing point of view, aspects of the MMN may reflect an automatic detection of divergence from a sensory prediction, also known as a prediction error (Friston, 2010).

If the auditory cortex implements an auditory regularity hierarchy, then one could expect a clear distinction between neuronal populations that correspond to their position in this hierarchy (Parras et al., 2017). Specifically, this distinction should be clear between recorded neuronal activity from the human primary auditory cortex (PAC) and the non-PAC. In addition, converging evidence suggests spatial differences in the processing of more abstract deviance, such as auditory irregularity derived from the inter-stimulus relationship, possibly reflecting a distributed deviance detection network (Dürschmid et al., 2016; Eckert et al., 2022; El Karoui et al., 2015; Johnson et al., 2020; Nourski et al., 2018). Neuroimaging approaches, like functional magnetic resonance imaging (fMRI), have contributed substantially to our understanding of the organization of human auditory processing.

However, they lack the signal-to-noise ratio and spatiotemporal resolution necessary to elucidate nuances between cortical fields, and functionally differentiate between the levels of a complex processing hierarchy (Rauschecker, 2020). In contrast, intracranial electroencephalography (iEEG) offers an excellent temporal resolution down to milliseconds (ms) and can achieve a spatial resolution to a few millimeters (mm), only restricted by electrode coverage of the exposed brain (McCarty et al., 2022). Thus, results based on data from iEEG may aid in answering key questions about the neural mechanisms involved in human auditory deviance detection without the aid of attention, and their regional distribution across the auditory hierarchy.

Research question and hypotheses

This study aimed to investigate the neural signatures and mechanisms of automatic deviance detection in the human auditory cortex and the loci of the MMN components leveraging on iEEG recordings. This yielded the following research questions:

What are the neural signatures of automatic deviance detection in the human primary and non-primary auditory cortex, and what are their precise anatomical locations?

These research questions were investigated with data gathered from intracranial depth electrodes implanted in the right hemisphere of three humans participating in two different tasks. Intracranial recordings and the anatomical positioning of the implanted electrodes are solely determined by clinical purposes and hence, the number of participants in this type of study is rather small. As a corollary, the investigation of the roles of PAC and non-PAC in auditory deviance detection in this empirical study was limited by electrode coverage. Therefore, the study was carried out by following hypothesis- and data-driven aspects.

This study had two objectives. The first aim was to investigate the distribution of tonotopic responses and their response onset latencies to establish a "tonotopic base map" to functionally delineate primary and non-primary auditory areas. The second aim was to assess, within auditory processing areas, the spatial distribution of brain responses to violations to statistically regular auditory stimuli when attention was directed towards a distractor task. For this aim, a passive oddball paradigm was used to isolate the effects of regularity violation from the effects auditory sensory processing of physical stimulus characteristics and stimulus violation probability. If the first aim succeeded, then deviance detection would be analyzed

for individual channels sensitive to specific tone frequencies. If not, responses would be analyzed as part of larger anatomical delineations defined by anatomical imaging techniques.

1.0 Outline

This study investigated deviance detection in the human auditory cortex leveraging on iEEG recordings. The thesis is divided into the following chapters: Chapter 1 presents relevant background information and a theoretical framework on auditory deviance detection in the human brain. Because iEEG was the key method used for investigating the research questions of this thesis, the chapter starts by introducing iEEG and what processes iEEG signals reflect. Chapter 2 presents the empirical study, including its materials and methods. The findings from the empirical study are presented and Chapter 3 and discussed in Chapter 4 with respect to previous empirical findings from iEEG, relevant theoretical frameworks, and their limitations. Lastly, Chapter 5 provides a conclusion to the research questions.

1.1 Intracranial Electroencephalography

Human iEEG is an invasive method in which electrode arrays are implanted into brain tissue in patients for direct recordings of the electrical activity from the exposed area (Helfrich & Knight, 2019). It is predominately used for presurgical monitoring and identification of seizure-generating loci in patients with pharmaco-resistant focal epilepsy who are candidates for resection surgery (Chauvel et al., 2019; Talairach & Bancaud, 1966). Since iEEG is combined with neuroimaging before and after implantation surgery to guide the localization of the electrodes and seizure loci, it also allows for a three-dimensional assessment of the functional human brain anatomy with excellent spatiotemporal precision over a prolonged time, from days to weeks (Helfrich & Knight, 2019; Lachaux et al., 2003). Thus, iEEG combines the high spatial resolution from neuroimaging and the high temporal resolution from EEG, which makes it an ideal approach for precise functional brain mapping.

1.1.1 Subdural and intracerebral electroencephalographic recordings

The two main approaches to iEEG are subdural grid electrodes referred to as electrocorticography (ECoG), and intracerebral depth electrodes referred to as stereotaxic electroencephalography (SEEG; Chauvel et al., 2019; Lachaux et al., 2003; Talairach & Bancaud, 1966). The key difference between the recorded signal from ECoG and SEEG lies in the spatial precision and coverage. Specifically, in SEEG, depth electrode arrays with

multiple single electrode contacts are implanted into the exposed brain through burr holes in the skull, while with ECoG, grid-formed electrode arrays are laid over the surface of the exposed brain tissue (Seeck & Schomer, 2017). The temporal resolution of the iEEG signal is excellent and only constrained by the sampling rate of the acquisition device, while its spatial resolution is defined by the center-to-center distance between adjacent electrode contacts (which typically is between 2 and 10 mm). The sensitivity of the iEEG signal, however, depends on the distance from the electrode contacts to the voltage source and the conductive properties of the brain tissue surrounding the electrode contacts (Lachaux et al., 2003).

1.1.2 The iEEG signal as an electrophysiological correlate of cognitive processing

The properties of the signal derived from iEEG allow for investigating various aspects of cognitive processing in the brain. The recorded raw iEEG signal reflects the local field potentials, which comprise the summation of voltage gradients from the postsynaptic potentials generated predominantly from pyramidal cells proximal to the electrode (Buzsáki et al., 2012). When neuronal cell populations fire, the extracellular currents generate a dipole and the polarity of the recorded voltage potential can vary between positive and negative values depending on the relative position of the electrode to the current dipole (Buser, 1955; Buzsáki et al., 2012). Hence, a change in the intracerebral voltage polarity in the measured signal between two adjacent electrode contacts on the same electrode array can provide an estimate of the neural generator of the recorded voltages (Buser, 1955; Lachaux et al., 2003).

The excellent frequency resolution and signal-to-noise ratio of the iEEG signal allow for investigating oscillations in various frequency bands in the time-frequency domain. Broadband high-frequency activity (HFA) is specifically used in iEEG as it represents the averaged summed changes in intracerebral voltage potentials from populations of neurons firing between 70 to 150 Hz (Crone et al., 1998; Helfrich & Knight, 2019). Although both intracranial ERP and HFA are derived from intracerebral post-synaptic currents, they do not overlap but reflect different aspects of the activity of neuronal ensembles. Specifically, the frequency component of the intracranial ERP is limited to synaptic activity up to 50 Hz, with larger amplitudes in the ERPs reflecting increase in either excitatory or inhibitory post-synaptic currents (Lachaux et al., 2012). In addition, activity in lower frequency bands is more prone to volume conduction and reflects the summation of voltages from larger neuronal ensembles (Helfrich, 2022). Conversely, HFA comprises faster synaptic activity and can reflect both synchronous and asynchronous firing meaning that the currents may cancel

each other out. As a corollary, the local field potentials reflected in HFA are more focal than in the ERPs (Lachaux et al., 2012; McCarty et al., 2022). HFA also correlates with local task-specific activity reflected in the blood-oxygen-level-dependent (BOLD) signal as measured in fMRI (Lachaux et al., 2012; Mukamel et al., 2005) and spiking multi-unit activity (Leszczyński et al., 2020; Ray et al., 2008). In addition, increase in the HFA magnitude correlates with behavior and task-specific neural activity (e.g., Blenkmann et al., 2019; Crone et al., 1998; Lachaux et al., 2012; Voytek & Knight, 2015). Because if its spatial resolution, changes in the functional properties of the HFA signal (e.g., power or response latency) may correspond to specific mechanisms that influence the synchronized firing of local neuronal ensembles.

Thus, correlative evidence supports that HFA indexes change in the local field potentials of neuronal ensembles involved in stimulus or cognitive processing, while polarity inversions in the intracerebral voltages reflect the anatomical source of such potentials. In the next section, we continue with presenting the human auditory system and how iEEG results can inform about auditory processing hierarchies.

1.2 The human auditory cortex as a processing hierarchy

The auditory cortex refers here to the supratemporal (Brodmann area; BA 41 and 42) plane and posterolateral regions of the STG (BA 22; Howard et al., 2012). Although selective neural responses to auditory input have been demonstrated in other brain regions such as parts of the parietal and frontal lobes (Howard et al., 2012), these are referred to by their anatomical labels. The auditory system is organized hierarchically in the sense that auditory information passes through multiple processing stages representing progressively more complex stimuli. In addition, the stages of this hierarchy, as early as the cochlea, receive feedback projections from later stages (McDermott, 2018). This suggests that auditory information is not projected in one-directional feedforward fashion but involves a complex interaction between ascending and descending information.

1.2.1 An overview of the subcortical processing stages

Auditory information enters the outer ear as sound waves that travel through the ear canal and are transmitted as vibrations on the tympanic membrane. These vibrations are conveyed via the ear ossicles as travelling waves until they reach the inner ear where they

stimulate the cochlea (Brodal, 2016; Rauschecker, 2020). The basilar membrane of the cochlea is filled with fluid and contains hair cells that are spatially organized as a function of sound frequency responsiveness. It is the width and stiffness of the membrane that determine the response properties of the inner hair cells. When auditory information stimulates the fluid membrane, this creates ripples that move the inner hair cells and leads to release of neurotransmitters that in turn stimulate the release of action potentials in the auditory nerve fiber the hair cell synapses with (McDermott, 2018). In addition, the membrane contains outer hair cells that can alter how the movement of the membrane and thus function to adjust the responses elicited by the inner hair cells (McDermott, 2018). From here on, auditory information continues onwards in the auditory ascending system as electrical impulses to the brain via the cochlear nucleus of the brain stem.

Much of the auditory information is computed with progressing complexity before it enters the cortex. These subcortical processing stages also contain efferent projections that return to the inner and outer hair cells, and allow for adaptive changes in audition (McDermott, 2018). The cochlear nucleus computes information about acoustic features such as sound onset and offset, and its temporal and spatial properties (Jasmin et al., 2019; McDermott, 2018). The thalamus represents a major relay and gating stage before the cortex. Here, most of the auditory information is projected via the medial geniculate body of the thalamus to the core of the PAC, while other thalamic subdivisions project to different subareas of the PAC in addition to non-primary auditory and non-auditory cortical brain areas (Jasmin et al., 2019; Scott et al., 2017).

1.2.2 Auditory processing in the human primary auditory cortex

Deep within the Sylvian fissure (also referred to as the lateral sulcus) on the planum temporale of the human temporal lobe lies Heschl's gyrus, which posteromedial portion comprises the human PAC or "the auditory core" (BA 41; Clarke & Morosan, 2012). The cytoarchitecture and myelination of this area are distinct from the surrounding cortex by being densely myelinated with thalamic and cortical projections (Clarke & Morosan, 2012). On a macroscopic level, the superior temporal plane is characterized by extensive cortical folding and convolutions that vary between individuals, making noninvasive investigations on the organization of the human PAC challenging (Clarke & Morosan, 2012; Nourski, 2017). Invasive investigations in non-human primates have thus been instrumental in developing models about the functional organization of the primate auditory cortex and the intricacy of its

many connections (Kaas et al., 1999; Nourski, 2017). These findings support a hierarchical organization of the primate auditory cortex, with a primary core being surrounded by a non-primary belt, which is again surrounded by a parabelt (Nourski, 2017), with additional extrinsic and intrinsic pathways connecting these and other cortical areas (Jasmin et al., 2019; Kaas & Hackett, 2000; Rauschecker, 2020; Scott et al., 2017). To what degree this organization translates to humans remains unclear, but one can assume that the human PAC is at least as complex (Rauscheker, 2020). In addition, there is evidence supporting a functional delineation between regional differences in the response properties of auditory cortical neurons, depicting a cortical auditory hierarchy (Nourski, Steinschneider, McMurray et al., 2014; Nourski, Steinschneider, Oya et al., 2014).

It is the width of the frequency tuning of an auditory cortical neuron that determines what features it is sensitive to and fire in response to (Howard et al., 2012). We differentiate here between variants of neuronal responsiveness to acoustic stimulation. Some neurons have a narrow tuning curve while others have a broader tuning curve. For pure sounds (i.e., sinusoids), the term *best frequency* refers to the center of a range of sound frequencies a neuron fire in response to (i.e., its neural tuning is not discrete). Thus, *frequency selectivity* refers to the degree of tuning width, meaning that a neuron with a narrow tuning width may demonstrate a high level of frequency selectivity to acoustic stimulation of one sound frequency. Conversely, a neuron with a wider tuning width may demonstrate less frequency selectivity and respond to a larger range of sound frequencies (Howard et al., 2012). Frequency preference thus refers to responses recorded from neuronal assemblies (e.g., local-field potentials) with individual tuning curves at the neuronal level, that may collectively demonstrate an overall stronger response (i.e., synchronized firing), or preference, to a category of sound frequencies (e.g., higher > lower) or a specific sound frequency compared to other frequencies used as stimuli (e.g., 1200 Hz > 1000 Hz).

The posteromedial portion of Heschl's gyrus contains neurons with short response onset latency to auditory stimulation, high level of frequency selectivity, and narrow tuning width compared to the surrounding cortex (Clark & Morosan, 2012; Howard et al., 2012; Nourski, Steinschneider, McMurray et al., 2014). In addition, the spatial organization of frequency responses in this area mirrors the tonotopic organization of the basilar membrane of the cochlea, rendering this area likely to comprise the human PAC (Clark & Morosan, 2012; McDermott, 2018). There is, however, some uncertainty about the number and orientation of

frequency gradients of the human PAC, and their functional importance. Most studies support a high-low-high frequency gradient, with the core of the PAC in the middle responding primarily to low frequencies, while a high-frequency gradient extends to the STG (Formisano et al., 2003; Moerel et al., 2014). Some evidence supports that the core is oriented along a posterior-anterior axis; other findings rather support a perpendicular (medial-lateral) orientation, while still other evidence suggests multiple local frequency gradients being distributed on the supratemporal plane (Moerel et al., 2014). Although they cover a more spatially restricted area, findings from iEEG also shed light upon the response properties of the human PAC, with one study reporting a high-to-low frequency gradient going from posterior to anterior parallel to the long axis of Heschl's gyrus (Howard et al., 1996).

Hence, while tonotopy can be an organizing principle of neurons in the PAC, large heterogeneity between individuals and group samples, besides restricted temporal resolution with standard methods such as fMRI, may lead to diverging results regarding the exact orientation of neural responses in the human PAC.

1.2.3 Auditory processing in the human non-primary auditory cortex

The PAC and the thalamus project auditory information to non-primary cortical areas such as the lateral portion of the STG, the parietal lobes, and the frontal lobes, and these may project further to additional parts of the neocortex (Howard et al., 2012; Jasmin et al., 2019; McDermott, 2018). As auditory information is propagated in the auditory system in both a serial and parallel manner, with the presence of multiple feedback projections, it is challenging to disentangle the exact order of each region in this processing hierarchy. For simplicity, we refer to these auditory cortical areas as non-PAC or secondary auditory cortex.

We can functionally delineate the cortical neurons of the non-PAC from those in the PAC based on their response properties. Besides a broader frequency tuning, neurons in the non-PAC have prolonged response latencies and broader frequency tuning in the early evoked auditory responses occurring within 100 ms post stimulus-onset compared with neurons in PAC (Brugge et al., 2008; Hall & Barker, 2012; Howard et al., 1996; Liégois-Chauvel et al., 1991, 1994; Nourski, Steinschneider, McMurray et al., 2014). Moreover, neuronal ensembles in these regions demonstrate regional selective responsiveness to more complex stimuli such as rhythm, music, speech, sound recognition, sound location, songs, sentence expectancy and expectancy violations, and integration of auditory and visual information (Jasmin et al., 2019;

McDermott, 2018; Norman-Haignere et al., 2022). Thus, tonotopy is a less likely organizing principle in non-PAC given such higher-order cognitive functions (Clarke & Morosan, 2012; McDermott, 2018).

In sum, the human PAC mirrors the spatial tonotopic organization of the cochlea, but its exact orientation remains unknown. Still, cumulative evidence supports that neurons in the core of the PAC have shorter response latency and stronger preference for lower frequencies than the neighboring non-PAC. There are also findings supporting that auditory information is computed at subcortical levels before and after it enters the PAC, and the many synaptic connections suggest that information is transmitted back and forth in this hierarchy.

1.3 Auditory deviance detection in the human auditory cortex

1.3.1 The mismatch negativity and other neural correlates of auditory irregularity

Regularity encoding and deviance detection in the auditory domain are traditionally studied with variants of the oddball paradigm (Näätänen et al., 1978). In the classic oddball paradigm, two physically distinct stimuli (e.g., two different sound frequencies) are randomly presented as a stream of sounds with different occurrence probabilities. One stimulus is presented frequently and hence considered more probable, while the second stimulus occurs infrequently and represents a deviant (Näätänen et al., 1978). When an unexpected deviant stimulus occurs instead of the standard stimulus, an ERP component known as the MMN can be observed (Näätänen et al., 1978). The MMN results from the subtraction of the ERPs to frequent standard stimuli from infrequent deviant stimuli (deviant - standard), reflected in scalp-EEG as a difference waveform of negative polarity (hence the name) that peaks between 150 to 250 ms after stimulus onset (Näätänen et al., 2007). The MMN was originally proposed to reflect an automatic mechanism for stimulus discrimination based on a comparison between the actual input with a short-term auditory memory trace for the standard repeated stimulus (Fitzgerald & Todd, 2020; Näätänen et al., 2007). An alternative explanation for the MMN component proposes that the repetition of a stimulus (i.e., a standard) causes stimulus-specific adaptation, or reduced sensitivity in neurons that fire in response to the specific stimulus (May & Tiitinen, 2010). Presentation of a novel or deviant stimulus with subsequent change in the recorded brain signal thus reflects the firing of neurons not sensitive to the standard stimulus.

ERP components are labelled according to the polarity of the waveform in the scalp EEG signal and the peak latency of their amplitudes (Luck, 2014). Changes in these properties may therefore reflect changes in the underlying neural mechanisms comprising the ERPs. For example, variability in the latency and amplitude of the MMN has been interpreted as reflecting the complexity of the standard-deviant comparison, with increased peak latency implying a more "complex" (i.e., more difficult) decision, and increased amplitude indicating more discriminable stimuli (Fitzgerald & Todd, 2020). Given its temporal peak properties, it has been debated whether the MMN reflects a distinct process or a modulation in the auditory N1-P2 ERP complex, which is elicited in response to auditory sensory processing (May & Tiitinen, 2010; Polich, 2007). However, the MMN and its counterparts have also been proposed to emerge from neural activity involved in processing violations of stimulus transition probability rather than auditory sensory processing (Fitzgerald & Todd, 2020; Winkler, 2007). Some of the strongest pieces of evidence for this argument is the elicitation of mismatch responses like the MMN to abstract rule violations and even stimulus omissions timed at an expected stimulus presentation (see e.g., Bekinschtein et al., 2009; Heilbron & Chait, 2018; Hughes et al., 2001; Nordby et al., 1988; Todorovic et al., 2011; Winkler, 2007). From this perspective, the repetition of standard stimuli in oddball paradigms represents auditory regularity, and it is the statistical inter-stimulus relationship, instead of the physical acoustic feature itself, that represents the standard (i.e., expected event) in auditory oddball paradigms (Winkler, 2007). Hence, in an alternating two-sound sequence (e.g., ABABA), the regularity rule is that sound B always follows sound A, and vice versa. Expanding upon this argument, an alternative interpretation of the MMN and its correlates is that they reflect violation to encoded auditory regularity, rather than the mismatch from an auditory sensory memory trace (Winkler, 2007). The elicitation of MMN to more complex stimulus violations thus suggests that the brain has generated an internal predictive model extrapolated from the statistical relationship between the auditory regularities (Winkler, 2007).

P300. Another electrophysiological correlate of deviance detection is the P300 (also known as the P3), which is a positive-polarity ERP component that peaks circa 300 ms after presentation of a deviant stimulus such as in the oddball paradigm (Kok, 2001; Polich, 2007; Sutton et al., 1965). Since the P300 often follows the MMN, it may represent the next step in the processing of auditory (ir)regularity (Polich, 2007). The P300 component has a differential scalp distribution pattern and peak latency that depends on the task instructions (i.e., an active or passive paradigm), and hence categorized into two subtypes (Polich, 2007).

The frontocentral P3a component peaks circa 220 to 300 ms post stimulus onset, in response to presentation of infrequent stimuli (e.g., a distractor). It has thus been interpreted as an involuntary attention-reorienting mechanism, with neural generators localized to the hippocampus, supramarginal gyrus and anterior cingulate gyrus (Fonken et al., 2020; Polich, 2007; Squires, et al., 1975). The other subtype is the parietal P3b, which has a prolonged peak latency (250 to 600 ms) localized to temporoparietal and frontal regions in response to target-detection and tasks that require selective attention, for example stimulus evaluation (Fonken et al., 2020; Kok, 2001; Picton et al., 1992; Polich, 2007; Soltani & Knight, 2000).

Converging findings from EEG and fMRI support a functional and anatomical distinction between the P3a and P3b, implying that they reflect activity in different attentional networks (Kim, 2014; Polich, 2007). The P3a can be elicited by unattended or novel stimuli such as in passive oddball paradigms, indicating that it reflects more stimulus-driven mechanisms (Kim, 2014). Meta-analytic evidence supports this suggestion, showing that presentation of unattended auditory oddballs in passive paradigms was associated with increased BOLD signal in a ventral attention network comprising the temporoparietal junction (TPJ), the STG, supramarginal gyrus, frontal operculum, anterior cingulate cortex, anterior insula, and inferior frontal gyrus (Kim, 2014). The TPJ may represent a key region in generating P3a-related activity (Kim, 2014; Polich, 2007), and may hence play a crucial role during deviance detection and be related to the MMN. Since the P3 succeeds the MMN, one hypothesis states that activity in the TPJ reflects an update of an internal contextual model with new information (Donchin & Coles, 1988; Polich, 2007). Reduction of the BOLD signal from the TPJ with repeated presentation of the same deviants supports this suggestion, implying that the internal model gets "saturated" with contextual information (Polich, 2007). Another hypothesis is that the right TPJ functions as a stimulus-driven "circuit breaker", signaling the need for allocation and reorientation of attentional resources towards an unattended stimulus (Corbetta & Shulman, 2002; Corbetta et al., 2008).

HFA. Auditory deviance detection is also associated with modulations in the spectral components in the time-frequency domain. Specifically, increased broadband activity in the high-gamma (>70 Hz) band has been suggested to reflect the augmented firing to unexpected stimuli or an error signal (Arnal & Giraud, 2012; Bastos et al., 2012). Lately, findings from iEEG studies in awake surgical patients showed increased local activity in the HFA range in a spatially restricted number of electrodes during processing of auditory deviance (e.g.,

Blenkmann et al., 2019; Edwards et el., 2005; El Karoui et al., 2015; Ishishita et al., 2019), thus indicating that increase in HFA reflects local deviance detection-like cortical activity.

1.3.2 Hierarchical predictive processing perspectives on auditory deviance detection

The overarching idea of our brains anchoring predictions about sensory experiences from an internal model derived from previous experience is at least as old as modern psychology itself (Helmholtz, 1867). In recent years, predictive coding, or hierarchical predictive processing frameworks, have regained attention as theoretical models explaining sensory processing and perception in terms of computational principles (Clark, 2013; Friston, 2005, 2010; Rao & Ballard, 1999). The hierarchical predictive processing framework postulates that the brain is organized hierarchically and involves two interacting units at each level in the hierarchy: Units that generate predictions about upcoming sensory stimuli based on an internal model of the sensory world, and error units that signal if a prediction is erroneous (Friston, 2005, 2010; Tabas & von Kriegstein, 2021; Walsh et al., 2020). The predictions are conveyed from higher to lower levels in the hierarchy, where they are compared to the actual incoming stimuli. (Friston, 2010; Walsh et al., 2020). If incoming stimuli deviate from the prediction, the error units generate a prediction error signal that is propagated up the hierarchy to higher processing levels, where the internal model is updated with new information about the current context (Garrido et al., 2009; Walsh et al., 2020). This process may thus enable more efficient information processing, allowing the brain to selectively attend to important (i.e., unpredictable) stimuli and ignore irrelevant (i.e., predictable) stimuli (Feldman & Friston, 2010). Sensory adaptation effects, such as attenuation of brain signal amplitudes from repeated stimulation, can hence be interpreted as attenuation to predictable stimuli that save neural resources (Auksztulewicz & Friston, 2016).

1.3.3 Intracranial evidence for auditory deviance detection in the human brain

The numerous projections within and between auditory-processing areas make it appealing to assume that these areas involve local and global network activity, as part of a larger hierarchy. However, the exact contribution of cortical fields in the human auditory cortex during auditory regularity and deviance encoding remains unclear. The fine-tuned spatiotemporal resolution of iEEG makes it ideal to differentiate between activity in neighboring auditory cortical fields when investigating violations to auditory regularity. For example, iEEG studies have located a neural generator of the intracerebral voltages that

comprise mismatch responses to the STG (Halgren et al., 1995; Kropotov et al., 2000) and frontal regions (Näätänen et al., 2007; Rosburg et al., 2005), thus confirming findings from scalp-EEG and MEG (Näätänen et al., 2007). However, the exact generators may depend on what physical features and abstract task rules the deviant represents (Fitzgerald & Todd, 2020). Thus, investigating responses to different types of auditory irregularity across cortical response profiles with iEEG can provide information at a level of detail that is not possible with other methods.

For example, by combining an active listening paradigm with unexpected repetitions and omissions of alternating sounds, Halgren et al. (1995) reported that such auditory deviants elicited a distinct positive waveform that peaked at approximately 150 ms after onset of the rare events. The polarity of this waveform became inverted at electrode contacts implanted superior to the Sylvian fissure, possibly reflecting a neural generator of the recorded waveform (Halgren et al., 1995). Notably, deviance-related activity and no polarity inversions were observed in channels implanted in the posteromedial portion of Heschl's gyrus (i.e., the PAC; Halgren et al., 1995). Others have also reported local spatial disparity in the effects of auditory deviance on neural activity. Nourski et al. (2018) reported a spatial difference in neural sensitivity to local (i.e., a switch between two tones) and global (i.e., violation of the presentation pattern) rule violations, with the latter being more prominent in HFA recorded from lateral STG compared to PAC (Nourski et al., 2018). By comparing neural responses in the high-gamma (> 70 Hz) range to standard and deviant tone pitches, including their spatial distribution in the distal superior temporal cortex, an iEEG study by Ishishita et al. (2019) showed that the deviant tone pitch elicited a significant increase in induced high-gamma power compared to the standard pitch. Their results also indicted that a relatively small contribution of neural adaptation to tones varied with the anatomical location of the grid electrodes on the posterior STG. Thus, some auditory lateral cortical fields may be more robust to adaptation effects (Ishshita et al., 2019).

The findings from Ishishita et al. (2019) are in line with other iEEG studies showing MMN or auditory deviance-related increase in local neural activity in the STG (Blenkmann et al., 2019; Edwards et al., 2005; El Karoui et al., 2015; Halgren et al., 1995; Rosburg et al., 2005), but also spatial disparity in the effect of stimulus repetition on cortical activity (Eckert et al., 2022). While violations to auditory regularity have received a lot of attention, how different brain regions respond to predictable stimuli remains less known. Based on data from

a passive oddball paradigm, Eckert and colleagues (2022) reported from two interacting networks distributed in temporal, frontal and parietal channels during stimulus processing: A network for stimulus-responses and a network of neurons involved in a repetition-suppression network (Eckert et al., 2022). Moreover, Dürschmid et al. (2016) showed regional differences in sensitivity to auditory predictions during a passive listening paradigm with ECoG. Auditory deviants that represented local and global rule violations elicited increased neural activity in the HFA range in temporal regions, but only global auditory deviants increased HFA in frontal regions (Dürschmid et al., 2016). Other areas involved in auditory deviance detection include the posterior insula (Blenkmann et al., 2019). When comparing HFA to deviants recorded from the posterior insula and superior temporal cortex during a passive listening task, the authors reported increased HFA to deviants relative to standards in both insula, STG, and superior temporal sulcus. However, the increase in insular activity occurred later, suggesting that it fulfills a later role in a processing hierarchy (Blenkmann et al., 2019). Thus, iEEG results expand on those from other approaches by replicating their previous findings on where in the human cortex auditory deviance processing occurs, and by suggesting involvement of other cortical areas as part of a deviance hierarchy.

1.4. Introduction to the empirical study and its research questions and hypotheses

While there is evidence suggesting a distributed network of cortical areas involved in regularity processing and deviance detection (Eckert et al., 2022; Johnson et al., 2020), there are still unanswered questions. Specifically, although the reviewed literature implies that the temporal cortex is involved in processing of unexpected deviants in regular sound streams, it is unclear what is the precise role of different stages in the auditory hierarchy when attention is directed towards an irrelevant task. The hierarchical predictive processing framework predicts that deviance detection (i.e., prediction errors) may take place at specific levels and ascend to the next level in the processing hierarchy (Walsh et al., 2020). In addition, higher-level regions such as the TPJ may represent a key role in later processing of auditory deviants (Chennu et al., 2013; Corbetta & Shulmann, 2002; Corbetta et al., 2008) that may extend to a predictive processing hierarchy. Thus, the current study aimed to investigate auditory irregularity processing in the cortical auditory hierarchy with the following hypotheses:

Hypothesis 1: Acoustic stimulation during the tonotopic mapping task would elicit tonotopic responses in Heschl's gyrus reflected as polarity inversions in the ERPs and channel-specific increase in HFA. The posteromedial portion of Heschl's gyrus was expected

to comprise the PAC, reflected as earlier response onset latencies than surrounding non-primary regions. However, given the prior diverging results and individual differences in the tonotopic organization of this area, no a priori predictions were made about the orientation of any spatially distributed frequency gradient. This hypothesis was based on previous functional differentiation based on response latencies using iEEG (e.g., Brugge et al., 2003; Liégois-Chauvel et al., 1991; Nourski, Steinschneider, McMurray et al., 2014).

Hypothesis 2: Previous iEEG findings have demonstrated increased power in the high-gamma range and polarity inversions in the ERPs in the lateral aspects of the STG when processing auditory deviants (Edwards et al., 2005; Halgren et al., 1995; Ishishita et al., 2019; Nourski et al., 2018). Unexpected auditory deviants in the oddball task were therefore hypothesized to elicit increased HFA in the STG compared to expected standard stimuli in the control condition. Similarly, we expected deviance detection effects in PAC, however to a lesser extent (Parras et al., 2017). Specifically, if tonotopic areas are dissociated within PAC, then areas tuned to the expected tone were expected to respond with increased HFA. This hypothesis was based on the PAC representing a lower-order processing stage compared to non-PAC, and the postulate from the hierarchical predictive processing frameworks stating that lower-order sensory stages encode predictions errors (Clark, 2013; Friston, 2005).

Hypothesis 3: The right TPJ, a key node in the ventral attention network, has been proposed a prominent role in reorienting attention towards unattended stimuli (Corbetta & Shulman, 2002). Thus, we investigated if unpredictable auditory irregularity influenced the ERPs and HFA elicited in this region. Based on meta-analytic evidence from previous fMRI studies showing increased BOLD signal to oddball stimuli localized to the right TPJ (Kim, 2014), combined with the correlation between the BOLD and HFA signals (Lachaux et al., 2012; Mukamel et al., 2005), we hypothesized that auditory deviants would evoke increased HFA in the right TPJ. In contrast, responses elicited by auditory deviants in other cortical areas were investigated with an exploratory approach to the extent that polarity inversions in the ERPs reflect neural generators. We also explored if unexpected auditory deviants relative to standards in the oddball task delayed response onset latencies of the HFA. This was investigated based on previous iEEG findings demonstrating a functional differentiation between primary and non-primary auditory cortical sites based on the response onsets of HFA (Nourski, Steinschneider, McMurray et al., 2014). Thus, changes in the latencies of the HFAs would allow exploring spatial disparity between stages in the auditory processing hierarchy.

2 Methods

2.1 Ethical considerations

This study was conducted as part of the "Oscillatory mechanisms supporting human cognition" project funded by The Norwegian Research Council. The project and the research protocol were approved by the Regional Committees for Medical and Health Research Ethics, Region North Norway (REK 2015/175/REK Nord) and *personvernombudet* (eng. Data protection officer) at Oslo University Hospital Rikshospitalet. Before participating in the study (and after the electrodes were implanted), the participants gave written informed consent under the Declaration of Helsinki. Before each experimental session, the experimenter reminded the participants that they could withdraw their participation at any time, and without providing any reason for that. If a participant experienced seizures or expressed discomfort during an experimental session, the experimenter would end the session and ask the participant a minimum of two hours later if they wanted to continue. Designated personnel anonymized all personal information and stored it on a secure server, with restricted access to staff members according to the project's data management plan.

2.2 Study participants

The participants were three adults (referred to individually as SUB1, SUB2, SUB3) with drug-resistant epilepsy who underwent iEEG monitoring as part the clinical assessment for resection surgery recruited at Oslo University Hospital Rikshospitalet. The participants (one male) were all in their 30s, and right-handed (score > 40 on the Edinburgh Handedness Inventory; Oldfield, 1971), fluent Norwegian speakers with self-reported normal hearing. The participants underwent pre-surgical iEEG monitoring as part of their diagnostic evaluation. None of the participants had undergone previous neurosurgical procedures.

2.3 Procedures

The current study comprised two experiments presented together. Dr Alejandro Blenkmann designed the experiments and stimuli and collected the data in the current study. The dataset for this study is constrained to recordings obtained from electrodes implanted in the right superior temporal plane (including auditory cortex, 10 to 12 contacts per depth electrode

array, one depth electrode implanted in the auditory cortex of each participant and one depth electrode implanted in the TPJ in two of the participants) that were not generating epileptic activity as revealed by the monitoring. The electrodes of interest were labelled by the operating neurosurgeon for each participant (SUB1: U; SUB2: T and H; SUB3: H and W). Recordings obtained from other brain locations were outside the scope of the current study and were not analyzed. All electrode implantations and data collection occurred at the Department of Neurosurgery at Oslo University Hospital Rikshospitalet, which has the national function for this type of iEEG monitoring and surgery in patients with drug-resistant epilepsy.

2.3.1 Stimuli and experimental design

Two auditory tasks, tonotopic mapping and repetition oddball task, were administered to investigate the distribution of functional properties and neuronal tuning in the auditory cortex. Both tasks had a similar approach, hence the general experimental procedures are reported together, and unique procedures reported separately. Because inter-individual differences in the spatial distribution of neuronal tuning and response properties represent a risk for whether any tone frequency-specific response was recordable in the implanted electrodes (Moerel et al., 2014), the oddball task was assessed on two separate sessions with different tone-pairs. However, given the time constraints and page limits for this thesis, we only present the dataset from the first oddball task session in each participant here.

The first experimental session occurred two days after implantation surgery and comprised either a tonotopic mapping task followed by an auditory repetition oddball task (SUB2 and SUB3), or only the oddball task (SUB1). In the next session (one to four days later), the tonotopic mapping task was tested on SUB1 and the oddball task was retested on all participants with different sound stimuli. To avoid patients' tiredness, a break lasting at least five minutes between each task was introduced. Both tasks were administered as passive listening paradigms by asking the participants to read a book and not pay attention to the stimuli. This was done to prevent interference from attentional processes in the recorded brain activity (Näätänen et al., 2007). Before the onset of each experimental session, the experimenter adjusted speaker volume and balance between the left and the right ear to each subjects' preferred comfort level. The balance was adjusted until it reached perceptual equilibrium because some participants had their ears partially covered with bandages.

Tonotopic Mapping. Five blocks comprising sequences of pure sinusoidal tones (frequencies were: 220, 311, 440, 622, 800, 1245, 1760, 2480, 3450, 4978, and 7040 Hz) were played binaurally in a pseudo-randomized order. Each tone lasted 100 ms and was randomly repeated ten times within each block with 600 to 900 ms (300 ms jitter, 10 ms fade in/out) between each tone, yielding 110 repetitions in each block.

Auditory repetition oddball task. This experiment was a modified version of the tone-alternation oddball paradigm (Alain et al., 1994; Nordby et al., 1988; Näätänen et al., 1978) and comprised the presentation of standard and deviant tones in four blocks with a few minutes break between blocks. The participants decided the duration of each break. In the first block, namely the alternation block, a low-frequency tone (e.g., A) and a high-frequency tone (e.g., B) were played in an alternating manner (e.g., ABAB). These two standard tones were played for at least 30 repetitions at the beginning of each block to establish the most frequent presentation pattern before the onset of any deviants. In 20 % of the trials, the previously played tone was repeated instead of the expected alternation tone (e.g., ABA**A**B), hence the repeated tone represents an unexpected event or Repetition Deviant tone (deviant indicated in bold font). In the second block, namely the repetition block, tones were presented in pairs (e.g., AABBAABB) 80% of the time (i.e., the standard condition). In 20% of the cases, tones were exchanged producing different types of deviants (AAB**A**ABB or AABB**B**ABB). In this study, we focused on the Alternation Deviant tone (AAB**A**ABB).

The deviants were temporally distributed in a pseudo-randomized manner to avoid presenting a deviant tone immediately after another deviant. Each tone was presented for 100 ms (including 10 ms rise and decay time) every second, yielding a total of 1240 repetitions in each block. This design enables comparing brain responses elicited in response to Repetition and Alternation Deviant tones contrasted to responses from control conditions when the same tones were presented as Standards in the complementary blocks. This yielded the following comparisons in the current study: deviant AA and deviant BB (i.e., Repetition Deviants) from the alternation block versus respectively standard AA and standard BB from the repetition block. In addition, deviant AB, and deviant BA (i.e., Alternation Deviants) from the repetition block versus standard AB and BA from the alternation block. Figure 1 illustrates the experimental design and stimuli presentation in the tonotopic mapping and oddball task.

Figure 1. *Illustration of Stimuli Presentation and Experimental Design*

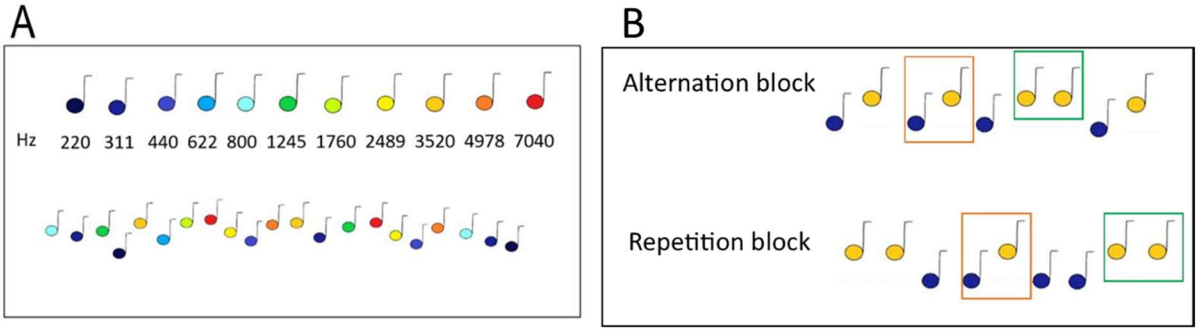

Note. **A**: Tonotopic mapping. Eleven different tone frequencies played in random order. **B**: A sequence of two distinct tones A (blue) and B (yellow) played in a repetitive pattern in each block. The color-coded rectangles illustrate the comparisons made between different tone patterns from each block. Green boxes: deviant BB (alternation block; upper row) versus standard BB (repetition block; lower row). Orange boxes: deviant AB (repetition block; lower row) versus standard AB (alternation block; upper row).

2.4 Data acquisition

2.4.1 Imaging data acquisition.

Before undergoing implantation surgery, T1-weighted MRI for each participant was obtained with a 3 Tesla scanner (Siemens Medical Solutions, Erklangen, Germany) with a 24-channel head coil to get a detailed anatomical description of each participant's brain. Depth electrode implantation may cause brain swellings in which the electrodes move 1 to 2 millimeters from their original coordinates. This was corrected by co-registering pre-surgery MRI with post-surgery CT that the participants underwent as a part of their post-surgical control. These MRI and CT images were co-registered individually for each subject for localization of the intracranial electrodes in native space.

2.4.2 Stereotaxic electroencephalography recordings

SEEG signals were recorded with subdural depth electrodes (DIXI Medical, France) made of platinum-iridium alloy (0.8 mm in diameter, 8 to 18 contacts per electrode, 2 mm between contacts). The signal was amplified and high-pass filtered at 0.15 Hz during the

recording and sampled at 2048 Hz (Participant SUB1 and SUB3) or 1024 Hz depending on the recording system (Atlas System, Neuralynx, USA or BrainQuick, MicroMed, Treviso, Italy). Scalp electrodes were used as a reference during recording. The channels were numbered in increasing order, starting medially from the tip of the electrode shaft, and increasing laterally along the electrode shaft.

2.4.3 Stimuli presentation

A pair of headphones (DT770 Pro, Beyerdynamic) was used to present the stimuli binaurally. The stimuli were created in Matlab version R2019b (MathWorks Inc., USA) and presented with PsychToolbox version 3 for Matlab (Kleiner et al., 2007) on a laptop. To synchronize the stimuli presentation with the recording, triggers were sent to the analog or digital input of the recording system.

2.5 Data preprocessing

2.5.1 Electrode localization

To determine the anatomical location and coordinates of the electrodes, pre-surgery MRI was segmented and preprocessed with Freesurfer (version 6.0; Dale et al., 1999), and post-implantation CT was co-registered to the MRI with SPM 12, using normalized mutual information (Studholme et al., 1999). Images were then loaded to the iElectrodes toolbox (Blenkmann et al., 2017) for manual localization and labelling of the electrodes using Freesurfer parcellations from the Desikan-Killiany atlas (Desikan et al., 2006). The individual cortical electrode coordinates and labels were confirmed by visual inspection of the MRI and CT images guided by the Duvernoy anatomical atlas (Naidich et al., 2009). The images were normalized to Montreal Neurological Institute (MNI)-152 space with SPM 12 (Ashburner & Friston, 1999). To reduce uncertainty and potential bias introduced from noise, electrode contacts with their center implanted in white matter more than 3 mm from the cortex were removed from further analyses. If less than 3 mm, the recorded activity was assigned to the closest cortical area.

The electrode coordinates were plotted on brain models in both native and normalized space. Cortical electrode coordinates in native space were plotted on tailored mesh surface reconstructions of the auditory cortex for each participant, created from individual brain segmentation data with an open-source Matlab toolbox (Dalboni da Rocha et al., 2020) and

anatomical labels from the Destrieux atlas (Destrieux et al., 2010). The normalized electrode coordinates were projected onto a standard MNI-152 brain model using Python (version 3.7) and the Visbrain toolbox (Combrisson et al., 2019).

2.5.2 The SEEG signal

Referencing method. The raw recorded SEEG signal was preprocessed using custom Matlab scripts and the FieldTrip toolbox (Oostenveld et al., 2011). Channels and segments that displayed epileptic or other abnormal activity were removed from the dataset and any further analyses. The cleaned data was re-referenced using the bipolar referencing method in which the recorded signal in one contact is subtracted from its adjacent lateral contact on the same electrode array (*N* contacts yield *N*-1 bipolar channels; Luck, 2014). This re-referencing method assumes that adjacent contacts record activity from the same brain region with the same impedance and noise levels. Thus, by subtracting activity that is common to two adjacent contacts, the preserved signal reflects only local activity related to the observed phenomenon (Bastos & Schoffelen, 2016; Li et al., 2018; however, see Zaveri et al., 2006). The bipolar referenced signal between two adjacent contacts is relabeled to show which contacts the bipolar signal originated from (e.g., the bipolar referenced signal obtained from contacts X1 and X2 is relabeled to X1-X2). All subsequent performed on the activity from these bipolar channels are henceforth called channels throughout this thesis. References made to single contacts on the electrode array are referred to as contacts.

The waveform of the ERPs can provide indications about the localization of the sources from where the signals originate (Buser, 1955; Halgren et al., 1995; Liégois-Chauvel et al., 1991). If there is a change in polarity between channels in the ERP waveform, this can imply that one contact is close to the source. Although using the bipolar referencing method is considered standard in the intracranial EEG field, its weakness is clear when attention to small details in the voltage differences between anatomical sites is crucial. This is because one might risk canceling out the local field potential if two neighboring contacts are recording from the same source, and the signal from this source is very strong. Thus, the ERPs were computed with the average referencing method by referencing the signal from each contact against the common average signal from all contacts on the electrode shaft (Luck, 2014). This was performed to functionally describe the implanted electrodes, the functional delineations between primary and non-primary auditory areas, and to localize the neural generator(s) of the evoked potentials.

Filtering. The data was low-pass filtered at 180 Hz using a Hann window and notch filtered at 50, 100, and 150 Hz to remove line noise. To avoid edge artifacts from the filtering, a buffer of 750 ms (corresponding to three cycles of 4 Hz; Cohen, 2014) was added to the data before it was re-epoched to 1-s epochs. All filters were applied in forward and backward directions (zero-phase). Abnormal trials in the time domain were removed from the epoched data if the amplitude was more than five standard deviations from the mean in time windows larger than 25 ms. Next, to remove trials with abnormal power-spectral density, a fast Fourier transformation with multitapers was carried out using a Hanning window for frequencies from 1 to 180 Hz in steps of 2 Hz. Trials that had power-spectral density larger than five standard deviations from the mean for over 6 Hz, were rejected from further analyses.

2.6 Data analysis

Data analysis and statistical testing were performed with custom-written scripts in Matlab (version 2022b), except the Bayesian *t* tests, which were performed in JASP (version 0.17.1).

2.6.1 High-frequency broadband activity

HFA was extracted from the preprocessed data. The data were band-pass filtered into seven frequency bands ranging from 75 to 145 Hz with 10 Hz frequency bandwidth around the center frequencies and Hanning window. Power was computed as the squared signal of the amplitude envelope of the analytical signal, using the Hilbert transformation (Hilbert, 1912). The power time-series were then baseline-corrected 200 ms pre-stimulus onset by using the absolute baseline method (Cohen, 2014). The power-time series were further normalized channel-wise relative to the baseline activity by dividing the activity in each frequency band by the standard deviation of all trials during the baseline period. After baseline correction, the HFA was computed as the average of the seven frequency bands. Finally, outliers within each tone-frequency condition defined as HFA trials with power (i.e., amplitudes) over three standard deviations from the mean within a time of 100 ms pre- to 500 ms post-stimulus onset that lasted over 50 ms, were excluded from the analysis.

Significance testing. Non-parametric cluster-based Monte Carlo permutation tests, implemented in the FieldTrip toolbox (Maris & Oostenveld, 2007), were used to test for significant differences in the magnitude of the ERP and HFA epochs (0 to 400 ms post-stimulus onset) between standard and deviant stimuli. The permutation tests were conducted

individually for each participant and performed channel-wise. The parameter configurations were similar for all hypotheses (5000 iterations, ERP: two-tailed independent *t* test, alpha = .025; HFA: one-tailed independent *t* test, alpha = .05). The decision to use permutation tests was based on the non-parametric nature of SEEG data and to control for multiple comparisons by using the mass inferred *t* statistic approach (Maris & Ostenveld, 2007). This permutation test identifies clusters in time and space based on the test statistic for the differences between the standard and deviant conditions for each channel. Differences between conditions that exceed the max test statistic threshold are then compared with clusters drawn from a population generated under the null hypothesis (i.e., no significant difference between the HFA elicited in standard or deviant condition; Maris & Ostenveld, 2007; Sassenhagen & Draschkow, 2019). Note that the independence in independent *t* tests refers to the comparison between observational units in each trial within one participant.

2.6.2 Response onset latency and peak latency of high-frequency activity

The response onset latencies and peak latencies of the HFAs were investigated to identify if there was a temporal distinction between anatomical sites' responsiveness to the different stimulus types. To investigate functional differentiation between primary and nonprimary cortical sites' temporal response profile, the response onsets during the tonotopic mapping task was estimated as the time after stimulus onset when the lower 99% bootstrapped (2000 permutations) confidence interval (CI) of the mean HFA was larger than zero for at least 30 ms within 200 ms after the onset of the stimulus. This criterion is based on a similar test on differences between the response latency properties in the auditory cortex in which more primary auditory areas demonstrated shorter response onsets than non-primary areas (Nourski, Steinschneider, McMurray et al., 2014). However, a more conservative criterion (99% versus 95% CI in Nourski, Steinschneider, McMurray et al., 2014) was administered to enhance spatially distributed differences. The same estimation procedure was applied to the data from the oddball task to investigate if the HFA latencies differed between expected and unexpected stimuli. The time window was extended to within 400 ms after stimulus onset to include mechanisms associated with later onset latencies such as the P300. Similarly, the peak latencies of the HFAs within the same time window were compared between standard and deviant stimuli to investigate if violations to contextual acoustic predictability influenced mechanisms associated with peak latency.

Bayesian *t* tests. Bayesian *t* tests were conducted to quantify group-level differences between primary and non-primary cortical areas in the subtracted differences in response onsets and peak latencies. Group-wise response onset latencies were calculated to deviant and standard tones for HFAs within 200 ms from stimulus onset and were tested for significance within each brain region of interest with two-tailed Bayesian one-sample *t* tests. The subtracted difference in latency between deviant and standard tones was calculated for each channel (deviant – standard) and pooled groupwise per brain area of interest. Because neural responsiveness could be moderated by stimulus predictability, the difference was calculated by subtracting the response onset latency for a standard tone from the response onset latency to the corresponding deviant tone for each channel separately. Using the subtracted difference from the same channel may thus control for spatial differences in responsiveness that are related to tonotopic response properties. A large positive difference thus indicates that the response onset was slower for the deviant compared to the standard tone.

Assumptions of normality were checked with Shapiro-Wilk's test before the Bayesian *t* tests. The Bayes factors were calculated using the default priors in JASP. The values of the Bayes factors are interpreted in favor of the alternative hypothesis (H_a) relative to the null hypothesis according to recommendations by Lee and Wagenmakers (2014; < 1: no evidence; 1 to 3: anecdotal evidence in support of the null hypothesis; 3 to 10: moderate evidence in support of H_a; 10 to 30: strong evidence for H_a; 30 to 100: very strong evidence for H_a; > 100: extremely strong evidence for H_a).

3 Results

The following section starts by describing how anatomical locations were determined based on the co-registered CT and MRI images, ERP waveforms, and HFA responses from the tonotopic mapping tasks. Then, the section presents the results from the analysis of the oddball task and the effects of violations to auditory regularity.

3.1 Determination of anatomical localization of implanted electrodes

None of the electrodes included in this study showed ictal or interictal epileptic activity. However, two electrode contacts (H2 and H12) from participant SUB3 were removed from the analyses because of a technical issue with the recording system in contact H2, and because H12 was implanted outside the cortex. Consequently, the bipolar referenced signal from electrode H1 in the same participant was removed from further analyses because the distance between H1 and H3 was larger than the other pairs, precluding comparison to the other channels. The electrode coordinates in MNI space are presented in Table X.1 in the Appendix.

3.1.1 Anatomical localization of electrodes based on neuroimaging

Visual inspection of the preselected electrode arrays on the fused MRI and CT scans revealed that contacts were situated in locations corresponding to the insula, Heschl's gyrus, superior temporal sulcus, STG, posterolateral fissure, supramarginal gyrus, and planum temporale. From here and continuing throughout this thesis, we refer to the regions covered by electrodes implanted in the posterolateral fissure and supramarginal gyrus (electrodes H in SUB2 and W in SUB3) as TPJ, while we use the term auditory cortex to refer to the areas covered by the remaining electrodes (electrodes U in SUB1, T in SUB2, and H in SUB3). Table 1 displays the anatomical position of each electrode contact based on automatic anatomical labels in Freesurfer and iElectrodes, and visual corroboration of using the Duvernoy's atlas. Figure 2 presents the merged MRI and CT images with electrodes implanted and illustrates that although the anatomical coordinates in Table 1 imply that the electrodes were implanted close to each other in anatomical coordinates, there was also individual differences in the volume and shape of Heschl's gyrus.

Figure 2. *Brain Morphometry and Electrode Implantation in Native Space and MNI Space*

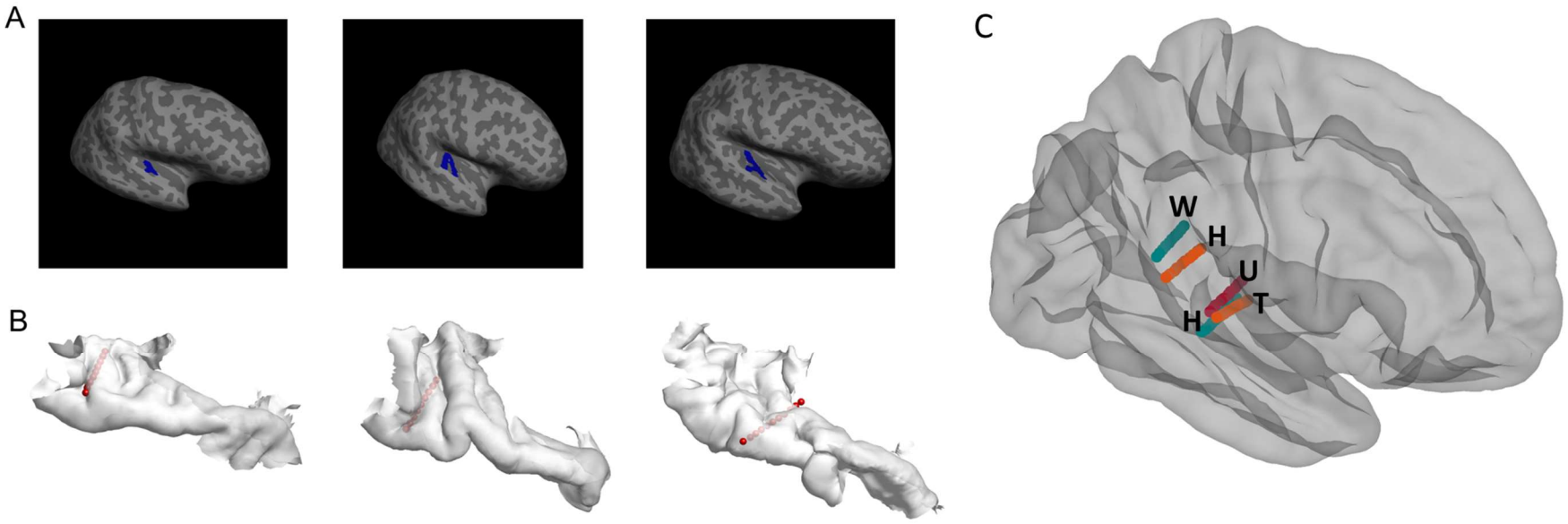

Note. **A:** Inflated brains for SUB1, SUB2, and SUB3, respectively. The blue area represents the primary auditory cortex and corresponds to the mesh figures in row B. **B:** Mesh figures of auditory cortex with implanted electrodes (in red) in horizontal view. **C**: Normalized brain (MNI space) with implanted electrodes color-coded for each participant: SUB1 (red; label U), SUB2 (orange; label H and T), and SUB3 (green; label W and H).

Table 1. *Anatomical Localization for Each Electrode Contact Number*

Patient	Electrode array	Electrode contact number and anatomical location (native space)										
		1	2	3	4	5	6	7	8	9	10	11
SUB1	U	Ins	Ins/HG	HG	HG	TTS	iPT	iPT	iPT	STG	STG	-
SUB2	T	Ins	Ins	HG	HG	WM	STS	iPT	iPT	STG	STG	-
	H	pLF	pLF	pLF	pLF	pLF	sPT	sPT	SMG	SMG	SMG	-
SUB3	H	**Ins**	**Ins/HG**	HG	HG	WM	STS	STS	STS	STG	STG	STG
	W	pLF	pLF	pLF	pLF	STG	SMG	SMG	STG	STG	STG	-

Note. Each cell indicates the anatomical region of each electrode contact. Electrodes implanted on the edge between two brain areas are indicated with "/". Labels in bold indicate electrode contacts that were removed from the analysis. Abbreviations: HG = Heschl's gyrus, Ins = Insula, iPT = inferior planum temporale, pLF = posterior lateral fissure, SMG = supramarginal gyrus, sPT = superior planum temporale, STG = superior temporal gyrus, STS = superior temporal sulcus, TTS = transverse temporal sulcus, WM = white matter.

3.1.2 Analysis of event-related potential waveforms during the tonotopic mapping task

Polarity inversions in the averaged evoked potentials between adjacent electrode contacts in the tonotopic mapping data, suggested that the sources of the recorded signals were located close to the electrode (see Fig. 3). This was observed on the innermost part of the electrode arrays implanted in the auditory cortex (i.e., Heschl's gyrus in Table 1). The changes in polarity in these channels were observed for most (~90%) of the presented acoustic stimuli. Figure 3 panels A and C also show a waveform complex in Heschl's gyrus comprising a small peak around 50 ms at circa 80 to 100 µV post-stimulus onset succeeded by a larger waveform of opposite polarity at 200 ms. Panel B in the same figure shows for the higher tone frequencies a small peak at circa 50 ms and 30 µV followed by large waveforms that peaked at approximately -100 µV within 200 ms after stimulus onset. Electrode H3 in participant SUB3 (Fig. 3C) demonstrated the largest recorded potentials, with approximately -250 µV within 100 ms from stimuli onset to tones between 800 and 1760 Hz. The waveforms obtained from the remaining electrode contacts had similar response profiles without a clear frequency specificity but a more general response to all tones, with amplitudes peaking around 100 µV between 100 and 200 ms post-stimulus. ERPs and HFAs from all channels are presented in the Appendix.

Figure 3. *Polarity Inversions in the ERPs from Electrodes in the Auditory Cortex*

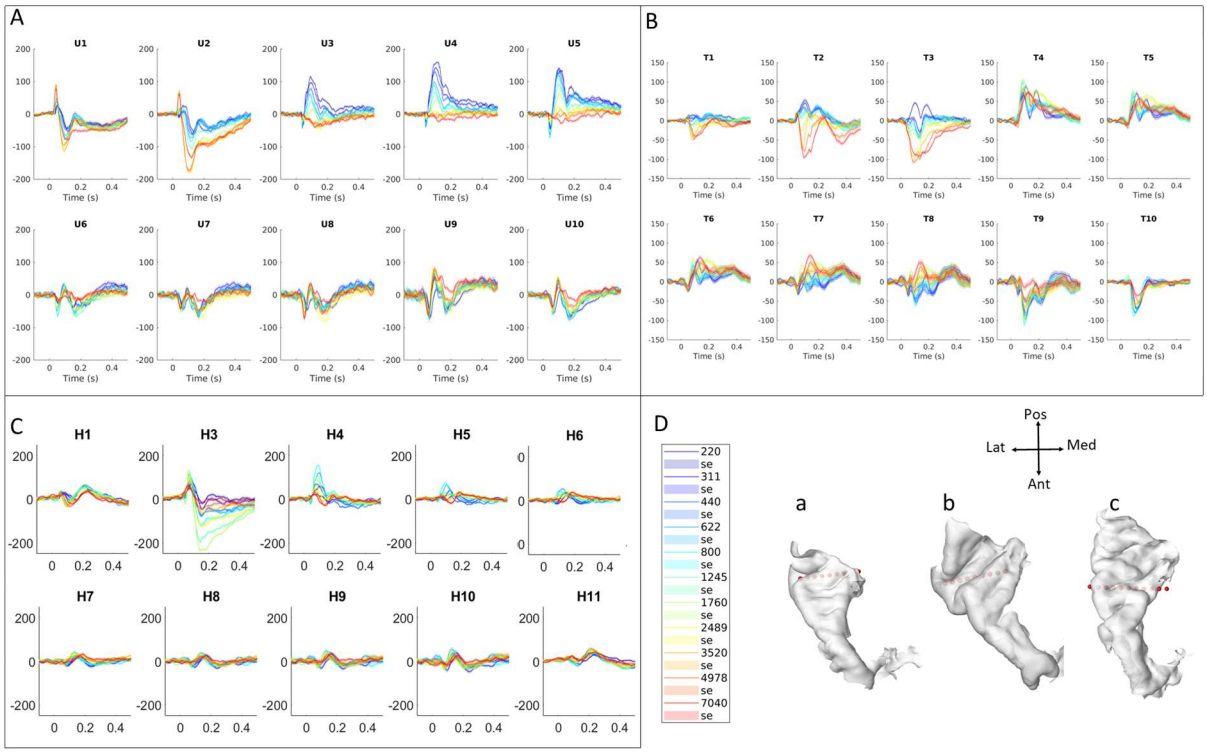

Note. The ERP plots show polarity inversions in the ERP from channels that correspond to Heschl's gyrus (A: SUB1; B: SUB2; C: SUB3). D: Color-coded lines for each stimuli tone with 95% standard error of the mean (se). Mesh figures of auditory cortex with implanted electrodes (in red) in for SUB1 (a), SUB2 (b) and SUB3 (c). Anatomical direction is indicated by the four-headed arrow indicating anatomical direction for the mesh figures (Ant = anterior, Pos = posterior, Med = medial, Lat = lateral). Note that for illustrative purposes, the y-axis (in μV) is scaled for each participant.

3.1.3 High-frequency activity during the tonotopic mapping task

On average, 12.7% of the trials in each condition in the tonotopic mapping was removed from the HFA data in each participant during the pre-processing. The frequency tuning response patterns varied between the participants. Figure 4 shows that some channels responded strongly to multiple tone-stimuli while other channels responded more selectively, and some stimuli evoked strong responses in multiple channels. Strong responses elicited to the medium to high tone-frequencies were observed in Heschl's gyrus (SUB3) and the more lateral electrodes in the superior temporal plane (SUB3; Fig. 4A) as well as the innermost

medial electrodes in the TPJ (Fig. 4C), corresponding to the posterior lateral fissure. Visual inspection of the corresponding latency maps in Figure 4 indicated shorter response onset latencies for the more medially oriented channels.

Figure 4. *Tonotopic Maps and Latency Maps from the Auditory Cortex and the TPJ*

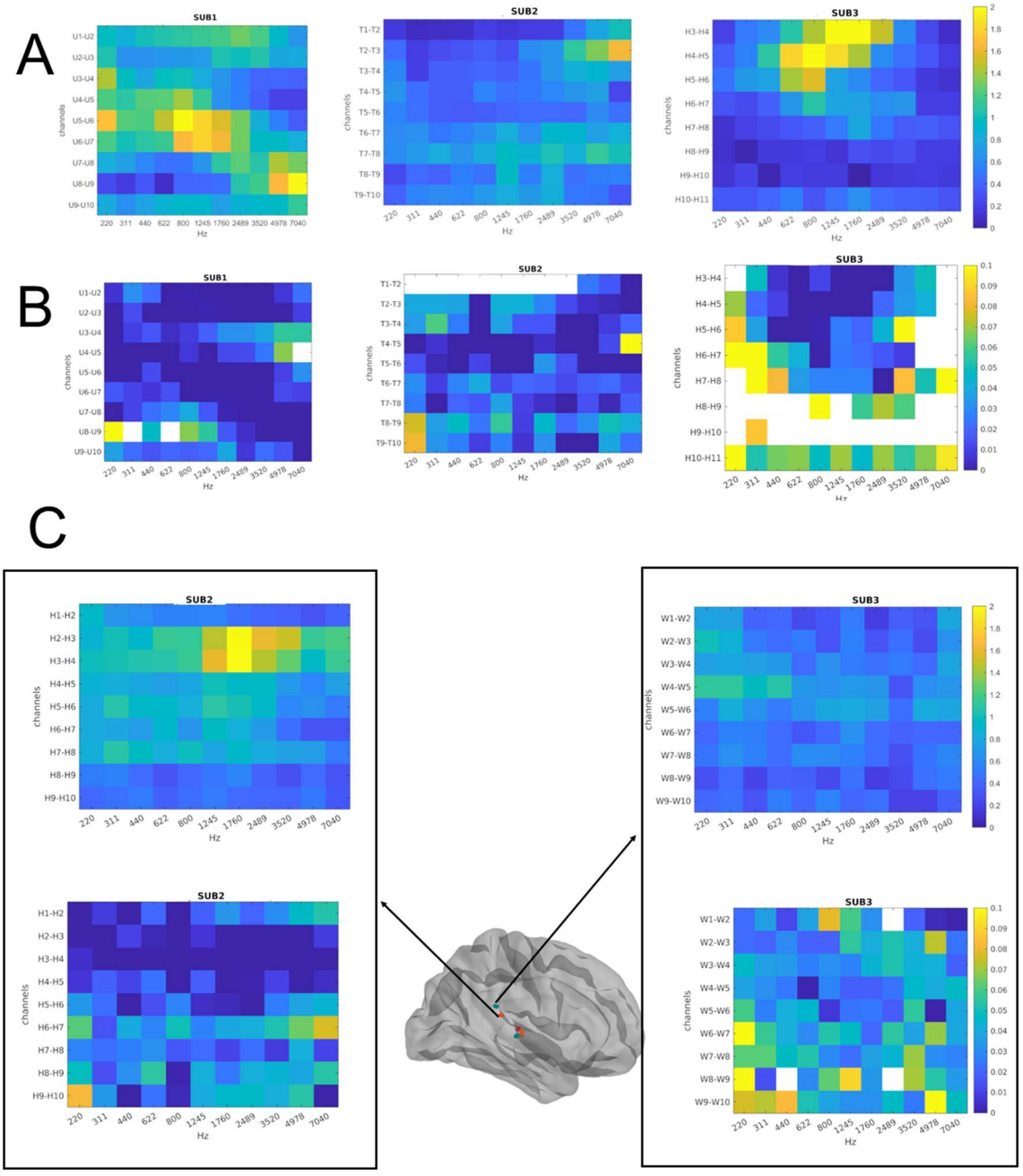

Note. Two-dimensional tonotopic (**A**) and latency maps (**B**) from recordings in the auditory cortex. **C**: Tonotopic maps (upper row) and latency maps (lower row) from recordings in the

TPJ (the arrows indicate the spatial location within the TPJ for all the maps). Each cell in the tonotopic maps shows for each tone the mean HFA magnitudes obtained from the full-width half-maximum period of the average HFA time courses across all trials. Each cell in the latency maps shows for each tone the average response onset latency for the HFA across all trials. Channels are presented row-wise, and each stimuli frequency (in Hz) is presented column-wise. The color-coding in the tonotopic maps is constrained to be within a range of 0 to 2 in all maps due to individual variations in power relative to baseline. For the same reason, the color-coding in the latency maps is constrained to be within 0 to 100 ms in all latency maps. White cells indicate that the channel did not respond to the tone according to the inclusion criteria (see Section 2.6.2 in Methods).

Figure 4 also illustrates spatial differences in neural responsiveness in the HFA range during the tonotopic mapping task. Participant SUB1 appeared to reflect stronger HFA responses to lower and middle tone-frequencies medially and to higher tone-frequencies across a medial-lateral axis. This gradient, however, was not observed in the other participants, in which the HFA rather reflected a general preference (i.e., higher amplitude) to sound frequencies above 1245 Hz relative to lower sound frequencies. Channels implanted in Heschl's gyrus in SUB3 (H3 and H4) displayed strongest preference (i.e., largest magnitude) to tone frequency 1245 Hz. The medial channels W4 and W5 implanted in the TPJ in SUB3 showed responses to 311 Hz and 7040 Hz, respectively. In contrast, the strongest tonotopic responses in SUB2 were recorded from the medial aspects of the posterolateral fissure to tones around 1245 Hz, and from channels implanted in Heschl's gyrus to the higher tone frequencies between 3520 to 7040 Hz.

Because of unspecific tonotopic responses for most participants (SUB2 and SUB3) in the tonotopic mapping task, the following investigation of deviance detection was focused on primary and non-primary cortices based on the labels derived from anatomical imaging. Stronger average responses were overall observed to tone frequencies equal to or larger than 1245 Hz. Figure 5 presents HFA responses across channels for each participant to tone frequencies that were used as stimuli in the oddball task (tone A = 311 Hz; tone B = 3520 Hz: SUB1 and SUB2, or 1245 Hz: SUB3).

Figure 5. *HFA Responses to Selected stimuli Tones During Tonotopic Mapping Task*

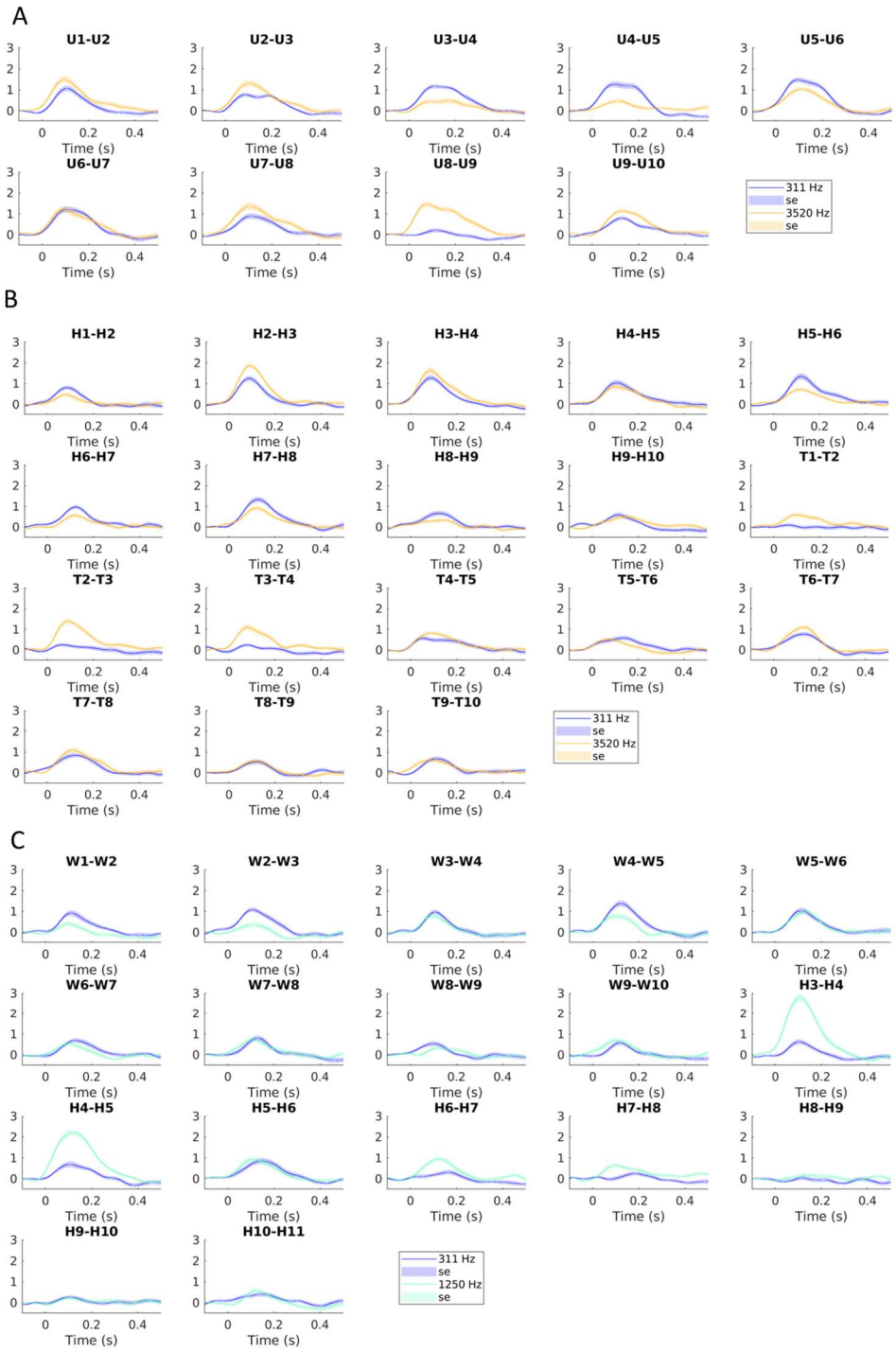

Note. HFA responses to selected acoustic stimuli during the tonotopic mapping task from channels implanted in the auditory cortex and the TPJ. The plots are presented channel-wise for each participant (Panel A: SUB1; Panel B: SUB2; Panel C: SUB3) with 95 % standard

error (se) of the mean HFA response. The y-axis represents the magnitude of the power for the HFA responses and the x-axis the time scale where zero indicates stimulus-onset.

3.2 Effects of violations to auditory regularities on neural activity

3.2.1 Localization of polarity inversions to deviant tones in the event-related potentials

Figure 6 shows the intracerebral ERPs from channels located in the TPJ and the auditory cortex from one participant (SUB2). The permutation test yielded statistically different responses to Repetition Deviants relative to standard condition in channels in the TPJ (SUB2: channels H2 to H9; SUB3: channels W1, W2, W5 to W9) with peak latency between 120 to 150 ms after the onset of the deviant tone. There was no clear evidence of polarity inversion to only deviants. All ERP plots are presented in the Appendix.

Figure 6. Spatial Disparity in Event-Related Potentials to Repetition Deviants

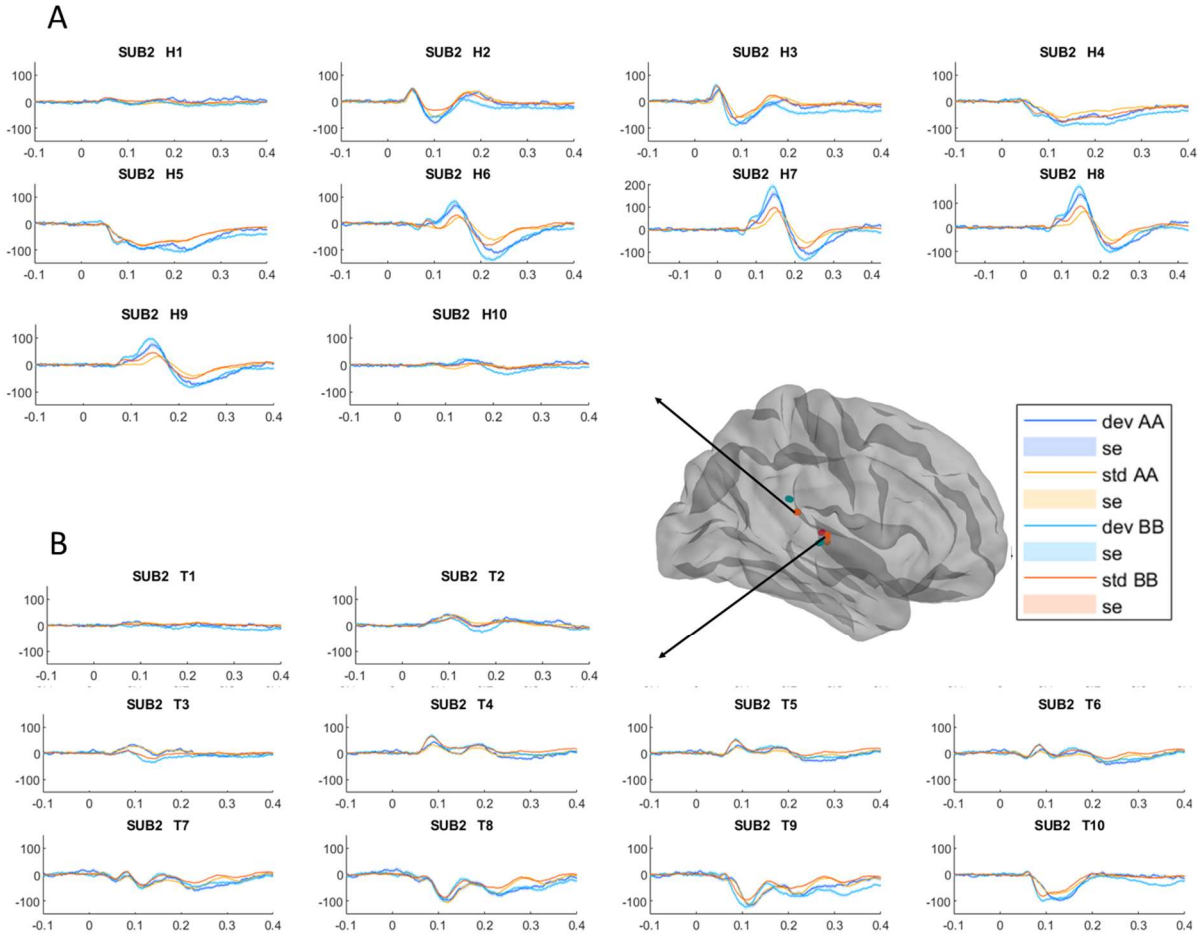

Note: ERP responses along contacts of depth electrode arrays. The average-referenced ERPs denote different patterns (from SUB2). Deviant tones (dev; in blue) elicit larger intracerebral voltages in the TPJ (Panel A) in electrode contacts H2 to H10, and in the auditory cortex (Panel B) in electrode contacts T1, T2, T4, T5, and in T9 and T10, compared to standard tones (std; in yellow and red). See also Figures X.2.3 and X.2.3.4 in the Appendix for the time samples at which the permutation test yielded significant differences in the ERPs between conditions. Note that there seems to be a polarity inversion between electrode contacts H5 and H6 starting approximately 80 ms after stimulus onset. Standard errors of the mean (se) are based on the 95% bootstrapped CI of the mean (2000 permutations). The y-axis represents intracerebral voltage in μV. The x-axis represents time scale in seconds where zero indicates stimulus-onset. Panel **A**: Electrode H = TPJ. **B:** Electrode T = Auditory cortex.

3.2.2 Violations to auditory regularity increase high-frequency activity

During the pre-processing of the HFA data from the oddball task, an average of 16% of the trials in each condition was removed. Figure 7 illustrates modulations in the induced power spectra (i.e., ERPs subtracted) by auditory Repetition Deviants. These modulations were more prominent in channels in the STG and the TPJ compared to channels in Heschl's gyrus. The overall strong increase in post-stimulus high-frequency broadband power relative to baseline demonstrates the validity of the upcoming HFA analyses. The permutation test revealed widespread significant enhancements in the HFA magnitudes to Repetition Deviants (i.e., deviant AA and BB in the alternation blocks) compared to the standard condition (i.e., standard AA and BB in the repetition blocks) in all subjects. There was no significant increase in HFA by Alternation Deviants (i.e., deviant AB and BA in the repetition blocks) compared to standard conditions (i.e., standard AB and BA in the repetition blocks) in any of the participants. Thus, the following results are presented with respect to Repetition Deviants only. Plots showing the HFA and ERPs for the Alternation Deviants in the repetition block are presented in the Appendix. Plots of HFA from all channels and participants are presented in the Appendix.

Figure 7. *Induced Power Spectra to Deviant and Standard Tones Across the Auditory Cortex*

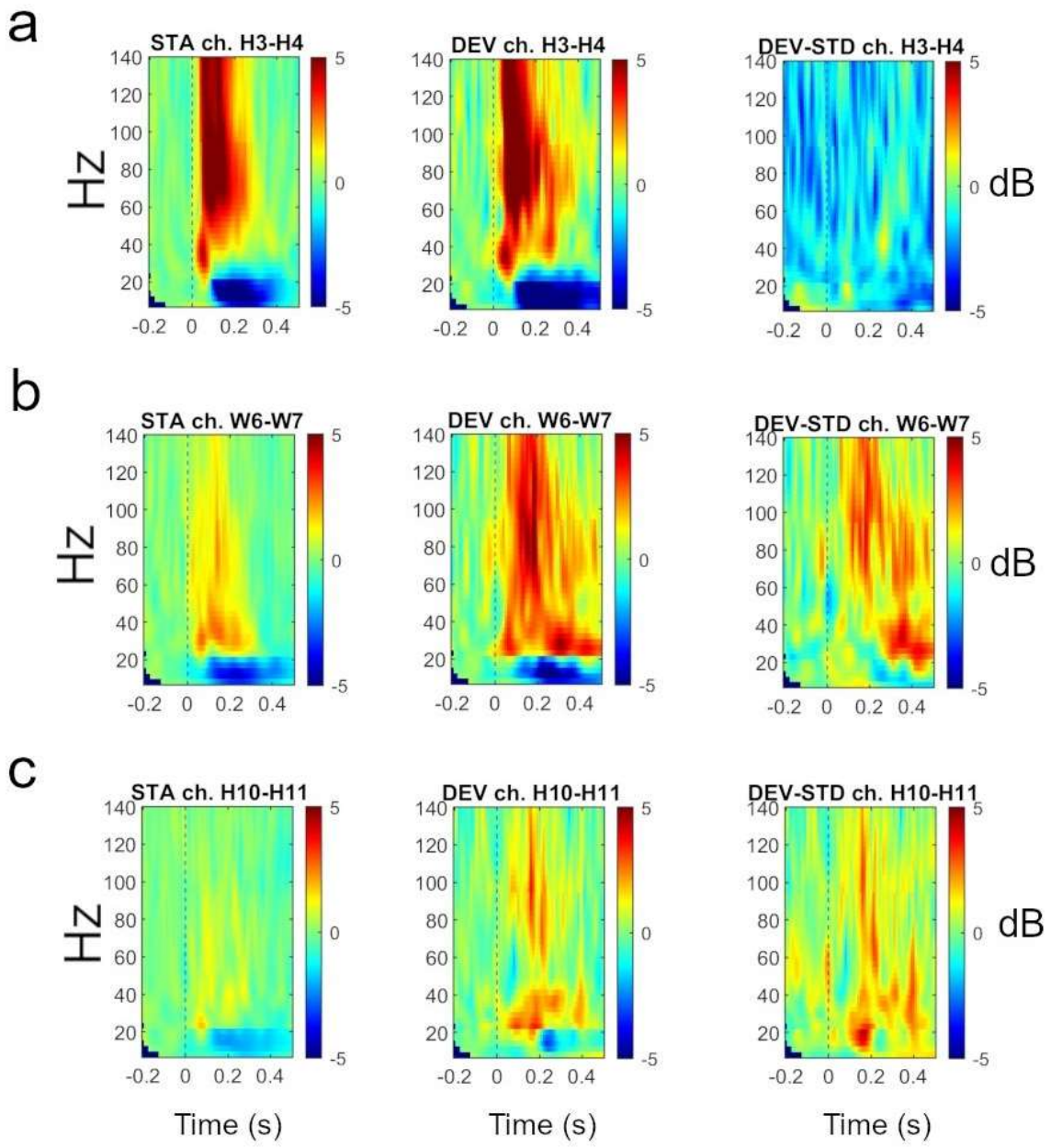

Note. Exemplary channels showing induced power spectra responses in SUB3. The power spectra show the relative change in decibel (dB) to baseline for deviant and standard tones and the subtracted difference between these (Deviant - Standard). Only responses to one tone (1245 Hz) are shown. Rows for each channel and columns for each tone. **Row a** = H3-H4 (Heschl's gyrus), **row b** = W6-W7 (supramarginal gyrus), and **row c** = H10-H11 (STG). Abbreviations: STA/STD = standard condition, DEV = deviant condition.

Figure 8 illustrates exemplary results of significantly increased HFA to deviant tones being more prominent in some cortical areas than others. This HFA appeared within 200 ms after stimulus-onset and were widespread across channels in the lateral aspects of the TPJ, and spatially restricted in the auditory cortex to channels implanted in the superior temporal sulcus and gyrus. In addition, visual inspection suggested that the significantly enhanced HFA magnitudes occurred earlier in the lateral aspects of the TPJ compared to other cortical areas. A later increase in HFA could also be observed in responses to Repetition Deviants in channels in the TPJ, which occurred approximately 250 to 400 ms after stimulus-onset.

Figure 8. *HFA to Repetition Deviants Compared to Standards*

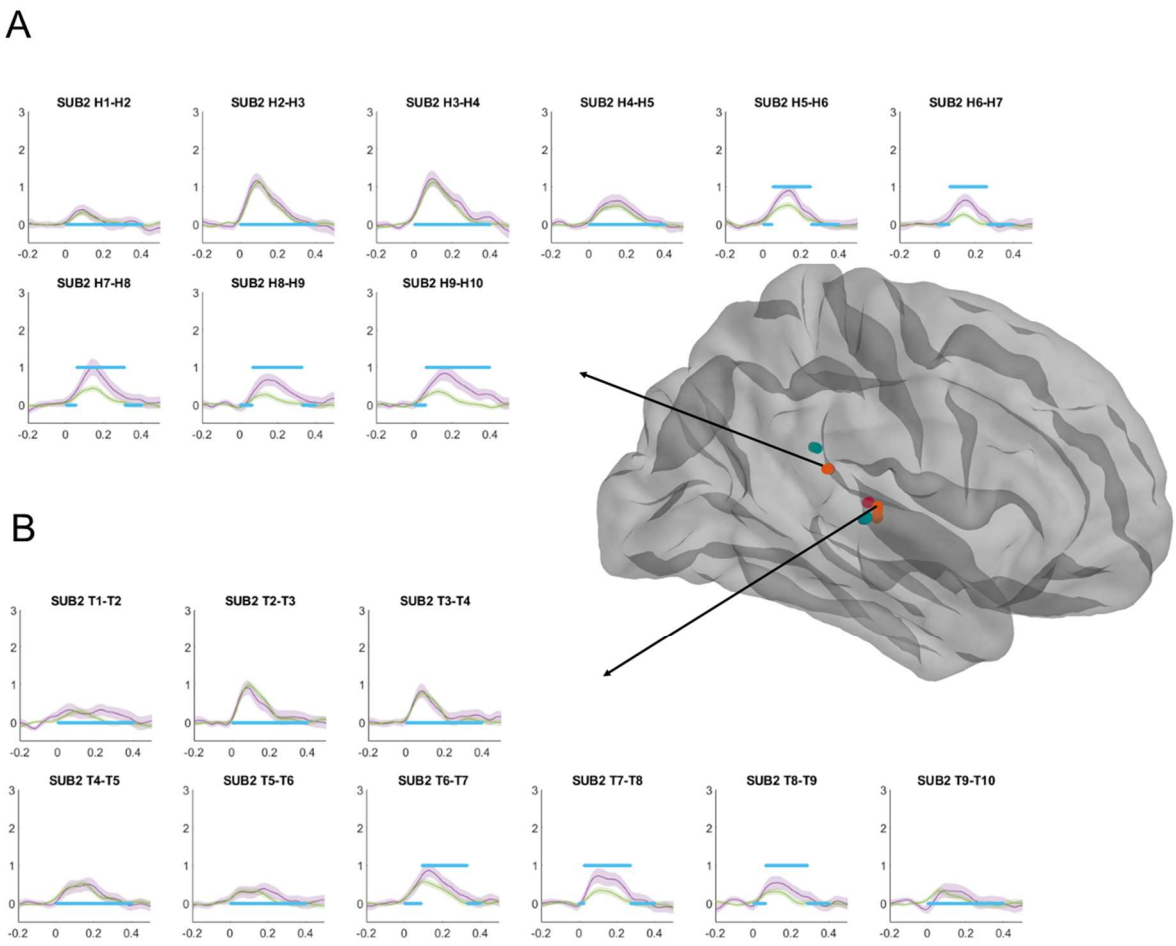

Note. Significant enhancement in HFA from one participant (SUB2) elicited by Repetition Deviants (only tone BB is shown) presented channel-wise. Channels labelled with the prefix "H" are implanted in the TPJ (Panel A), while channels labelled with "T" are implanted in the auditory cortex (Panel B). The blue bar illustrates the time samples at which the permutation

tests yielded clusters in which Repetition Deviants responses were significantly stronger compared to the control condition. The y-axis represents the magnitude of the HFA while the x-axis represents the time in seconds where zero indicates stimulus onset. The arrows depict which electrode (orange) the activity is recorded from.

Post hoc testing. To quantify if there was group-level support for spatially increased activity to a deviant tone, versus a null hypothesis of no change, the difference between HFA calculated as full-width half-maximum to deviant and standard tones from all channels in Heschl's gyrus, posterolateral fissure, supramarginal gyrus, planum temporale and the STG were pooled based on their anatomical labelling presented in Table 1 and tested with post hoc Bayesian *t* tests. The superior temporal sulcus was excluded from this post hoc test and the latency analyses, because only three channels were implanted in these areas. Before running this post hoc test, the data was evaluated group-wise per region of interest for normality with Shapiro-Wilk test, which yielded non-significant results. Thus, the post hoc testing proceeded with Student's *t* test. Table 2 shows the results from this post hoc testing, in which the Bayes factors indicated evidence in support of increase in HFA by Repetition Deviants in all regions except for Heschl's gyrus. This post hoc test supported an effect of deviance in the TPJ, with extremely strong evidence in support of an effect of Repetition Deviants on HFA in the supramarginal gyrus (Lee & Wagenmakers, 2014).

Table 2.
Differences in HFA to Deviant and Standard Tones Between Anatomical Regions

ROI	Mean	Median	*SD*	BF	*n*
HG	.05	.035	.083	1.39	12
pLF	.146	.106	.141	42.478	16
infPT	.132	.154	.15	3.376	10
supPT	.359	.3	.195	9.72	6
STG	.134	.065	.158	4.644	12
SMG	.328	.357	.1	68697.282	12

Note. Group-level descriptive statistics for difference in HFA based on full-width half-maximum. The Bayes factors are derived from two-tailed Bayesian Students *t* test in favor of the alternative hypothesis (i.e., that the difference in HFA is not equal zero) relative to the null hypothesis. Abbreviations: BF = Bayes factors, HG = Heschl's gyrus, lateral PT = inferior planum temporale, *n* = number of channels, pLF = posterolateral fissure, ROI =

region of interest, *SD* = standard deviation, SMG = superior marginal gyrus, STG = superior temporal gyrus, supPT = superior planum temporale.

3.2.3 Spatial discrepancy in the temporal effects of deviance on high-frequency activity

Comparisons between the latency to respond in the HFA in the oddball tasks and the tonotopic mapping task, revealed overall shorter latencies in the oddball tasks relative to the tonotopic mapping. Although the overall difference in onset latency was more delayed to tone AA (median = 14 ms, *SD* = 38, *n* = 31) than tone BB (median = 2 ms, *SD* = 29, *n* = 31), the differences in temporal response properties of the HFA between the two tones were not significant (response onset: $p = .191$, $n = 62$; peak latency: $p = .297$, $n = 68$), and the Shapiro-Wilk test for normality was non-significant. Thus, differences in latencies to both tones AA and BB were pooled and tested groupwise per region of interest. Table 3 shows spatial differences in the effect of deviance on response delays and peak delays. The Bayes factors indicated more evidence in support of a delaying effect by Repetition Deviants on channels located in the posterolateral fissure, while there was more evidence supporting the null hypothesis (i.e., no effect of deviance on the onset of HFA response) in the remaining regions. Table 3 also displays descriptive data and Bayes factors suggesting no evidence in support of an effect of Repetition Deviants on peak latency for the grouped HFA.

Table 3. *Regional Differences in Latency (s) in HFA to Deviant and Standard Tones*

ROI	Mean	Median	*SD*	BF	*n*
Response onset latency					
HG	.0	.07	.01	1.819	12
pLF	.008	.006	.013	6.003	16
infPT	.002	.008	.011	.978	10
supPT	.023	.017	.028	1.246	6
STG	.022	.014	.024	1.845	7
SMG	-0.003	.002	.044	.303	11
Peak latency					
HG	.0	.0	.016	.288	12
pLF	.02	.001	.044	1.146	16
infPT	.013	.01	.02	1.393	10
supPT	.032	.027	.031	2	6
STG	-.051	.004	.144	.537	12
SMG	.024	.025	.033	2.817	12

Note. Group-level descriptive statistics for difference in HFA response onset latencies and peak latencies in seconds. The Bayes factors are derived from two-tailed Bayesian Student's *t* test assessing the alternative hypothesis that the difference in latency between deviant and standard tones is not equal zero. Abbreviations: BF = Bayes factors, HG = Heschl's gyrus, infPT = inferior planum temporale, *n* = number of channels, pLF = posterolateral fissure, ROI = region of interest, *SD* = standard deviation, SMG = superior marginal gyrus, STG = superior temporal gyrus, supPT = superior planum temporale.

4 Discussion

Our overarching goals were to investigate the neural signatures of automatic deviance detection and their anatomical locations in the human PAC and non-PAC. First, we aimed at establishing at tonotopic base-map based to functionally delineate PAC and non-PAC in the right hemisphere. Then, we aimed at investigating effects of violations to auditory regularity within auditory-processing areas in the PAC and non-PAC with a passive oddball paradigm. The results revealed inter-individual variation in the distribution of tonotopy, and differences in neural activity between PAC and non-PAC to the effects of auditory irregularity. Violations to predictable sequences of acoustic stimuli generated deviance detection-like activity in higher-order cortical areas, such as the STG and the supramarginal gyrus. Except for channels in the right posterolateral fissure, auditory irregularity did not affect the temporal properties of the HFA responses.

The next section starts by discussing the results on the organization of frequency gradients from the tonotopic mapping task. Then, we discuss the neural signatures of automatic auditory deviance detection recorded from the auditory cortex and the TPJ, from a hierarchical predictive processing perspective. Finally, this chapter addresses the limitations of the current study and provides suggestions for future research.

4.1 Inter-individual variability in distributed tonotopy

The implantation of the electrodes used in this experiment went across Heschl's gyrus as well as lateral aspects of the auditory cortex and surrounding areas. The combination of overall

responsiveness to auditory stimuli and shorter response onset latencies implies that electrode contacts number two to five in the auditory cortex were within, or nearby, Heschl's gyrus in all participants, which is in line with the anatomical demarcation of the electrode contacts. In agreement with previous findings on tonotopy in the human auditory cortex (e.g., Besle et al., 2019; Moerel et al., 2014; Saenz & Langers, 2014), an area of Heschl's gyrus demonstrated preference for lower frequencies while non-primary auditory cortices preferred higher tone frequencies. However, there was no clear sign of a common tonotopic gradient or map across the participants. This may reflect inter-individual variability in location, orientation, morphology, volumetry, myelination, response patterns, and functional organization of the auditory cortex, as previously reported (e.g., Abdul-Kareem & Sluming, 2008; Rademacker et al., 1993, 2001). It is possible that this variation is related to the interaction of inter-individual differences in the functional anatomy and the relative positioning of the electrodes. Despite differences in tonotopy between participants, there were consistent within-electrode responses to specific sound frequencies across sessions in the individual participants. Thus, it is possible that the broad and detailed tonotopic maps and frequency gradients reported in the neuroimaging literature, reflect the effect of pooling multiple subjects and their individual tonotopic maps.

Another possibility is that the between-participant variability in frequency gradients reflects a high anatomical specificity for tonotopy, as indicated by previous iEEG studies (Nourski, Steinschneider, Oya et al., 2014). In our study, the normalized coordinates for each electrode indicate that the relative positioning of the electrodes between participants differed by various mm in both the x-, y- and z-plane. In addition, the approximate 1 mm error range in the co-registered CT and MRI images impacts the manual and semi-automatic localization of the electrodes. Thus, because the electrodes were not implanted in the same position across subjects, the response patterns to the various sound frequencies might differ between participants. Individual differences between participants in their HFA and ERP responses during the tonotopic mapping task can hence also be attributed to the electrodes being implanted in different cortical layers (Howard et al., 2000).

One challenge with fMRI is that the statistical contrasts used to compare conditions do not allow defining specific frequency selectivity, but preference (i.e., higher frequencies > lower frequencies). Here, the intracranial results show that all three participants had the strongest stimulus-evoked responses near the third electrode contact on the electrode arrays

implanted in the auditory cortex (i.e., in Heschl's gyrus). The overall shorter response onset latencies and strong HFA, in addition to polarity inversions to the acoustic stimuli, support that this area corresponds to the human PAC. Yet, it is difficult to determine if the recorded responses reflect a consistent tonotopic organization or not, because most channels demonstrated unspecific frequency preference to more than one tone. It is possible that this ambiguity is influenced by physiological properties, such as differences in neuronal tuning width, adaptation effects, or that the electrodes recorded additional frequency-specific responses from nearby neurons. Also, since it is viable that some channels recorded activity from non-PAC, the responses might have some spatial dispersion. Such irregular stimulus-driven distributed response patterns are, however, consistent with frequency preferences extending to non-PAC such as the STG, as reported in neuroimaging studies (De Martino et al., 2015; Dick et al., 2017; Saenz & Langers, 2014).

Tonotopic responses from non-auditory cortices. The recorded signals from channels implanted in non-auditory cortical sites in the medial aspects of the TPJ raise further questions about the tonotopic organization of the human auditory cortex. Although the HFA and ERPs were not as strong as the signals recorded from the PAC, they indicated sensory auditory processing and frequency preference. Specifically, the very strong HFA response to 1245 Hz recorded from channels in the posterior lateral fissure (in SUB2) had similar response onset latency as responses recorded from channels in PAC/Heschl's gyrus, although they were spatially separated by 5.5 centimeters. Hence, the short response onset latencies suggest that this area is more "primary" than previously assumed. Moreover, the finding contrasts with the assumption that the lateral fissure corresponds to the parabelt in non-human primates (Kass et al., 1999; Kaas & Hackett, 2000), and raises further questions about the functional organization of the human auditory system. This area of the TPJ might correspond to the parakoniocortex, a subregion of the auditory cortex in macaques that may extend to the posterior superior temporal sulcus and the supramarginal sulcus (Galaburda & Sanides, 1980; Sweet et al., 2005). On the other hand, this finding was limited to one patient, and because we cannot exclude whether rare responses like these result from epilepsy and reorganization of the cortex, this finding and its interpretation should be treated with caution. Yet, previous findings from studies on tonotopy in humans have also indicated that auditory stimuli can elicit selective activation in non-primary cortices that may extend to the lateral part of the STG, and deeper regions dorsomedial to Heschl's gyrus and medial to the supramarginal gyrus (Humphries et al., 2010).

It is possible that methodological restrictions with neuroimaging from prior findings can explain why tonotopy in the posterolateral fissure has, to the best of our knowledge, not been reported before. For example, volume conductance, levels of cortical folding and convolutions, and the orientation of neuronal populations limit the spatial resolution in EEG and MEG, while low temporal resolution and artifactual effects from different filters and preprocessing pipelines limit fMRI (Lindquist et al., 2019). In addition, tonotopic responses reported from neuroimaging findings cannot, in contrast to iEEG findings, clearly differentiate between response properties in posterolateral superior temporal cortices across time (Nourski, Steinschneider, Oya et al., 2014). Therefore, substantial information about the anatomical distribution of response properties and frequency tuning might stay undetected when interpreting fMRI data.

The discrepancy between the observed tonotopy in non-primary areas here and the results from others (e.g., Howard et al., 1996; Nourski, Steinschneider, Oya et al., 2014) might be related to the positioning of the implanted electrodes. It is possible that the electrodes in the current study were positioned relative to tonotopic gradients that extended along an anterior-posterior axis or a medial-lateral axis of Heschl's gyrus. In addition, the broad frequency range used here may have evoked activity in the secondary cortices to a greater degree than tones with less spectral distance. For example, Humphries et al. (2010) found responses in secondary areas when using frequencies up to 6400 Hz and the highest tone tested in the current study was 7040 Hz. Moreover, the presentation rate in the current study was less than 2 Hz, which is slower than what were used in studies such as those by Woods et al. (2009) and Humphries et al. (2010), which used 4 and 10 Hz, respectively. Hence, different stimulus presentation rates evoke distinct activations of PAC and non-PAC.

As a partial conclusion before we discuss the results from the oddball task, the limited electrode coverage of Heschl's gyrus in this study, combined with large inter-individual variability in tonotopy, renders it difficult to disentangle ambiguity in inter- and intra-area frequency preference.

4.2 Violations to acoustic regularity during a passive oddball task

4.2.1 Automatic deviance detection in primary versus non-primary auditory cortex

As hypothesized in Hypothesis 2, and consistent with previous iEEG results (Blenkmann et al., 2019; Edwards et al., 2005; El Karoui et al., 2015; Halgren et al., 1995; Ishishita et al., 2019, auditory deviants evoked increased HFA when compared to a control (i.e., a standard) condition. The loci of these significant increases did, however, vary with anatomical regions. In part, the results from our study are in line with previous human iEEG studies reporting auditory deviance detection reflected as increased neural activity in the HFA range being prominent in the lateral aspects of the STG and superior part of the Sylvian fissure (e.g., Edwards et al., 2005; Ishishita et al., 2019). Bayes factors are continuous with values between zero and infinity (Lee & Wagenmakers, 2014), thus the group-level Bayes factors indicated only anecdotal to no evidence of an effect of auditory deviance in HFA in Heschl's gyrus being more probable (Lee & Wagenmakers, 2014). In contrast, the Bayes factors indicated moderate to extreme effects of Repetition Deviants on HFA in non-PAC regions (Lee & Wagenmakers, 2014). The lack of deviance detection-like activity in Heschl's gyrus, however, contrasts with prior findings on the MMN generator using MEG (Näätänen et al., 2007), and our Hypothesis 2 about increased power in HFA in the PAC, which was informed by the principles of hierarchical predictive processing (Clark, 2013; Friston, 2005, 2010; Rao & Ballard, 1999) and previous rodent studies (Parras et al., 2017). This spatial disparity in responsiveness to deviant stimuli proposes a functional differentiation between primary and non-primary regions related to auditory regularity encoding. Specifically, only electrodes implanted in the most lateral part of the auditory cortex (i.e., the STG) captured automatic auditory deviance detection within the auditory cortex. Because this finding was replicated in all participants, it implies that the results were not caused by chance.

Although previous iEEG findings from the temporal lobe and the Sylvian fissure (Edwards et al., 2005; El Karoui et al., 2015; Ishishita et al., 2019) agree with the anatomical loci of increased HFA elicited by deviants in our study, there are some methodological differences. For example, the results in earlier studies were derived from the classic oddball paradigm (Edwards et al., 2005) or an active listening task (El Karoui et al., 2015; Ishishita et al., 2019), while the current study was a passive listening task where deviants violated higher-order regularity rules, and, by design, were less sensitive to stimulus-specific adaptation. Notably, Edwards et al. (2005) tested significance relative to baseline, while the present study compared standard and deviant conditions. The pre-stimulus baseline period in Edwards et al. (2005) may hence have involved increased beta power, as reported elsewhere (e.g., Fujioka et al., 2009; Morillon & Baillett, 2017; Todorovic et al., 2011). In addition, El Karoui et al.

(2015) used an active oddball discrimination task that required participants to pay attention and push a button to deviant stimuli. Their task may thus have evoked processes more related to the P3b component, while we used a passive oddball paradigm that likely involves processes more related to the P3a and involuntary reorientation of attention (Fonken et al., 2020). Therefore, our results expand upon previous findings by suggesting that the lateral aspects of the STG are involved in auditory deviance detection when the deviants represent a violation to a higher-order statistical regularity, irrespective of whether attention is directed towards the task.

Deviance detection in the temporoparietal junction. If we compare the HFA to the tonotopy stimuli corresponding to tones A and B in the oddball task (see Fig. 5), there was no clear frequency preference nor frequency selectivity in the supramarginal gyrus, implying that this area corresponds to non-PAC. As predicted in Hypothesis 3, auditory deviants elicited significant increase in HFA in the TPJ, which suggests that the supramarginal gyrus plays a dedicated role in automatic auditory deviance detection. The very strong Bayes factors derived from group-wise differences in HFA to deviant versus standard tones provide additional support to this interpretation, as the supramarginal gyrus yielded Bayes factors with magnitudes more than a thousand times stronger than other brain regions. This finding could be consistent with the proposed alerting role of the TPJ during processing of stimulus-driven deviance, as part of a ventral attention network (Corbetta et al., 2008), and the context update model (Polich, 2007). However, the peak latency of the significantly enhanced HFA in the TPJ was within the range of the MMN, thus making the significant HFA observed here less likely to reflect the P300 from scalp-EEG. Notably, a smaller peak succeeding the significantly increased HFA at circa 250 to 400 ms after onset of a deviant stimulus could, however, be observed in the TPJ, which might be related to the P300. Therefore, it is possible that these two peaks are related to neural processes involved in a prediction error, followed by an update of a prediction-generating contextual model.

When considering the myeloarchitectonic organization of the PAC and its projections to both subcortical areas and non-PAC (Jasmin et al., 2019; Scott et al., 2017), one may speculate if the activity observed in the TPJ subserves adaptive changes in the auditory processing at subcortical stages based on predictive feedback. An alternative interpretation is that the supramarginal gyrus and the TPJ are sensitive to prolonged stimulus repetition by standard stimuli, causing an attenuation of the HFA amplitudes to standards (Eckert et al.,

2022). Since the permutation test did not reveal any significant increase in the HFA to Alternation Deviants, it is possible that other mechanisms underlay the present results, such as differences in regional sensitivity to stimulus repetition. From this perspective, HFA in Heschl's gyrus or PAC appears to be more robust, while HFA in non-PAC is more sensitive to auditory stimuli repetition. Our results thus suggest both sensitivity to auditory regularity and stimulus repetition as possible organizing principles in non-PAC.

Importantly, we must address one significant cluster from the permutation test for the arguments above about deviance detection in PAC versus non-PAC to be valid. The permutations testing yielded one significant cluster in channel U2-U3 in SUB1 (see Fig. X.3.2 in the Appendix), suggesting evidence for deviance detection proximal to Heschl's gyrus. In contrast to the significant clusters in the STG and the TPJ, only one deviant tone frequency (3520 Hz) elicited a significant increase in HFA. Based on its anatomical position, it is possible that the activity recorded from this channel corresponds more to insular activity, which is lately ascribed a role in deviance detection (Blenkmann et al., 2019, however, see Nourski et al., 2021 for a recent update on the functional separation between anterior and posterior insula). Alternatively, Figure 5A illustrates that this channel showed frequency preference for 3520 Hz relative to 311 Hz. It is thus possible that the increased HFA recorded by this channel reflected tonotopic responses from nearby neurons in Heschl's gyrus.

4.2.2 Spatial disparity in the temporal effects of auditory deviants on neuronal responses

The results support a possible temporal effect by auditory deviants being present in the response onsets of HFA in the posterolateral fissure. HFA responses to deviant tones in this area were on average only 8 ms delayed compared to standard tones and yet, the magnitude of the Bayes factor indicated moderate evidence supporting an effect of deviance (Lee & Wagenmakers, 2014). For the remaining areas, there was more evidence in support of null effects from deviants on the temporal properties of HFA. The tonotopy and latency maps in Figure 4C suggest that the posterolateral fissure is a more primary auditory region compared to other areas in the TPJ region. It is thus tempting to speculate what role the posterolateral fissure and its projections fulfill in an auditory predictive processing hierarchy, and if the delay in HFA onset is related to processing of deviants or propagation of prediction errors. Since there was no evidence in support of a temporal delay in the HFA by auditory deviance from the other areas, including those showing deviance detection, it is also possible that the posterolateral fissure is involved in later processes or functions not covered here.

4.2.3 The loci of the neural generators

Polarity inversions in the ERPs from adjacent electrode contacts can indicate that they are recording activity from a neural generator (Lachaux et al., 2003). Possible polarity inversions in the ERPs to Repetition Deviants occurred here between electrode contacts H5 and H6 in SUB2, in an area that may correspond to the border between the posterolateral fissure and the posterior part of superior planum temporale. The tonotopic mapping results suggest that these contacts were implanted in non-PAC, illustrated by more general responsiveness to acoustic stimuli and prolonged response onset latency in Figure 4C. The permutation test and the ERP plots indicate that responses to deviants were overall stronger and more widespread in electrodes in the TPJ than in the auditory cortex. This is consistent with iEEG studies reporting that the polarity of an MMN-like ERP component depended on the position of the electrode relative to the Sylvian fissure (Edwards et al., 2005; El Karoui et al., 2015; Halgren et al., 1995). However, the polarity inversions were not as clear as the inversion observed in Heschl's gyrus during the tonotopic mapping task.

Although polarity inversions were observed in the ERPs from Heschl's gyrus during the oddball task, these inversions occurred in the same contacts to both standard and deviant stimuli and during the tonotopic mapping. Thus, the polarity inversions in Heschl's gyrus might reflect activity from tonotopically tuned neurons in the PAC and not activity related to auditory regularity encoding and deviance detection. Moreover, similar polarity inversions between electrode contacts H5 and H6 in SUB2 were also observed during the tonotopic mapping task (Fig. X.1.3 in the Appendix) to all stimulus tones, which renders it unlikely that the voltages reflect a unique neural generator for deviance detection. Rather, no clear frequency preference (Fig. 4C and Fig. X.1.3 in the Appendix), combined with unique ERP waveforms to auditory deviants (Fig. 6A), imply that the neural activity that comprises the MMN results from a combination of underlying processes in neurons with broader frequency tuning in non-PAC. Moreover, the HFA may here be a more valid reflection of local neural activity to auditory deviants (Lachaux et al., 2012; McCarty et al., 2022).

4.3 Limitations and future directions

The current study had some limitations warranting discussion. First, although a strength with iEEG is the excellent temporal resolution, this is not necessarily helpful when comparing responses and non-responses from the same channel. A consequence of the exclusion criteria

used for the latency analyses of the oddball task is that the differences between conditions in response onsets were calculated as the subtracted difference. Hence, if a channel did not respond to a standard or deviant tone, data from both conditions were removed from the analyses. It is possible that these criteria were too conservative, rendering increased risk of a type 2 error (i.e., a true effect was not found).

Stimuli range. Next, the stimuli in the oddball task were restricted to three different sound frequencies, namely 311 Hz, 1245 Hz, and 3520 Hz. Hence, sound frequencies less separated from each other in spectral distance may yield different results. However, as demonstrated in the tonotopic mapping task, some auditory cortical fields responded to multiple tones, and it is therefore possible that even SEEG electrode contacts have the necessary precision to distinguish between fine-tuning in responsiveness. More narrow spectral distance in the auditory stimuli may also impact the responsiveness because of adaptation effects and/or lateral inhibition from nearby tonotopic fields (May & Tiitinen, 2010).

Hemispheric differences. Other limitations include that data were collected from a small clinical population and limited to the right hemisphere. Although it is custom clinical practice to only record from the hemisphere where the epileptic activity is most likely generated, not having samples from the left hemisphere restricts the overall generalizability of the current results. The impact of this limitation is further emphasized given the large interindividual variability in the response properties and morphology of the auditory cortex. Hence, it is possible that the current results on tonotopy and deviance detection differ between the left and the right hemisphere, and that a larger sample would yield more conclusive results.

Anatomical labelling. We focused on brain regions defined by automatic anatomical labeling software combined with visual inspection of the fused preoperative MRI and postoperative CT scans. Since the brain swells (i.e., edema) up to 2 mm after implantation of the electrodes, the electrodes may move slightly, and the anatomical label may consequently not be entirely correct. The labels used to investigate group-wise differences between anatomical regions in auditory deviance detection may hence contain some imprecision in the anatomical details. This impacts conclusions about the role of specific brain regions and their involvement in auditory deviance detection. Thus, larger spatial electrode coverage would be ideal to fully investigate auditory deviance detection in these regions.

Counterbalancing. A major limitation is that the design of the oddball task did not control for order-effects since the repetition and the alternation blocks were not counterbalanced. Specifically, the repetition block (in which a repetition of the preceding tone was expected) was always presented after the alternation block (in which a repetition of the preceding tone was not expected). It is thus possible that the responses recorded during the repetition block were confounded by habituation and adaptation effects, that reduced the overall responsiveness during this block. Previous intracranial findings have showed that the magnitude of activity in the HFA range recorded from non-PAC reduces with frequent stimulation, possibly reflecting a sensitivity to long-term adaptation effects (Eliades et al., 2014). Order effects could therefore potentially explain why the permutation tests yielded significantly enhanced HFAs to Repetition Deviants but not to Alternation Deviants. Hence, overall reduced responsiveness in the last blocks could generate an illusory deviance detection reflected as enhanced HFA amplitudes to auditory deviant but not to standard stimuli, when the true cause of this increase in HFA was attenuation of HFA from repeated acoustic stimulation (i.e., neural adaptation). Thus, to exclude or investigate order effects, future research applying the auditory repetition oddball task may benefit from using a counterbalanced design.

Alternatively, it is possible that the non-significant findings for the Alternation Deviants reflect the recent encounter with these tones as standard alternation tones A and B in the preceding alternation block. Hence, some form of synaptic learning took place and the Alternation Deviants in the repetition blocks were not unexpected, but *less* expected. Moreover, if the TPJ and the STG are involved in tracking stimulus regularity and violation to stimulus transition probability, then these tones were already incorporated in the current sampling space of possible auditory events (i.e., the cumulative encounters and thus the expectancy of tone A given tone B during the repetition block is larger than the expectancy of tone A succeeding to A during the alternation block [e.g., $E(A|B)_{\text{repetition block}} > E(A|A)_{\text{alternation block}}$]). In addition, there was an overall increased occurrence of expected A-B and B-A transitions relative to the A-A and B-B transitions in the repetition block (e.g., A**AB**BA**ABBAA**), relative to the A-A and B-B transitions in the preceding alternation block (e.g., ABABABABAB). Thus, the missing counterbalancing combined with increased A-B/B-A transition probability in the repetition block, makes the Alternation Deviants in the repetition block less "deviant" than the Repetition Deviant in the alternation block. However, if the Alternation Deviants represents a type of regularity violation that is tracked by lower

levels in the processing hierarchy not covered here (e.g., subcortical areas), then this could also explain why we did not find evidence of deviance detection to these deviants.

Yet, counterbalanced blocks may not allow for stimulus-specific adaptation effects to be distinguished from predictability effects. Conversely, comparing tonotopy and oddball task data to investigate difference in neural activity to expected but rare occurrences of unpredictable stimuli versus unexpected violations to frequent and predictable stimuli, would allow control of novelty (i.e., frequency change) as in Ishishita et al. (2019). This was not possible in the current study, as the inter-stimulus-intervals in the two tasks were not equal hence making comparisons between HFA to control for confounding adaptation effects less ideal (i.e., we cannot exclude confounding effects in neural activity from different inter-stimulus intervals). Thus, future studies may benefit from using equal inter-stimulus-intervals, to disentangle predictability effects and adaptation effects when comparing neural activity in different conditions.

5 Conclusions

5.1 Tonotopy in the human auditory cortex

Although it is possible that the tonotopic mapping was limited to a part of the auditory core corresponding more to frequencies around 1245 to 1760 Hz in SUB2 and SUB3, and a broader sound frequency range (220 to 7040 Hz) in SUB1, these brain areas responded strongly to acoustic stimuli. However, the combination of heterogeneity in neural responsiveness and the limited electrode coverage constrains any distinction between anterior and posterior portions of Heschl's gyrus. Hence, the current results do not provide sufficient evidence to draw firm conclusions regarding the organization of tonotopic gradients across Heschl's gyrus. Still, the results demonstrated that acoustic stimuli elicited selective responses reflected in the magnitudes and response-onsets of HFA in a limited area of the human auditory cortex, and the frequency tuning in this area showed large interindividual variability.

5.2 Automatic deviance detection in the human auditory cortex

We aimed to identify the neural signatures of automatic deviance detection in the human PAC and non-PAC, and their precise neural loci. The results suggest that a violation to acoustic stimuli presented as part of a temporally predictable and regular sound sequence, is reflected as increased HFA in non-PAC, namely the more lateral aspects of the STG, the posterolateral fissure and the supramarginal gyrus. Moreover, the onset of HFA in the posterolateral fissure was delayed to auditory Repetition Deviants. Altogether, our results show that the TPJ and lateral aspects of the STG automatically track and detect deviance to auditory regularities, without the aid of attention. In contrast, the PAC is unaffected by auditory deviants. Yet, despite these findings, no counterbalancing between experimental blocks hinders firm conclusions to be drawn from the current results. We therefore conclude that additional investigations are needed to fully understand the neural implementation of automatic auditory deviance detection in the human brain.

Literature

Abdul-Kareem, I. A., & Sluming, V. (2008). Heschl gyrus and its included primary auditory cortex: Structural MRI studies in healthy and diseased subjects. *Journal of Magnetic Resonance Imaging: JMRI*, *28*(2), 287–299. https://doi.org/10.1002/jmri.21445

Alain, C., Woods, D. L., & Ogawa, K. H. (1994). Brain indices of automatic pattern processing. *Neuroreport: An International Journal for the Rapid Communication of Research in Neuroscience*, *6*, 140–144. https://doi.org/10.1097/00001756-199412300-00036

Arnal, L. H., & Giraud, A.-L. (2012). Cortical oscillations and sensory predictions. *Trends in Cognitive Sciences*, *16*(7), 390–398. https://doi.org/10.1016/j.tics.2012.05.003

Ashburner, J., & Friston, K. J. (1999). Nonlinear spatial normalization using basis functions. *Human Brain Mapping*, *7*(4), 254–266. https://doi.org/10.1002/(SICI)1097-0193(1999)7:4<254::AID-HBM4>3.0.CO;2-G

Auksztulewicz, R., & Friston, K. (2016). Repetition suppression and its contextual determinants in predictive coding. *Cortex; a Journal Devoted to the Study of the Nervous System and Behavior*, *80*, 125–140. https://doi.org/10.1016/j.cortex.2015.11.024

Bastos, A. M., & Schoffelen, J.-M. (2016). A tutorial review of functional connectivity analysis methods and their interpretational pitfalls. *Frontiers in Systems Neuroscience*, *9*. https://www.frontiersin.org/articles/10.3389/fnsys.2015.00175

Bastos, A. M., Usrey, W. M., Adams, R. A., Mangun, G. R., Fries, P., & Friston, K. J. (2012). Canonical microcircuits for predictive coding. *Neuron*, *76*(4), 695–711. https://doi.org/10.1016/j.neuron.2012.10.038

Bekinschtein, T. A., Dehaene, S., Rohaut, B., Tadel, F., Cohen, L., & Naccache, L. (2009). Neural signature of the conscious processing of auditory regularities. *Proceedings of the National Academy of Sciences*, *106*(5), 1672–1677. https://doi.org/10.1073/pnas.0809667106

Besle, J., Mougin, O., Sánchez-Panchuelo, R.-M., Lanting, C., Gowland, P., Bowtell, R., Francis, S., & Krumbholz, K. (2019). Is human auditory cortex organization compatible with the monkey model? Contrary evidence from ultra-high-field functional and structural MRI. *Cerebral Cortex*, *29*(1), 410–428. https://doi.org/10.1093/cercor/bhy267

Blenkmann, A. O., Collavini, S., Lubell, J., Llorens, A., Funderud, I., Ivanovic, J., Larsson, P. G., Meling, T. R., Bekinschtein, T., Kochen, S., Endestad, T., Knight, R. T., & Solbakk, A.-K. (2019). Auditory deviance detection in the human insula: An intracranial EEG study. *Cortex; a Journal Devoted to the Study of the Nervous System and Behavior*, *121*, 189–200. https://doi.org/10.1016/j.cortex.2019.09.002

Blenkmann, A. O., Phillips, H. N., Princich, J. P., Rowe, J. B., Bekinschtein, T. A., Muravchik, C. H., & Kochen, S. (2017). iElectrodes: A comprehensive open-source toolbox for depth and subdural grid electrode localization. *Frontiers in Neuroinformatics*, *11*. https://www.frontiersin.org/articles/10.3389/fninf.2017.00014

Brodal, P., (2016). *The central nervous system: Structure and function* (Fifth edition). Oxford University Press

Brugge, J. F., Volkov, I. O., Garell, P. C., Reale, R. A., & Howard, M. A. (2003). Functional connections between auditory cortex on Heschl's gyrus and on the lateral superior temporal gyrus in humans. *Journal of Neurophysiology*, *90*(6), 3750–3763. https://doi.org/10.1152/jn.00500.2003

Brugge, J. F., Volkov, I. O., Oya, H., Kawasaki, H., Reale, R. A., Fenoy, A., Steinschneider, M., & Howard, M. A. (2008). Functional localization of auditory cortical fields of human: Click-train stimulation. *Hearing Research*, *238*(1), 12–24. https://doi.org/10.1016/j.heares.2007.11.012

Buser, P. A. (1955). *Analyse des réponses électriques du lobe optique à la stimulation de la voie visuelle chez quelques vertébrés inférieurs*. Masson & Cie, Éditeurs, Libraires de l'Académie de Médecine.

Buzsáki, G., Anastassiou, C. A., & Koch, C. (2012). The origin of extracellular fields and currents—EEG, ECoG, LFP and spikes. *Nature Reviews Neuroscience*, *13*(6), Article 6. https://doi.org/10.1038/nrn3241

Chauvel, P., Gonzalez-Martinez, J., & Bulacio, J. (2019). Presurgical intracranial investigations in epilepsy surgery. *Handbook of Clinical Neurology*, *161*, 45–71. https://doi.org/10.1016/B978-0-444-64142-7.00040-0

Chennu, S., Noreika, V., Gueorguiev, D., Blenkmann, A., Kochen, S., Ibáñez, A., Owen, A. M., & Bekinschtein, T. A. (2013). Expectation and attention in hierarchical auditory prediction. *The Journal of Neuroscience*, *33*(27), 11194–11205. https://doi.org/10.1523/JNEUROSCI.0114-13.2013

Clark, A. (2013). Whatever next? Predictive brains, situated agents, and the future of cognitive science. *Behavioral and Brain Sciences*, *36*(3), 181–204. https://doi.org/10.1017/S0140525X12000477

Clarke, S., & Morosan, P. (2012). Architecture, connectivity, and transmitter receptors of human auditory cortex. In D. Poeppel, T. Overath, A. N. Popper, & R. R. Fay (Eds.), *The human auditory cortex* (pp. 11–38). Springer. https://doi.org/10.1007/978-1-4614-2314-0_2

Cohen, M. X. (2014). *Analyzing neural time series data: Theory and practice*. https://doi.org/10.7551/mitpress/9609.001.0001

Combrisson, E., Vallat, R., O'Reilly, C., Jas, M., Pascarella, A., Saive, A., Thiery, T., Meunier, D., Altukhov, D., Lajnef, T., Ruby, P., Guillot, A., & Jerbi, K. (2019). Visbrain: A multi-purpose GPU-accelerated open-source suite for multimodal brain data visualization. *Frontiers in Neuroinformatics*, *13*. https://www.frontiersin.org/articles/10.3389/fninf.2019.00014

Corbetta, M., Patel, G., & Shulman, G. L. (2008). The reorienting system of the human brain: From environment to theory of mind. *Neuron*, *58*(3), 306–324. https://doi.org/10.1016/j.neuron.2008.04.017

Corbetta, M., & Shulman, G. L. (2002). Control of goal-directed and stimulus-driven attention in the brain. *Nature Reviews Neuroscience*, *3*(3), Article 3. https://doi.org/10.1038/nrn755

Crone, N. E., Miglioretti, D. L., Gordon, B., & Lesser, R. P. (1998). Functional mapping of human sensorimotor cortex with electrocorticographic spectral analysis. II. Event-related synchronization in the gamma band. *Brain: A Journal of Neurology*, *121 (Pt 12)*, 2301–2315. https://doi.org/10.1093/brain/121.12.2301

Dalboni da Rocha, J. L., Schneider, P., Benner, J., Santoro, R., Atanasova, T., Van De Ville, D., & Golestani, N. (2020). TASH: Toolbox for the automated segmentation of Heschl's gyrus. *Scientific Reports*, *10*(1), Article 1. https://doi.org/10.1038/s41598-020-60609-y

Dale, A. M., Fischl, B., & Sereno, M. I. (1999). Cortical surface-based analysis. I. Segmentation and surface reconstruction. *NeuroImage*, *9*(2), 179–194. https://doi.org/10.1006/nimg.1998.0395

De Martino, F., Moerel, M., Ugurbil, K., Goebel, R., Yacoub, E., & Formisano, E. (2015). Frequency preference and attention effects across cortical depths in the human primary auditory cortex. *Proceedings of the National Academy of Sciences*, *112*(52), 16036–16041. https://doi.org/10.1073/pnas.1507552112

Desikan, R. S., Ségonne, F., Fischl, B., Quinn, B. T., Dickerson, B. C., Blacker, D., Buckner, R. L., Dale, A. M., Maguire, R. P., Hyman, B. T., Albert, M. S., & Killiany, R. J. (2006). An automated labeling system for subdividing the human cerebral cortex on MRI scans into gyral based regions of interest. *NeuroImage*, *31*(3), 968–980. https://doi.org/10.1016/j.neuroimage.2006.01.021

Destrieux, C., Fischl, B., Dale, A., & Halgren, E. (2010). Automatic parcellation of human cortical gyri and sulci using standard anatomical nomenclature. *NeuroImage*, *53*(1), 1–15. https://doi.org/10.1016/j.neuroimage.2010.06.010

Dick, F. K., Lehet, M. I., Callaghan, M. F., Keller, T. A., Sereno, M. I., & Holt, L. L. (2017). Extensive tonotopic mapping across auditory cortex is recapitulated by spectrally directed attention and systematically related to cortical myeloarchitecture. *The Journal of Neuroscience*, *37*(50), 12187–12201. https://doi.org/10.1523/JNEUROSCI.1436-17.2017

Donchin, E., & Coles, M. G. H. (1988). Is the P300 component a manifestation of context updating? *Behavioral and Brain Sciences*, *11*(3), 357. https://doi.org/10.1017/s0140525x00058027

Dürschmid, S., Edwards, E., Reichert, C., Dewar, C., Hinrichs, H., Heinze, H.-J., Kirsch, H. E., Dalal, S. S., Deouell, L. Y., & Knight, R. T. (2016). Hierarchy of prediction errors for auditory events in human temporal and frontal cortex. *Proceedings of the National Academy of Sciences*, *113*(24), 6755–6760. https://doi.org/10.1073/pnas.1525030113

Eckert, D., Reichert, C., Bien, C. G., Heinze, H.-J., Knight, R. T., Deouell, L. Y., & Dürschmid, S. (2022). Distinct interacting cortical networks for stimulus-response and repetition-suppression. *Communications Biology*, *5*(1), Article 1. https://doi.org/10.1038/s42003-022-03861-4

Edwards, E., Soltani, M., Deouell, L. Y., Berger, M. S., & Knight, R. T. (2005). High gamma activity in response to deviant auditory stimuli recorded directly from human cortex. *Journal of Neurophysiology*, *94*(6), 4269–4280. https://doi.org/10.1152/jn.00324.2005

El Karoui, I., King, J.-R., Sitt, J., Meyniel, F., Van Gaal, S., Hasboun, D., Adam, C., Navarro, V., Baulac, M., Dehaene, S., Cohen, L., & Naccache, L. (2015). Event-related potential, time-frequency, and functional connectivity facets of local and global auditory novelty processing: An intracranial study in humans. *Cerebral Cortex (New York, N.Y.: 1991)*, *25*(11), 4203–4212. https://doi.org/10.1093/cercor/bhu143

Eliades, S., Crone, N., Anderson, W., Ramadoss, D., Lenz, F., & Boatman-Reich, D. (2014). Adaptation of high-gamma responses in human auditory association cortex. *JOURNAL OF NEUROPHYSIOLOGY*, *112*(9), 2147–2163. https://doi.org/10.1152/jn.00207.2014

Escera, C. (2017). The role of the auditory brainstem in regularity encoding and deviance detection. In N. Kraus, S. Anderson, T. White-Schwoch, R. R. Fay, & A. N. Popper (Eds.), *The frequency-following response: A window into human communication* (pp. 101–120). Springer International Publishing. https://doi.org/10.1007/978-3-319-47944-6_5

Escera, C., Leung, S., & Grimm, S. (2014). Deviance detection based on regularity encoding along the auditory hierarchy: Electrophysiological evidence in humans. *Brain Topography*, *27*(4), 527–538. https://doi.org/10.1007/s10548-013-0328-4

Feldman, H., & Friston, K. (2010). Attention, uncertainty, and free-energy. *Frontiers in Human Neuroscience*, *4*. https://www.frontiersin.org/articles/10.3389/fnhum.2010.00215

Fitzgerald, K., & Todd, J. (2020). Making sense of mismatch negativity. *Frontiers in Psychiatry*, *11*. https://www.frontiersin.org/articles/10.3389/fpsyt.2020.00468

Fonken, Y. M., Kam, J. W. Y., & Knight, R. T. (2020). A differential role for human hippocampus in novelty and contextual processing: Implications for P300. *Psychophysiology*, *57*(7), e13400. https://doi.org/10.1111/psyp.13400

Formisano, E., Kim, D.-S., Di Salle, F., van de Moortele, P.-F., Ugurbil, K., & Goebel, R. (2003). Mirror-symmetric tonotopic maps in human primary auditory cortex. *Neuron*, *40*(4), 859–869. https://doi.org/10.1016/S0896-6273(03)00669-X

Friston, K. (2005). A theory of cortical responses. *Philosophical Transactions of the Royal Society of London. Series B, Biological Sciences*, *360*(1456), 815–836. https://doi.org/10.1098/rstb.2005.1622

Friston, K. (2010). The free-energy principle: A unified brain theory? *Nature Reviews Neuroscience*, *11*(2), Article 2. https://doi.org/10.1038/nrn2787

Fuhrer, J., Glette, K., Ivanovic, J., Larsson, P. G., Bekinschtein, T., Kochen, S., Knight, R. T., Tørresen, J., Solbakk, A.-K., Endestad, T., & Blenkmann, A. (2022). Direct brain recordings reveal continuous encoding of structure in random stimuli (p. 2021.10.01.462295). *bioRxiv.* https://doi.org/10.1101/2021.10.01.462295

Fujioka, T., Trainor, L. J., Large, E. W., & Ross, B. (2009). Beta and gamma rhythms in human auditory cortex during musical beat processing. *Annals of the New York Academy of Sciences*, *1169*, 89–92. https://doi.org/10.1111/j.1749-6632.2009.04779.x

Galaburda, A., & Sanides, F. (1980). Cytoarchitectonic organization of the human auditory cortex. *Journal of Comparative Neurology*, *190*(3), 597–610. https://doi.org/10.1002/cne.901900312

Garrido, M. I., Kilner, J. M., Stephan, K. E., & Friston, K. J. (2009). The mismatch negativity: A review of underlying mechanisms. *Clinical Neurophysiology*, *120*(3), 453–463. https://doi.org/10.1016/j.clinph.2008.11.029

Gonzalez-Gadea, M. L., Chennu, S., Bekinschtein, T. A., Rattazzi, A., Beraudi, A., Tripicchio, P., Moyano, B., Soffita, Y., Steinberg, L., Adolfi, F., Sigman, M., Marino, J., Manes, F., & Ibanez, A. (2015). Predictive coding in autism spectrum disorder and attention deficit hyperactivity disorder. *Journal of Neurophysiology*, *114*(5), 2625–2636. https://doi.org/10.1152/jn.00543.2015

Gu, C., & Bi, H.-Y. (2020). Auditory processing deficit in individuals with dyslexia: A meta-analysis of mismatch negativity. *Neuroscience & Biobehavioral Reviews*, *116*, 396–405. https://doi.org/10.1016/j.neubiorev.2020.06.032

Hilbert, D. (1912). *Grundzüge einer allgemeinen theorie der linearen integralgleichungen*. Retrieved 2 April 2023, from https://archive.org/details/grundzugeallg00hilbrich/page/n7/mode/2up

Halgren, E., Baudena, P., Clarke, J. M., Heit, G., Liégeois, C., Chauvel, P., & Musolino, A. (1995). Intracerebral potentials to rare target and distractor auditory and visual stimuli. I. Superior temporal plane and parietal lobe. *Electroencephalography and Clinical Neurophysiology*, *94*(3), 191–220. https://doi.org/10.1016/0013-4694(94)00259-N

Hall, D., & Barker, D. (2012). Coding of basic acoustical and perceptual components of sound in human auditory cortex. In D. Poeppel, T. Overath, A. N. Popper, & R. R. Fay (Eds.), *The Human Auditory Cortex* (pp. 165–197). Springer. https://doi.org/10.1007/978-1-4614-2314-0_7

Heilbron, M., & Chait, M. (2018). Great expectations: Is there evidence for predictive coding in auditory cortex? *Neuroscience*, *389*, 54–73. https://doi.org/10.1016/j.neuroscience.2017.07.061

Helfrich, R. F. (2022). Human intracranial cognitive neurophysiology. In R. P. Vertes & T. Allen (Eds.), *Electrophysiological Recording Techniques* (pp. 221–245). Springer US. https://doi.org/10.1007/978-1-0716-2631-3_10

Helfrich, R. F., & Knight, R. T. (2019). Chapter 36 - Cognitive neurophysiology: Event-related potentials. In K. H. Levin & P. Chauvel (Eds.), *Handbook of Clinical Neurology* (Vol. 160, pp. 543–558). Elsevier. https://doi.org/10.1016/B978-0-444-64032-1.00036-9

Helmholtz, H. von. (1867). Handbuch der physiologischen Optik*: Mit 213 in den Text eingedruckten Holzschnitten und 11 Tafeln*. Voss.

Howard, M. A., Nourski, K. V., & Brugge, J. F. (2012). Invasive research methods. In D. Poeppel, T. Overath, A. N. Popper, & R. R. Fay (Eds.), *The Human Auditory Cortex* (pp. 39–67). Springer. https://doi.org/10.1007/978-1-4614-2314-0_3

Howard, M. A., Volkov, I. O., Abbas, P. J., Damasio, H., Ollendieck, M. C., & Granner, M. A. (1996). A chronic microelectrode investigation of the tonotopic organization of human auditory cortex. *Brain Research*, *724*(2), 260–264. https://doi.org/10.1016/0006-8993(96)00315-0

Howard, M. A., Volkov, I. O., Mirsky, R., Garell, P. C., Noh, M. D., Granner, M., Damasio, H., Steinschneider, M., Reale, R. A., Hind, J. E., & Brugge, J. F. (2000). Auditory cortex on the human posterior superior temporal gyrus. *Journal of Comparative Neurology*, *416*(1), 79–92. https://doi.org/10.1002/(SICI)1096-9861(20000103)416:1<79::AID-CNE6>3.0.CO;2-2

Hughes, H. C., Darcey, T. M., Barkan, H. I., Williamson, P. D., Roberts, D. W., & Aslin, C. H. (2001). Responses of human auditory association cortex to the omission of an expected acoustic event. *NeuroImage*, *13*(6), 1073–1089. https://doi.org/10.1006/nimg.2001.0766

Humphries, C., Liebenthal, E., & Binder, J. R. (2010). Tonotopic organization of human auditory cortex. *NeuroImage*, *50*(3), 1202–1211. https://doi.org/10.1016/j.neuroimage.2010.01.046

Ishishita, Y., Kunii, N., Shimada, S., Ibayashi, K., Tada, M., Kirihara, K., Kawai, K., Uka, T., Kasai, K., & Saito, N. (2019). Deviance detection is the dominant component of auditory contextual processing in the lateral superior temporal gyrus: A human ECoG study. *Human Brain Mapping*, *40*(4), 1184–1194. https://doi.org/10.1002/hbm.24438

Jasmin, K., Lima, C. F., & Scott, S. K. (2019). Understanding rostral–caudal auditory cortex contributions to auditory perception. *Nature Reviews Neuroscience*, *20*(7), Article 7. https://doi.org/10.1038/s41583-019-0160-2

Johnson, E. L., Kam, J. W. Y., Tzovara, A., & Knight, R. T. (2020). Insights into human cognition from intracranial EEG: A review of audition, memory, internal cognition, and causality. *Journal of Neural Engineering*, *17*(5), 051001. https://doi.org/10.1088/1741-2552/abb7a5

Kaas, J. H., & Hackett, T. A. (2000). Subdivisions of auditory cortex and processing streams in primates. *Proceedings of the National Academy of Sciences*, *97*(22), 11793–11799. https://doi.org/10.1073/pnas.97.22.11793

Kaas, J. H., Hackett, T. A., & Tramo, M. J. (1999). Auditory processing in primate cerebral cortex. *Current Opinion in Neurobiology*, *9*(2), 164–170. https://doi.org/10.1016/S0959-4388(99)80022-1

Kim, H. (2014). Involvement of the dorsal and ventral attention networks in oddball stimulus processing: A meta-analysis. *Human Brain Mapping*, *35*(5), 2265–2284. https://doi.org/10.1002/hbm.22326

Kleiner, M., Brainard, D., Pelli, D., Ingling, A., Murray, R., & Broussard, C. (2007). What's new in psychtoolbox-3. *Perception*, *36*(14), 1–16.

Kok, A. (2001). On the utility of P3 amplitude as a measure of processing capacity. *Psychophysiology*, *38*(3), 557–577. https://doi.org/10.1017/S0048577201990559

Kropotov, J. D., Alho, K., Näätänen, R., Ponomarev, V. A., Kropotova, O. V., Anichkov, A. D., & Nechaev, V. B. (2000). Human auditory-cortex mechanisms of preattentive sound discrimination. *Neuroscience Letters*, *280*(2), 87–90. https://doi.org/10.1016/S0304-3940(00)00765-5

Lachaux, J. P., Rudrauf, D., & Kahane, P. (2003). Intracranial EEG and human brain mapping. *Journal of Physiology-Paris*, *97*(4), 613–628. https://doi.org/10.1016/j.jphysparis.2004.01.018

Lachaux, J.-P., Axmacher, N., Mormann, F., Halgren, E., & Crone, N. E. (2012). High-frequency neural activity and human cognition: Past, present and possible future of intracranial EEG research. *Progress in Neurobiology*, *98*(3), 279–301. https://doi.org/10.1016/j.pneurobio.2012.06.008

Lee, M. D., & Wagenmakers, E.-J. (2014). *Bayesian cognitive modeling: A practical course* (1st ed.). Cambridge University Press. https://doi.org/10.1017/CBO9781139087759

Leszczyński, M., Barczak, A., Kajikawa, Y., Ulbert, I., Falchier, A. Y., Tal, I., Haegens, S., Melloni, L., Knight, R. T., & Schroeder, C. E. (2020). Dissociation of broadband high-

frequency activity and neuronal firing in the neocortex. *Science Advances*, *6*(33), eabb0977. https://doi.org/10.1126/sciadv.abb0977

Li, G., Jiang, S., Paraskevopoulou, S. E., Wang, M., Xu, Y., Wu, Z., Chen, L., Zhang, D., & Schalk, G. (2018). Optimal referencing for stereo-electroencephalographic (SEEG) recordings. *NeuroImage*, *183*, 327–335. https://doi.org/10.1016/j.neuroimage.2018.08.020

Liégeois-Chauvel, C., Musolino, A., Badier, J. M., Marquis, P., & Chauvel, P. (1994). Evoked potentials recorded from the auditory cortex in man: Evaluation and topography of the middle latency components. *Electroencephalography and Clinical Neurophysiology/Evoked Potentials Section*, *92*(3), 204–214. https://doi.org/10.1016/0168-5597(94)90064-7

Liégois-Chauvel, C., Musolino, A., & Chauvel, P. (1991). Localization of the primary auditory cortex area in man. *Brain*, *114A*(1), 139–153. https://doi.org/10.1093/oxfordjournals.brain.a101854

Lindquist, M. A., Geuter, S., Wager, T. D., & Caffo, B. S. (2019). Modular preprocessing pipelines can reintroduce artifacts into fMRI data. *Human Brain Mapping*, *40*(8), 2358–2376. https://doi.org/10.1002/hbm.24528

Luck, S. J. (2014). *An introduction to the event-related potential technique* (second edition). MIT Press.

Maris, E., & Oostenveld, R. (2007). Nonparametric statistical testing of EEG- and MEG-data. *Journal of Neuroscience Methods*, *164*(1), 177–190. https://doi.org/10.1016/j.jneumeth.2007.03.024

May, P. J. C., & Tiitinen, H. (2010). Mismatch negativity (MMN), the deviance-elicited auditory deflection, explained. *Psychophysiology*, *47*(1), 66–122. https://doi.org/10.1111/j.1469-8986.2009.00856.x

McCarty, M. J., Woolnough, O., Mosher, J. C., Seymour, J., & Tandon, N. (2022). The listening zone of human electrocorticographic field potential recordings. *ENeuro*, *9*(2). https://doi.org/10.1523/ENEURO.0492-21.2022

McDermott, J. H. (2018). Audition. In J. T. Wixted (Ed.), *Stevens' Handbook of Experimental Psychology and Cognitive Neuroscience* (pp. 1–57). John Wiley & Sons, Inc. https://doi.org/10.1002/9781119170174.epcn202

Moerel, M., De Martino, F., & Formisano, E. (2014). An anatomical and functional topography of human auditory cortical areas. *Frontiers in Neuroscience*, *8*. https://www.frontiersin.org/articles/10.3389/fnins.2014.00225

Morillon, B., & Baillet, S. (2017). Motor origin of temporal predictions in auditory attention. *Proceedings of the National Academy of Sciences*, *114*(42), E8913–E8921. https://doi.org/10.1073/pnas.1705373114

Mukamel, R., Gelbard, H., Arieli, A., Hasson, U., Fried, I., & Malach, R. (2005). Coupling between neuronal firing, field potentials, and FMRI in human auditory cortex. *Science (New York, N.Y.)*, *309*(5736), 951–954. https://doi.org/10.1126/science.1110913

Näätänen, R., Gaillard, A. W. K., & Mäntysalo, S. (1978). Early selective-attention effect on evoked potential reinterpreted. *Acta Psychologica*, *42*(4), 313–329. https://doi.org/10.1016/0001-6918(78)90006-9

Näätänen, R., Kujala, T., Escera, C., Baldeweg, T., Kreegipuu, K., Carlson, S., & Ponton, C. (2012). The mismatch negativity (MMN)—A unique window to disturbed central auditory

processing in ageing and different clinical conditions. *CLINICAL NEUROPHYSIOLOGY*, *123*(3), 424–458. https://doi.org/10.1016/j.clinph.2011.09.020

Näätänen, R., Paavilainen, P., Rinne, T., & Alho, K. (2007). The mismatch negativity (MMN) in basic research of central auditory processing: A review. *Clinical Neurophysiology*, *118*(12), 2544–2590. https://doi.org/10.1016/j.clinph.2007.04.026

Naidich, T. P., Duvernoy, H. M., Delman, B. N., Sorensen, A. G., Kollias, S. S., & Haacke, E. M. (2009). *Duvernoy's atlas of the human brain stem and cerebellum*. Springer. https://doi.org/10.1007/978-3-211-73971-6

Nordby, H., Roth, W. T., & Pfefferbaum, A. (1988). Event-related potentials to breaks in sequences of alternating pitches or interstimulus intervals. *Psychophysiology*, *25*(3), 262–268. https://doi.org/10.1111/j.1469-8986.1988.tb01239.x

Norman-Haignere, S. V., Feather, J., Boebinger, D., Brunner, P., Ritaccio, A., McDermott, J. H., Schalk, G., & Kanwisher, N. (2022). A neural population selective for song in human auditory cortex. *Current Biology: CB*, *32*(7), 1470-1484.e12. https://doi.org/10.1016/j.cub.2022.01.069

Nourski, K., Steinschneider, M., Rhone, A., Krause, B., Kawasaki, H., & Banks, M. (2021). Cortical responses to auditory novelty across task conditions: An intracranial electrophysiology study. *HEARING RESEARCH*, *399*. https://doi.org/10.1016/j.heares.2020.107911

Nourski, K. V. (2017). Auditory processing in the human cortex: An intracranial electrophysiology perspective. *Laryngoscope Investigative Otolaryngology*, *2*(4), 147–156. https://doi.org/10.1002/lio2.73

Nourski, K. V., Steinschneider, M., McMurray, B., Kovach, C. K., Oya, H., Kawasaki, H., & Howard, M. A. (2014). Functional organization of human auditory cortex: Investigation of response latencies through direct recordings. *NeuroImage*, *101*, 598–609. https://doi.org/10.1016/j.neuroimage.2014.07.004

Nourski, K. V., Steinschneider, M., Oya, H., Kawasaki, H., Jones, R. D., & Howard, M. A. (2014). Spectral organization of the human lateral superior temporal gyrus revealed by intracranial recordings. *Cerebral Cortex*, *24*(2), 340–352. https://doi.org/10.1093/cercor/bhs314

Nourski, K. V., Steinschneider, M., Rhone, A. E., Kawasaki, H., Howard, M. A., & Banks, M. I. (2018). Processing of auditory novelty across the cortical hierarchy: An intracranial electrophysiology study. *NeuroImage*, *183*, 412–424. https://doi.org/10.1016/j.neuroimage.2018.08.027

Oldfield, R. C. (1971). The assessment and analysis of handedness: The Edinburgh inventory. *Neuropsychologia*, *9*(1), 97–113. https://doi.org/10.1016/0028-3932(71)90067-4

Oostenveld, R., Fries, P., Maris, E., & Schoffelen, J.-M. (2011). FieldTrip: Open source software for advanced analysis of MEG, EEG, and invasive electrophysiological data. *Computational Intelligence and Neuroscience*, *2011*, 1:1-1:9. https://doi.org/10.1155/2011/156869

Paavilainen, P. (2013). The mismatch-negativity (MMN) component of the auditory event-related potential to violations of abstract regularities: A review. *International Journal of Psychophysiology*, *88*(2), 109–123. https://doi.org/10.1016/j.ijpsycho.2013.03.015

Parras, G. G., Nieto-Diego, J., Carbajal, G. V., Valdés-Baizabal, C., Escera, C., & Malmierca, M. S. (2017). Neurons along the auditory pathway exhibit a hierarchical organization of

prediction error. *Nature Communications*, *8*(1), Article 1. https://doi.org/10.1038/s41467-017-02038-6

Picton, T. W. (1992). The P300 wave of the human event-related potential. *Journal of Clinical Neurophysiology: Official Publication of the American Electroencephalographic Society*, *9*(4), 456–479. https://doi.org/10.1097/00004691-199210000-00002

Polich, J. (2007). Updating P300: An integrative theory of P3a and P3b. *Clinical Neurophysiology*, *118*(10), 2128–2148. https://doi.org/10.1016/j.clinph.2007.04.019

Rademacher, J., Caviness, V. S., Steinmetz, H., & Galaburda, A. M. (1993). Topographical variation of the human primary cortices: Implications for neuroimaging, brain mapping, and neurobiology. *Cerebral Cortex (New York, N.Y.: 1991)*, *3*(4), 313–329. https://doi.org/10.1093/cercor/3.4.313

Rademacher, J., Morosan, P., Schormann, T., Schleicher, A., Werner, C., Freund, H. J., & Zilles, K. (2001). Probabilistic mapping and volume measurement of human primary auditory cortex. *NeuroImage*, *13*(4), 669–683. https://doi.org/10.1006/nimg.2000.0714

Rauschecker, J. P. (2020). Chapter 37—The evolution of auditory cortex in humans. In J. H. Kaas (Ed.), *Evolutionary Neuroscience (Second Edition)* (pp. 891–898). Academic Press. https://doi.org/10.1016/B978-0-12-820584-6.00037-4

Rao, R. P. N., & Ballard, D. H. (1999). Predictive coding in the visual cortex: A functional interpretation of some extra-classical receptive-field effects. *Nature Neuroscience*, *2*(1), Article 1. https://doi.org/10.1038/4580

Ray, S., Crone, N. E., Niebur, E., Franaszczuk, P. J., & Hsiao, S. S. (2008). Neural correlates of high-gamma oscillations (60-200 Hz) in macaque local field potentials and their potential implications in electrocorticography. *The Journal of Neuroscience: The Official Journal of*

the Society for Neuroscience, *28*(45), 11526–11536. https://doi.org/10.1523/JNEUROSCI.2848-08.2008

Rosburg, T., Trautner, P., Dietl, T., Korzyukov, O. A., Boutros, N. N., Schaller, C., Elger, C. E., & Kurthen, M. (2005). Subdural recordings of the mismatch negativity (MMN) in patients with focal epilepsy. *Brain*, *128*(4), 819–828. https://doi.org/10.1093/brain/awh442

Saenz, M., & Langers, D. R. M. (2014). Tonotopic mapping of human auditory cortex. *Hearing Research*, *307*, 42–52. https://doi.org/10.1016/j.heares.2013.07.016

Sassenhagen, J., & Draschkow, D. (2019). Cluster-based permutation tests of MEG/EEG data do not establish significance of effect latency or location. *Psychophysiology*, *56*(6), e13335. https://doi.org/10.1111/psyp.13335

Scott, B. H., Saleem, K. S., Kikuchi, Y., Fukushima, M., Mishkin, M., & Saunders, R. C. (2017). Thalamic connections of the core auditory cortex and rostral supratemporal plane in the macaque monkey. *The Journal of Comparative Neurology*, *525*(16), 3488–3513. https://doi.org/10.1002/cne.24283

Seeck, M., & Schomer, D. L. (2017). C29Intracranial EEG Monitoring: Depth, subdural, foramen ovale, and microarrays. In D. L. Schomer, F. H. Lopes da Silva, D. L. Schomer, & F. H. Lopes da Silva (Eds.), *Niedermeyer's Electroencephalography: Basic Principles, Clinical Applications, and Related Fields* (p. 0). Oxford University Press. https://doi.org/10.1093/med/9780190228484.003.0029

Soltani, M., & Knight, R. T. (2000). Neural origins of the P300. *Critical reviews™ in Neurobiology*, *14*(3–4). https://doi.org/10.1615/CritRevNeurobiol.v14.i3-4.20

Squires, K. C., Squires, N. K., & Hillyard, S. A. (1975). Decision-related cortical potentials during an auditory signal detection task with cued observation intervals. *Journal of*

Experimental Psychology: Human Perception and Performance, *1*, 268–279. https://doi.org/10.1037/0096-1523.1.3.268

Studholme, C., Hill, D. L. G., & Hawkes, D. J. (1999). An overlap invariant entropy measure of 3D medical image alignment. *Pattern Recognition*, *32*(1), 71–86. https://doi.org/10.1016/S0031-3203(98)00091-0

Sutton, S., Braren, M., Zubin, J., & John, E. R. (1965). Evoked-Potential Correlates of Stimulus Uncertainty. *Science*, *150*(3700), 1187–1188. https://doi.org/10.1126/science.150.3700.1187

Sweet, R. A., Dorph-Petersen, K.-A., & Lewis, D. A. (2005). Mapping auditory core, lateral belt, and parabelt cortices in the human superior temporal gyrus. *Journal of Comparative Neurology*, *491*(3), 270–289. https://doi.org/10.1002/cne.20702

Tabas, A., & von Kriegstein, K. (2021). Adjudicating between local and global architectures of predictive processing in the subcortical auditory pathway. *Frontiers in Neural Circuits*, *15*. https://www.frontiersin.org/articles/10.3389/fncir.2021.644743

Talairach, J., & Bancaud, J. (1966). Lesion, 'irritative' zone and epileptogenic focus. *Confinia Neurologica*, *27*(1), 91–94. https://doi.org/10.1159/000103937

Todorovic, A., Ede, F. van, Maris, E., & Lange, F. P. de. (2011). Prior expectation mediates neural adaptation to repeated sounds in the auditory cortex: An MEG Study. *Journal of Neuroscience*, *31*(25), 9118–9123. https://doi.org/10.1523/JNEUROSCI.1425-11.2011

Voytek, B., & Knight, R. T. (2015). Dynamic network communication as a unifying neural basis for cognition, development, aging, and disease. *Biological Psychiatry*, *77*(12), 1089–1097. https://doi.org/10.1016/j.biopsych.2015.04.016

Walsh, K. S., McGovern, D. P., Clark, A., & O'Connell, R. G. (2020). Evaluating the neurophysiological evidence for predictive processing as a model of perception. *Annals of the New York Academy of Sciences*, *1464*(1), 242–268. https://doi.org/10.1111/nyas.14321

Winkler, I. (2007). Interpreting the mismatch negativity. *Journal of Psychophysiology*, *21*, 147–163. https://doi.org/10.1027/0269-8803.21.34.147

Woods, D. L., Stecker, G. C., Rinne, T., Herron, T. J., Cate, A. D., Yund, E. W., Liao, I., & Kang, X. (2009). Functional maps of human auditory cortex: Effects of acoustic features and attention. *PLoS ONE*, *4*(4), e5183. https://doi.org/10.1371/journal.pone.0005183

Zaveri, H. P., Duckrow, R. B., & Spencer, S. S. (2006). On the use of bipolar montages for time-series analysis of intracranial electroencephalograms. *Clinical Neurophysiology*, *117*(9), 2102–2108. https://doi.org/10.1016/j.clinph.2006.05.032

Appendix

Tonotopic mapping task

Figure X.1.1 SUB1: HFA Responses During Tonotopic Mapping Task

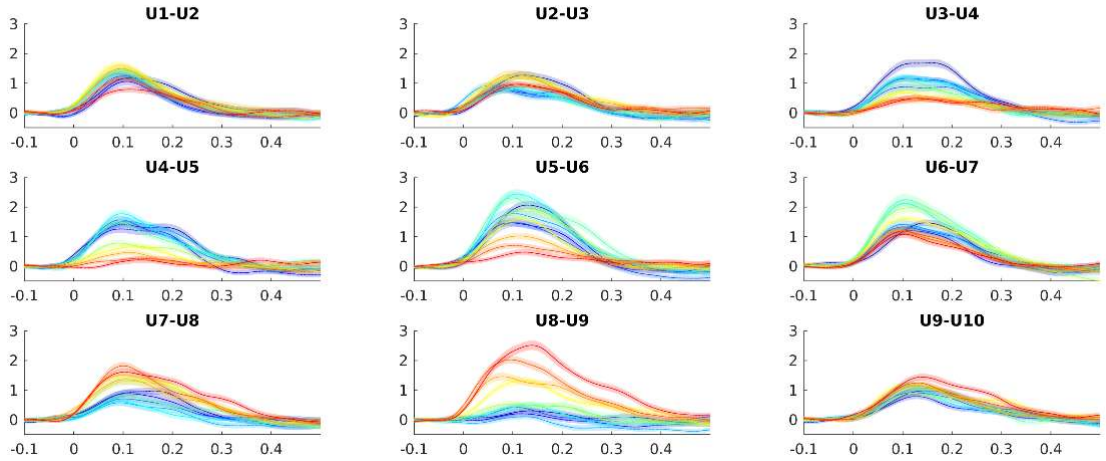

Note. HFA responses from SUB1 during tonotopic mapping task. The x-axis represents the time scale in seconds with zero indicating stimulus onset. The y-axis represents the magnitude of the HFA. Heschl's gyrus is located to channel U3-U4.

Figure X.1.2 SUB2: HFA Responses During Tonotopic Mapping Task

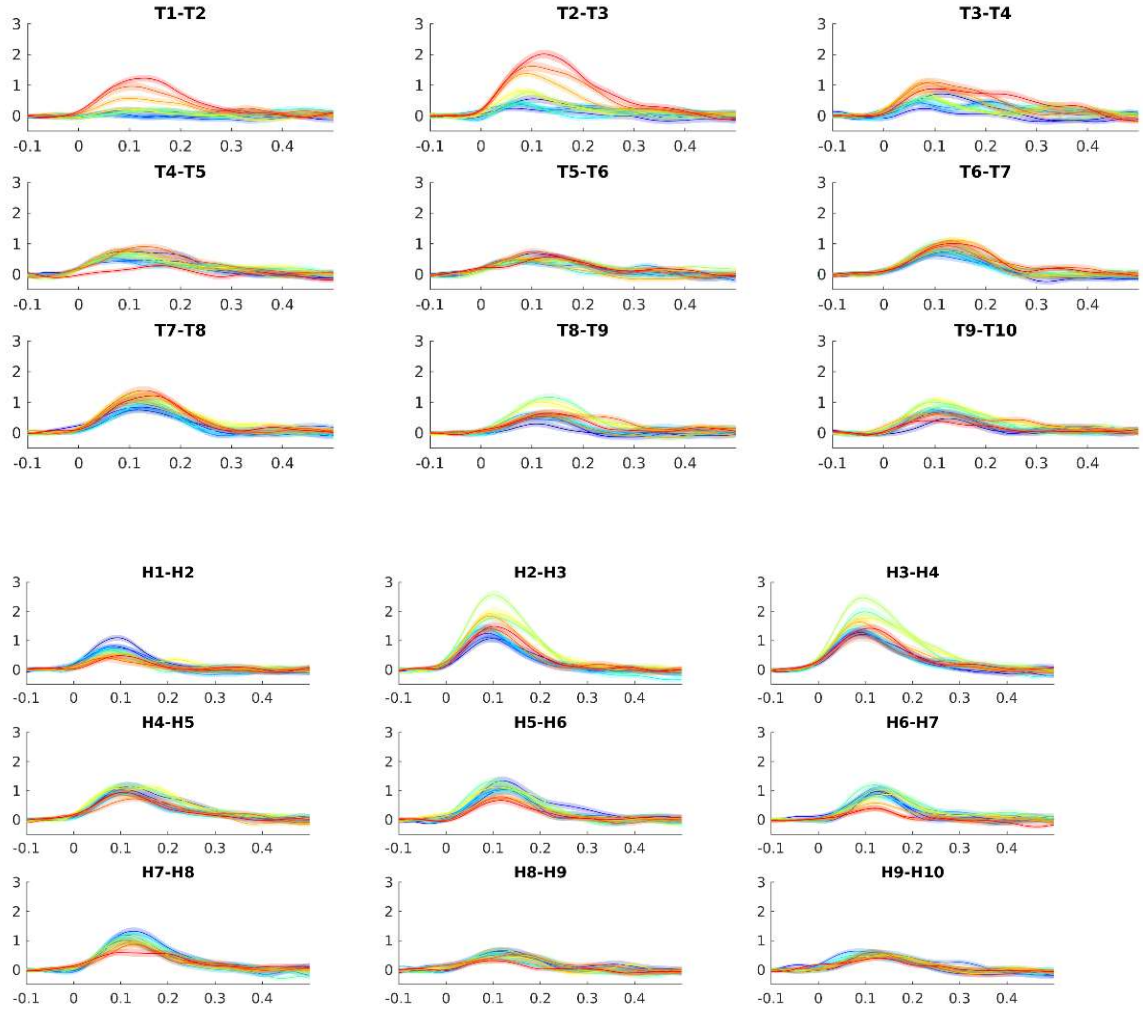

Note. HFA responses from SUB2 during tonotopic mapping task. Electrodes with prefix "T" are implanted in the auditory cortex while the prefix "H" indicate electrodes implanted in the TPJ region. The x-axis represents the time scale in seconds with zero indicating stimulus onset. The y-axis represents the magnitude of the HFA.

Figure X.1.3 SUB2: ERP Responses from TPJ During Tonotopic Mapping Task

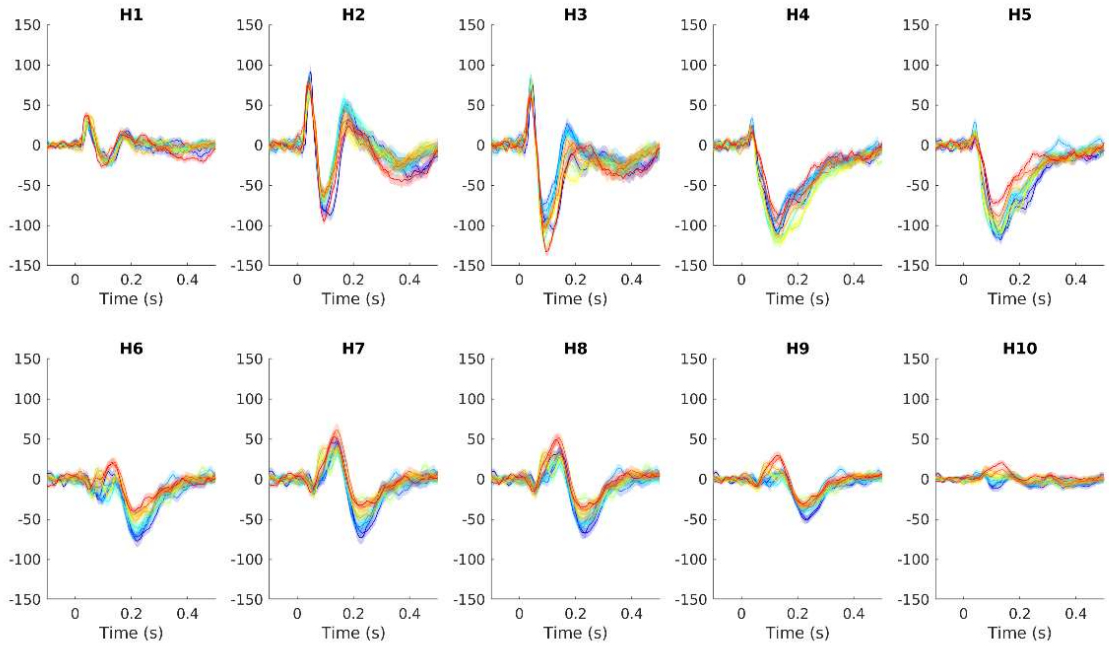

Note. Average-referenced ERPs from SUB2 during tonotopic mapping task from electrodes implanted in the TPJ region. The x-axis represents time scale in seconds with zero indicating stimulus onset. The y-axis represents the intracerebral voltages in μV.

Figure X.1.4 SUB3: HFA Responses During Tonotopic Mapping Task

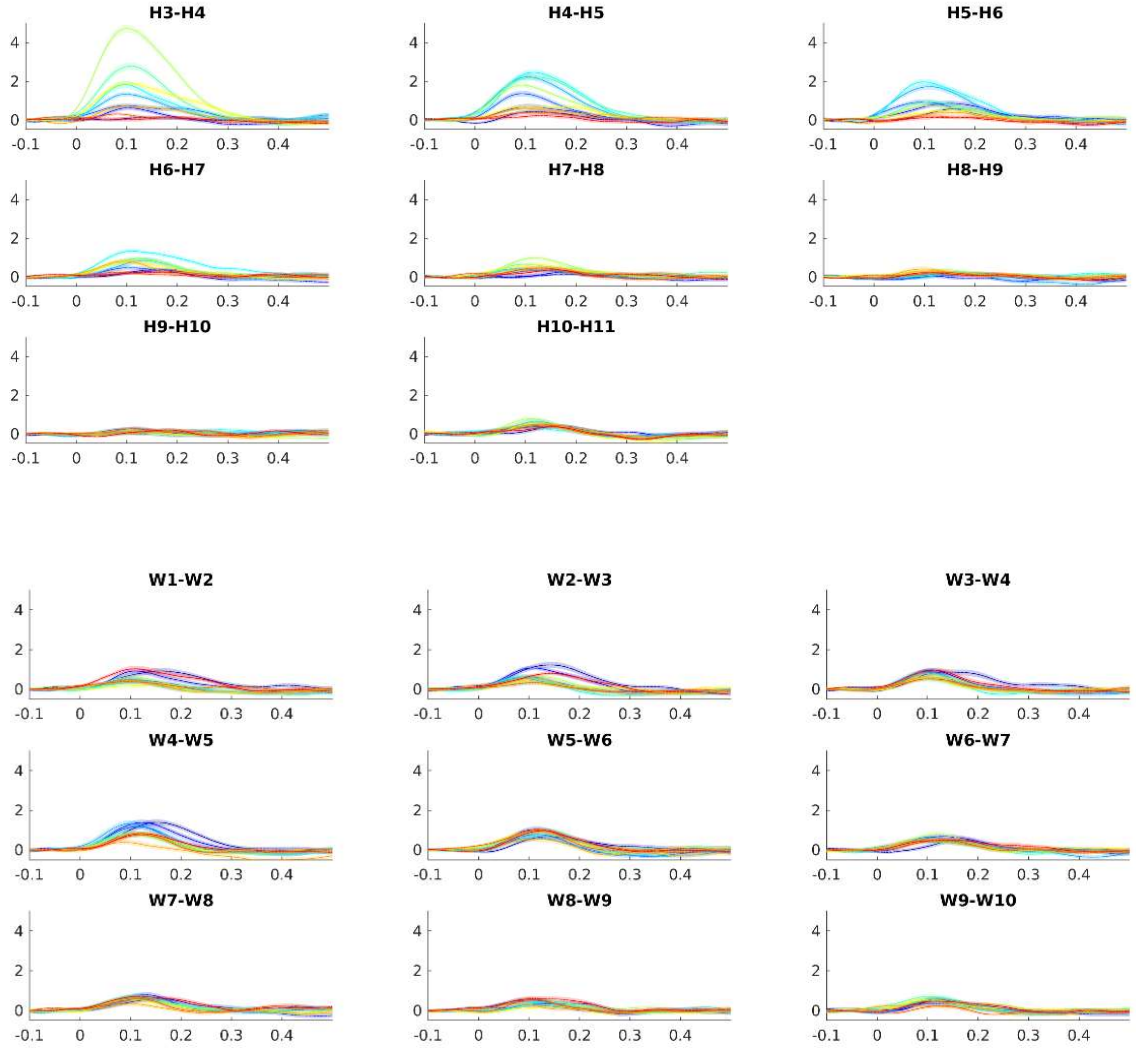

Note. HFA responses from SUB3 during tonotopic mapping task. Electrodes with prefix "H" are implanted in the auditory cortex while the prefix "W" indicate electrodes implanted in the TPJ region. The x-axis represents time scale in seconds with zero indicating stimulus onset. The y-axis represents the magnitude of the HFA.

Figure X.1.5 SUB3: ERP Responses from the TPJ During Tonotopic Mapping Task

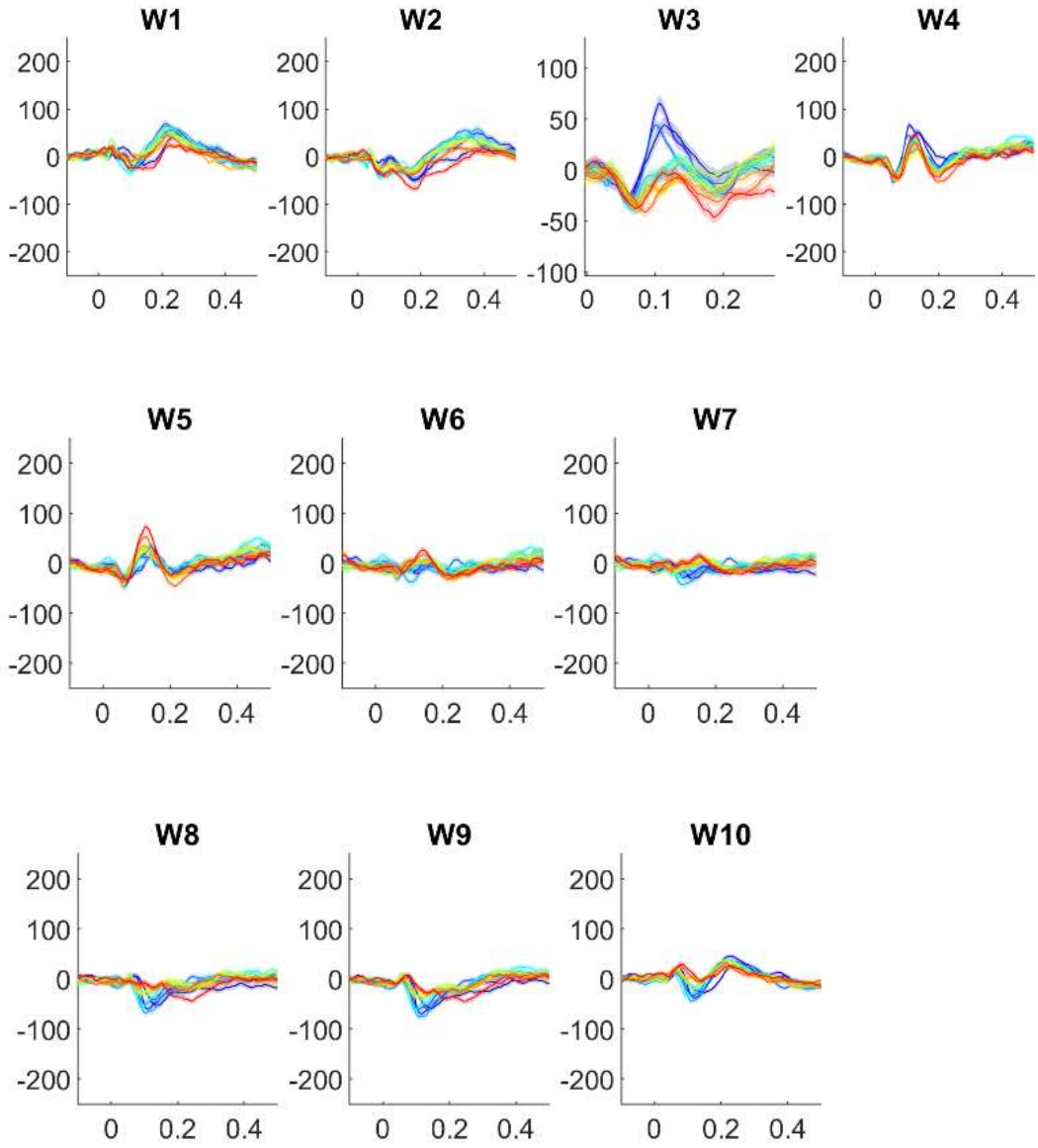

Note. Average-referenced ERPs from SUB3 during tonotopic mapping task from electrodes implanted in the TPJ region. The x-axis represents time scale in seconds with zero indicating stimulus onset. The y-axis represents the intracerebral voltages in μV.

Oddball task: ERPs

Stimuli in the oddball task: tone A = 311 Hz (all participants), tone B = 3520 Hz (SUB1 and SUB2) or 1245 Hz (SUB3).

Figure X.2.1 SUB1: ERP Responses to Repetition Deviants and Standard Control Tones

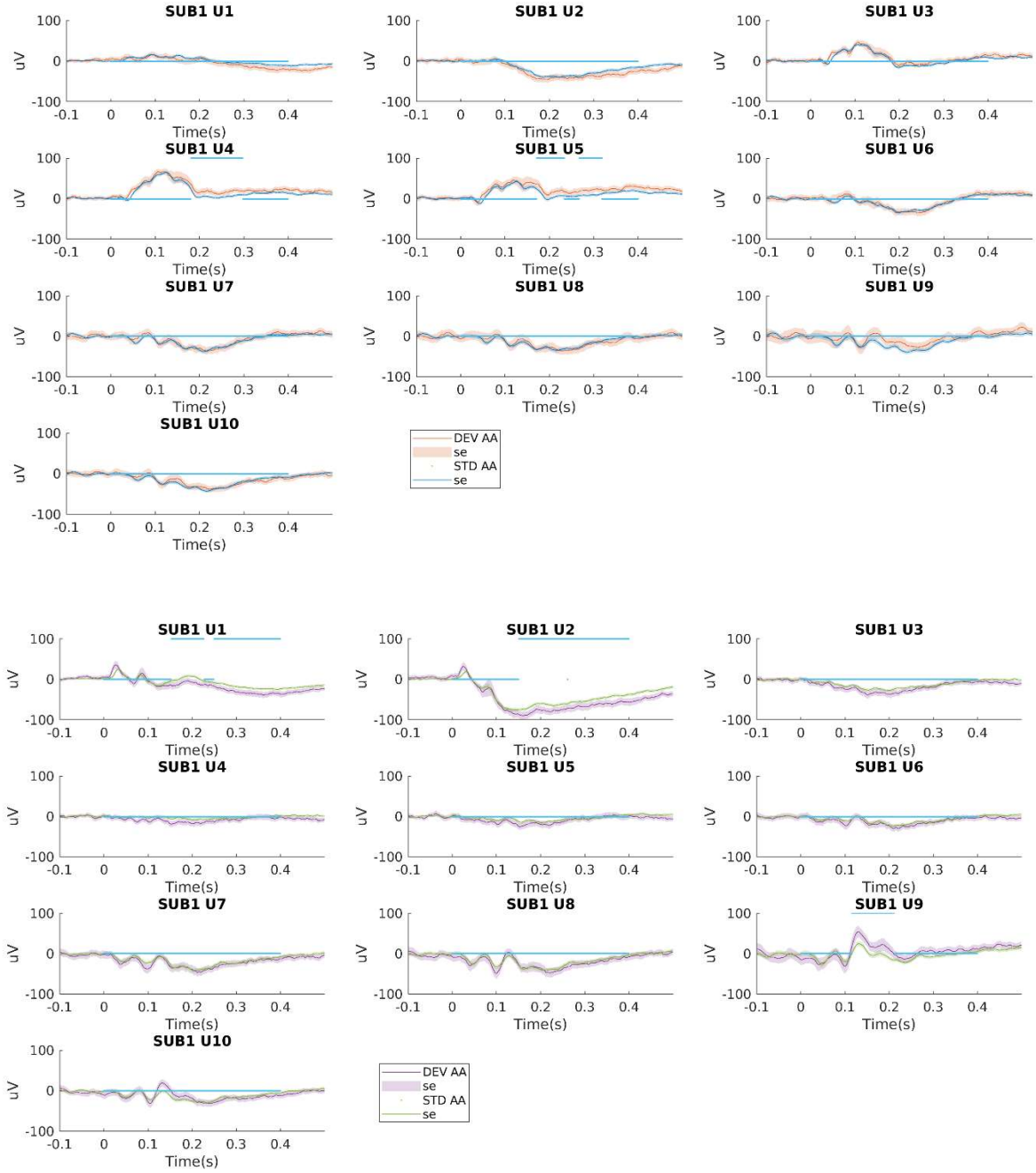

Note. Average-referenced ERPs elicited by Repetition Deviants versus standard controls to tone AA (311 Hz; upper panel) and tone BB (3520 Hz; lower panel). The blue bar illustrates

time samples at which the permutation test yielded significant differences ($p < .025$, two-tailed) between deviant and standard tones. The y-axis represents intracerebral voltage in μV. The x-axis represents time scale in seconds with zero indicating time of stimulus onset.

Figure X.2.2 SUB1: ERP Responses to Alternation Deviants and Standard Control Tones

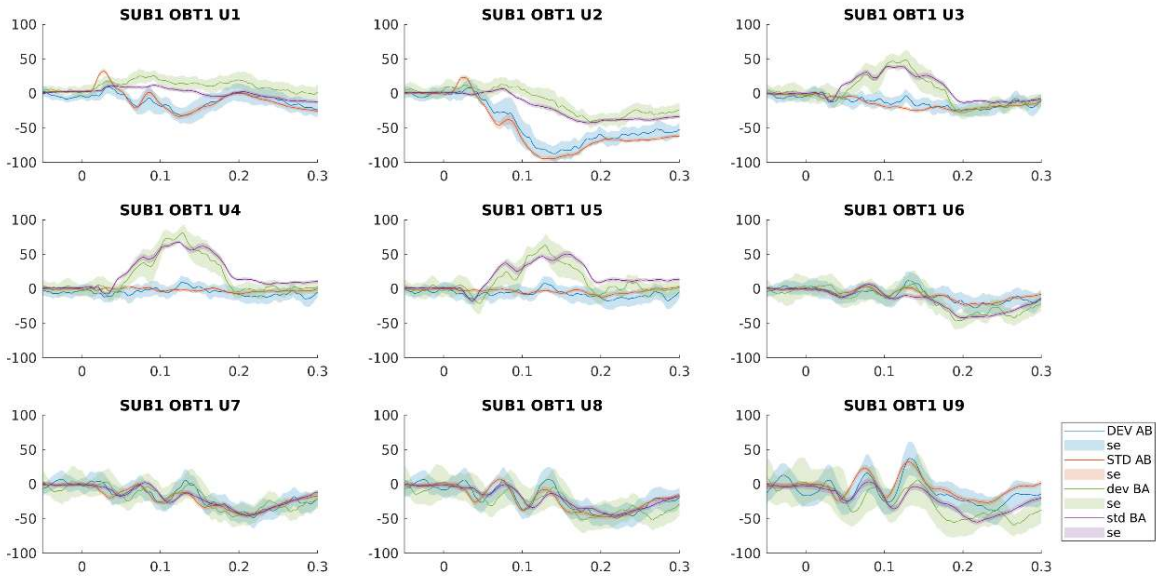

Note. Average-referenced ERPs elicited by Alternation Deviants versus standard controls. There was no significant difference between Alternation Deviants and standards. The y-axis represents intracerebral voltage in μV. The x-axis represents time scale in seconds with zero indicating time of stimulus onset.

Figure X.2.3 SUB2: ERP Responses to Repetition Deviants and Standard Control Tones

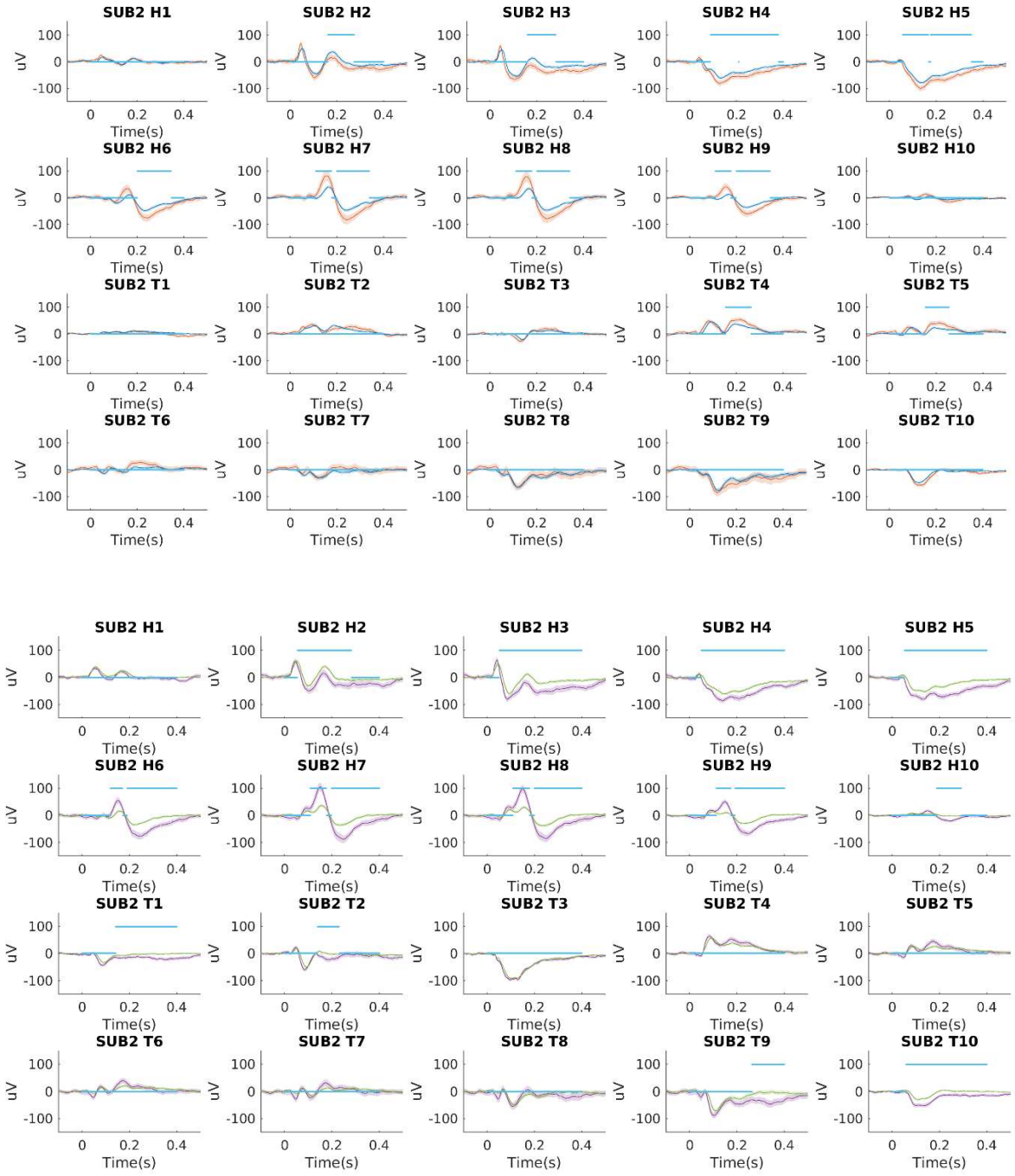

Note: Spatial difference in average-referenced ERPs from SUB3. Upper panel = tone AA, lower panel = tone BB. Deviant tones (DEV; in pink) elicit larger intracerebral voltages in all electrode contacts in the TPJ in electrode contacts H2 to H10, and in the auditory cortex in electrode contacts T1, T2, T4, T5, T9 and T10, compared to standard tones (STD; in green). The blue bar represents the time samples at which the permutation tests yielded clusters where the ERPs to Repetition Deviants differed significantly ($p < .025$, two-sided) from the control condition. Standard errors of the mean (se) are based on the 95% bootstrapped CI of the mean

(2000 permutations). The y-axis represents intracerebral voltage in μV. The x-axis represents time scale in seconds with zero indicating time of stimulus onset. Electrode W = TPJ. Electrode H = Auditory cortex.

Figure X.2.4 SUB2: ERP Responses to Alternation Deviants and Standard Control Tones

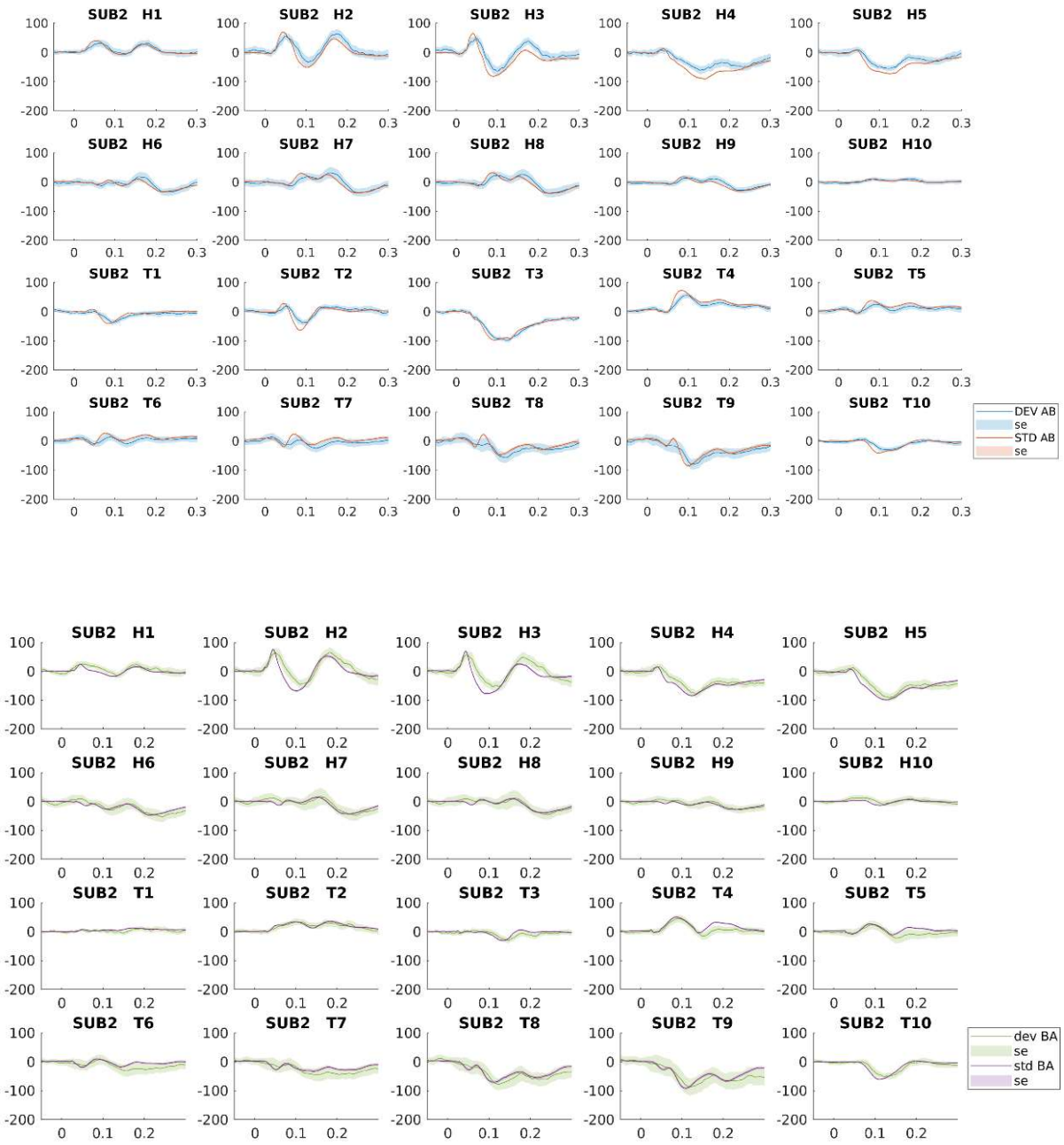

Note: Spatial distribution in average referenced ERPs from SUB2. Standard errors of the mean (se) are based on the 95% bootstrapped CI of the mean (2000 permutations). The y-axis

represents intracerebral voltage in μV. The x-axis represents the time scale in seconds with zero indicating time of stimulus onset. Electrode W = TPJ. Electrode T = Auditory cortex.

Figure X.2.5 SUB3: ERP Responses to Repetition Deviants AA and Standard Controls

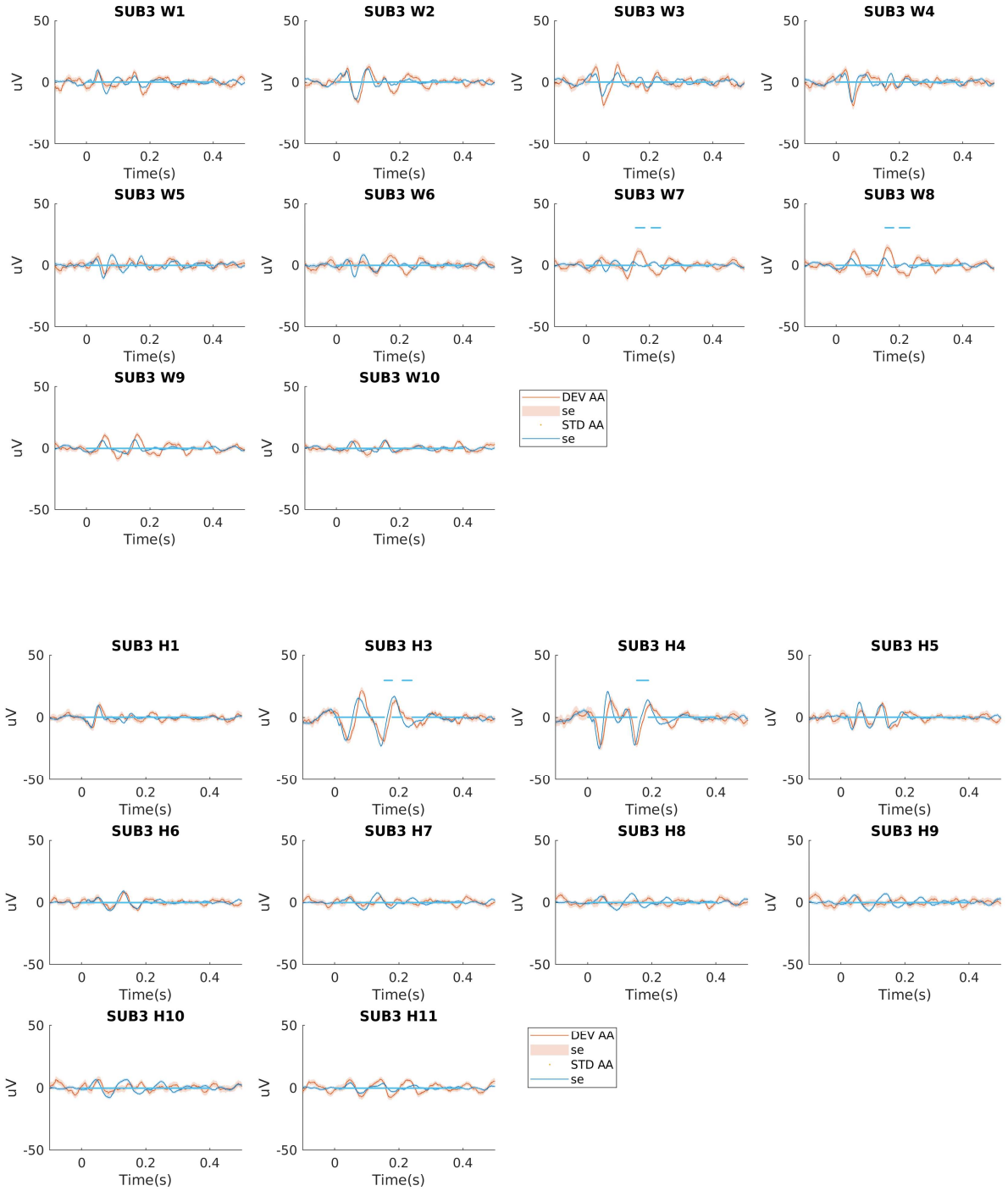

Note: Spatial difference in average-referenced ERPs from SUB3 from the TPJ (upper panel) and auditory cortex (lower panel) to tone AA. Repetition Deviants (DEV; in red) elicit larger intracerebral voltages in all electrode contacts in compared to standard tones (STD; in blue). The blue bar illustrates the time samples at which the permutation tests yielded clusters in which the ERPs to Repetition Deviants differed significantly ($p < .25$, two-sided) from the ERPs in the control condition. Standard errors of the mean (se) are based on the 95% bootstrapped CI of the mean (2000 permutations). Note that for illustrative purposes, the y-axis (in μV) is scaled differently between the TPJ and the auditory cortex. The x-axis represents time scale in seconds with zero indicating time of stimulus onset. Electrode W = TPJ. Electrode H = Auditory cortex.

Figure X.2.6 SUB3: ERP Responses to Repetition Deviants BB and Standard Controls

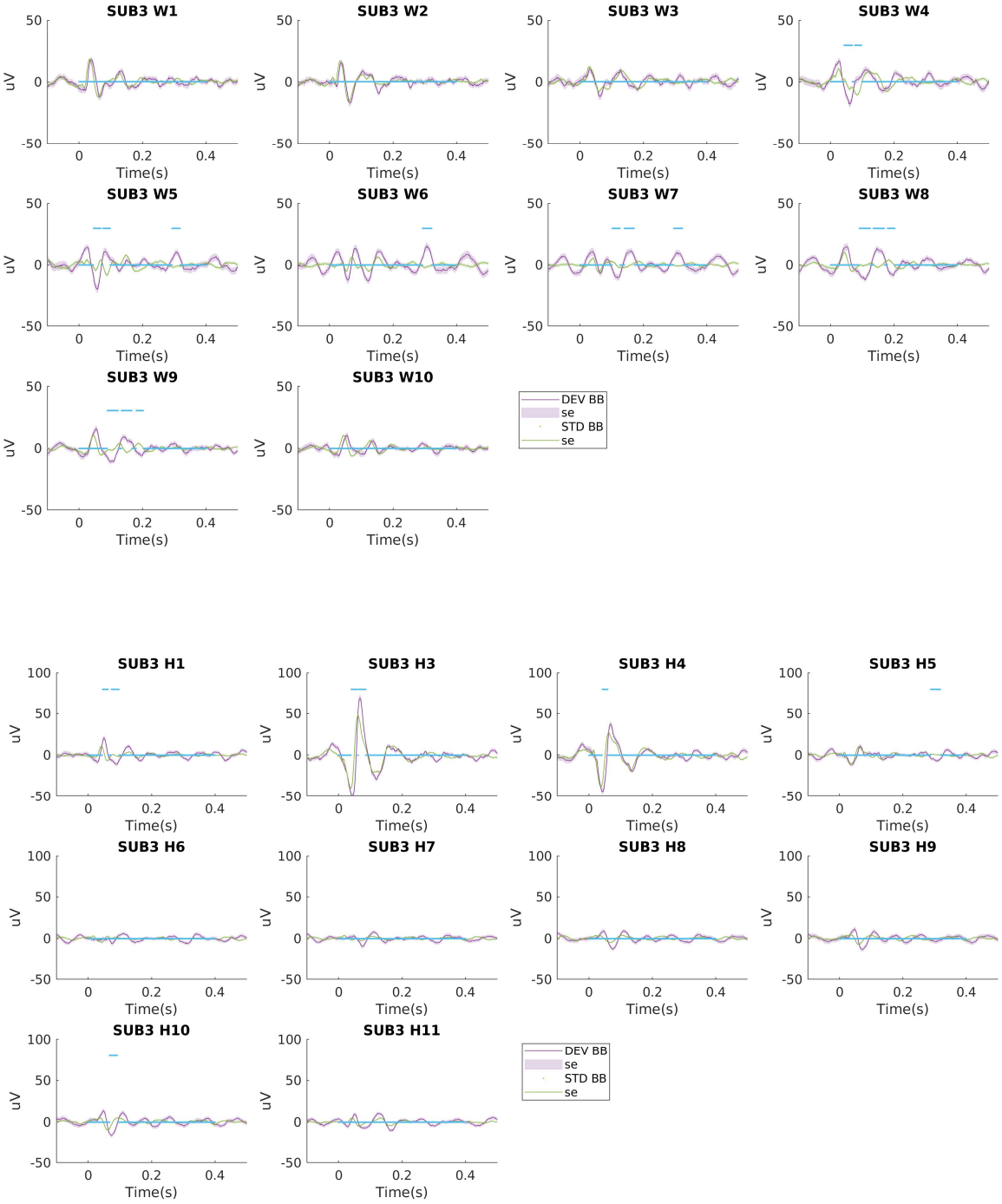

Note: Spatial difference in average-referenced ERPs from SUB3 from the TPJ (upper panel) and auditory cortex (lower panel) to tone BB. Repetition Deviants (DEV; in pink) elicit larger intracerebral voltages in all electrode contacts in compared to standard tones (STD; in green). The blue bar illustrates the time samples at which the permutation tests yielded clusters in which the ERPs to Repetition Deviants differed significantly ($p < .25$, two-sided) from the ERPs in the control condition. Standard errors of the mean (se) are based on the 95%

bootstrapped CI of the mean (2000 permutations). Note that for illustrative purposes, the y-axis (in μV) is scaled differently between the TPJ and the auditory cortex. The x-axis represents time scale in seconds with zero indicating time of stimulus onset. Electrode W = TPJ. Electrode H = Auditory cortex.

Figure X.2.7 SUB3: ERP Responses to Alternation Deviants AB and Control Tones

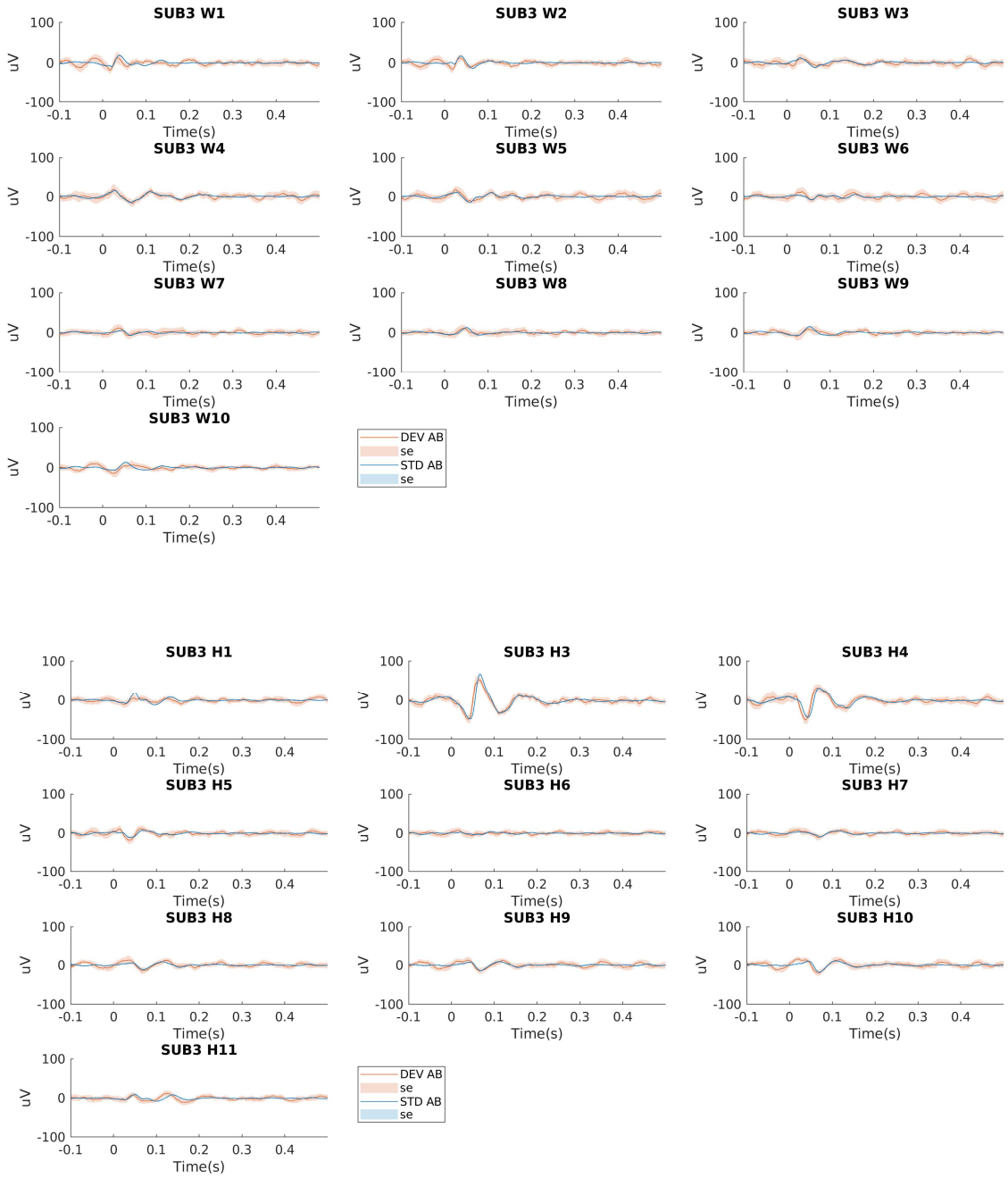

Note: Spatial difference in average-referenced ERPs to tone Alternation Deviants AB and standard control tones from SUB3. Standard errors of the mean (se) are based on the 95% bootstrapped CI of the mean (2000 permutations). Electrode W = TPJ. Electrode H = Auditory cortex.

Figure X.2.8 SUB3: ERP Responses to Alternation Deviants BA and Control Tones

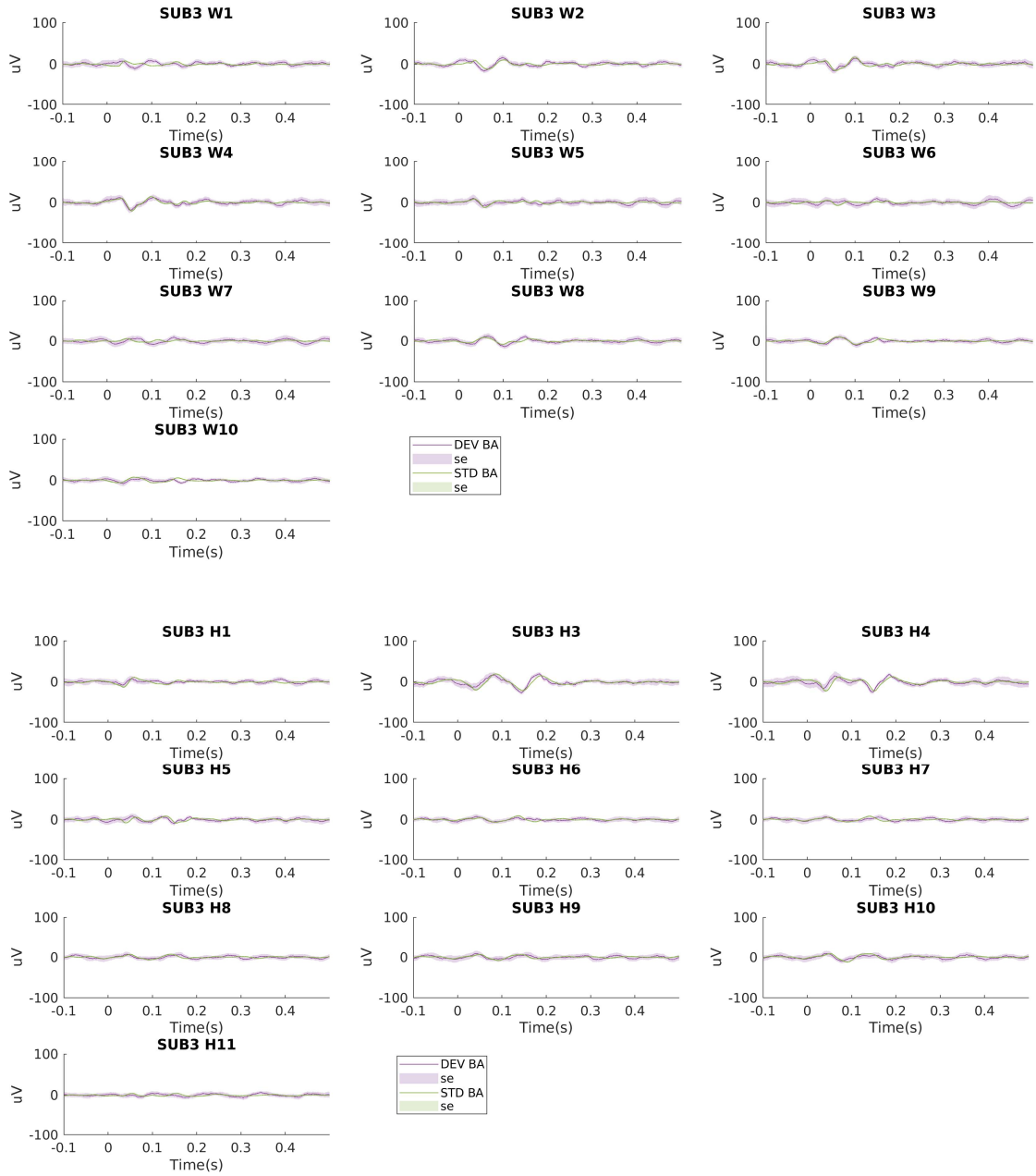

Note: Spatial difference in average-referenced ERPs to Alternation Deviants BA and standard control tones from SUB3. Standard errors of the mean (se) are based on the 95% bootstrapped CI of the mean (2000 permutations). The x-axis represents time scale in seconds with zero indicating time of stimulus onset. Electrode W = TPJ. Electrode H = Auditory cortex.

Oddball task: HFAs

Figure X.3.1 SUB1: HFA Responses to Alternation Deviants and Standards

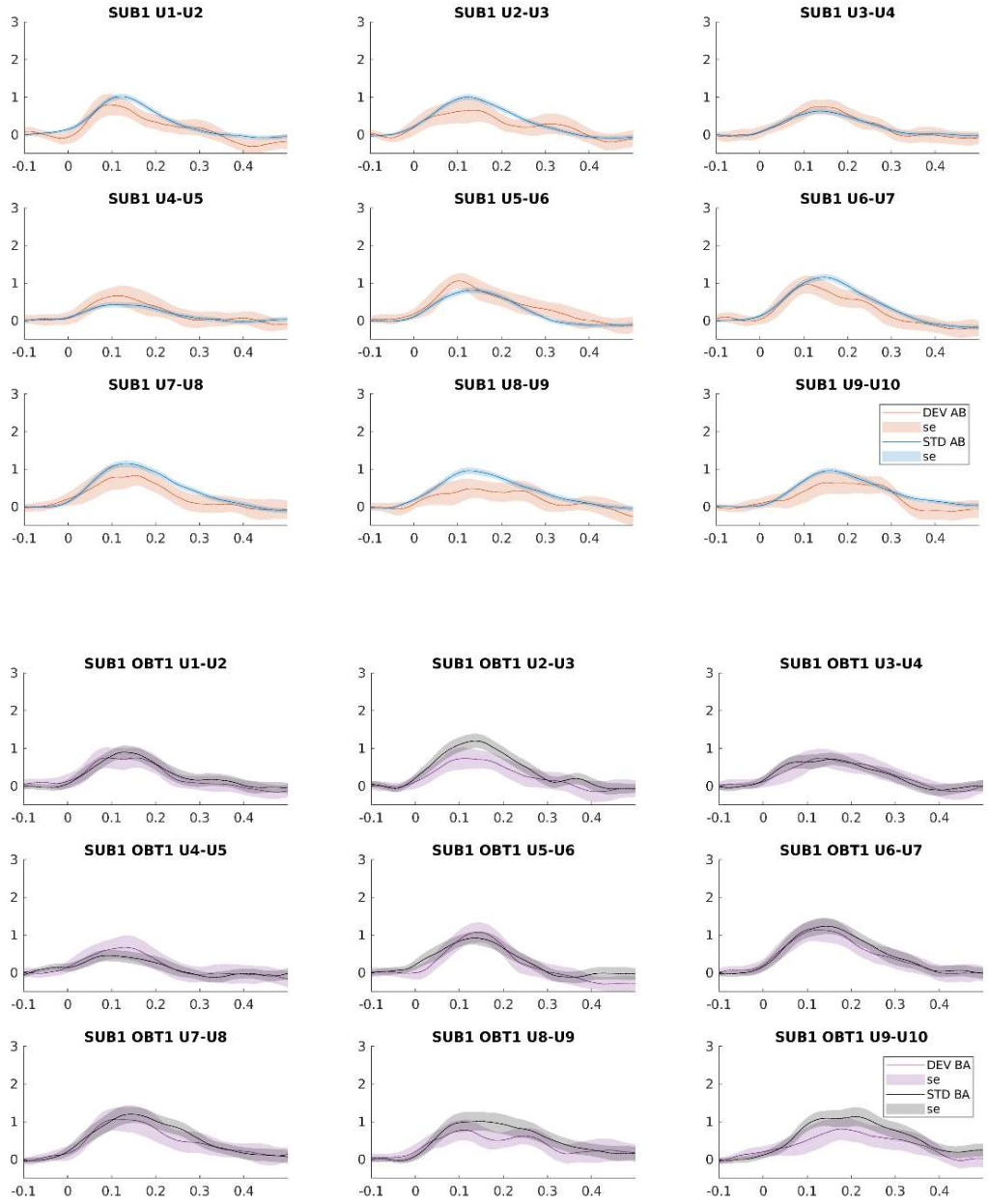

Note. HFA to Alternation Deviants (DEV AB/DEV BA) and standard condition (STD AB/STD BA) in SUB1 from channels implanted in the auditory cortex. The y-axis represents the magnitude of the HFA, and the x-axis represents the time in seconds with zero indicating time of stimulus onset. The standard errors of the mean (se) are calculated using the 95% bootstrapped CI (2000 permutations).

Figure X.3.2 SUB1: HFA Responses to Repetition Deviants and Standards

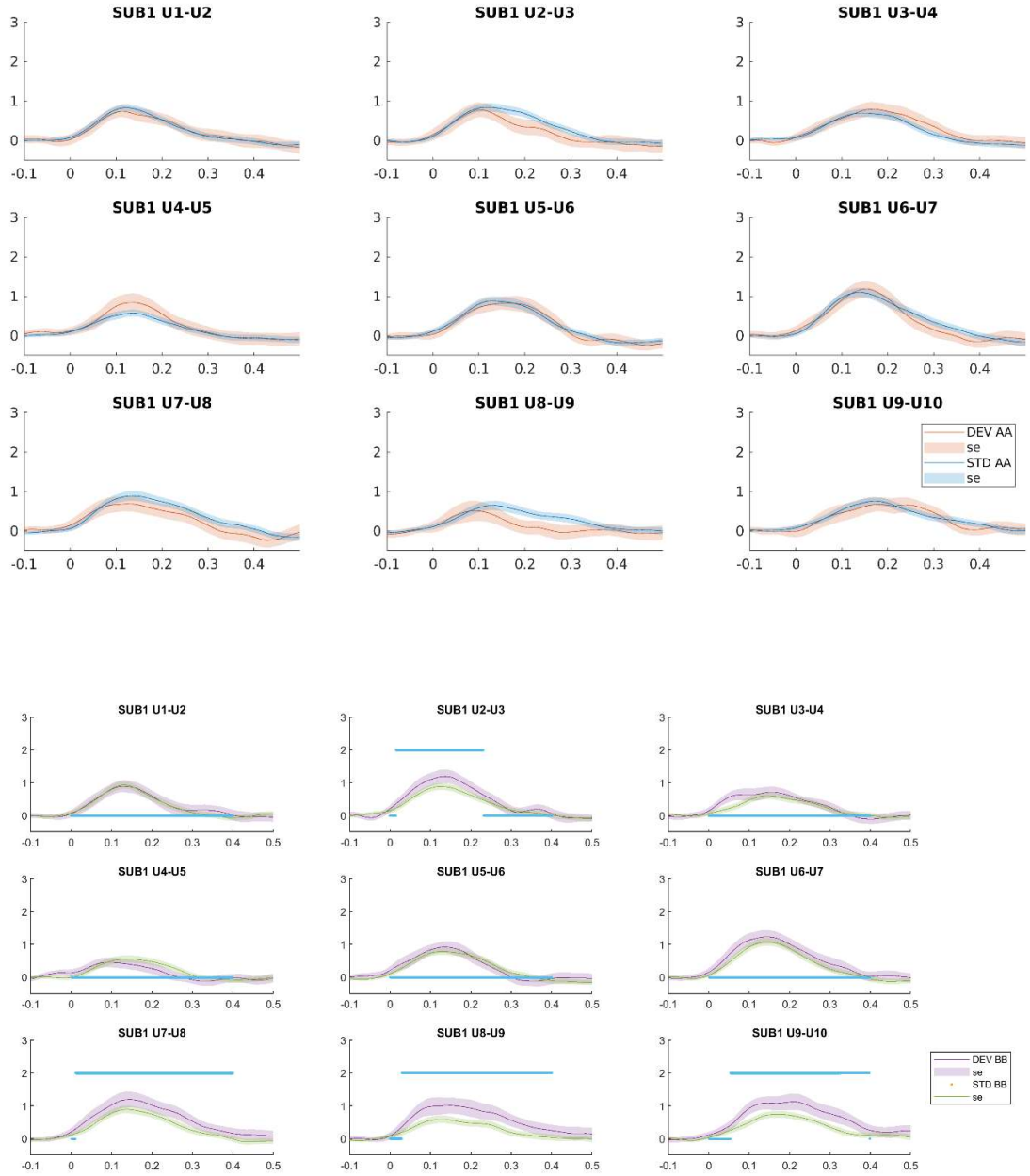

Note. HFA to Repetition Deviants (in red and pink; DEV AA/DEV BB) and standard condition (in blue and green; STD AA/STD BB) in SUB1 from channels implanted in the auditory cortex. The y-axis represents the magnitude of the HFA, and the x-axis represents the time in seconds with time equal zero indicating time of stimulus onset. The blue bar represents the time samples at which the permutation tests yielded clusters in which the HFA to Repetition Deviants were significantly stronger compared to the control condition. The

standard errors of the mean (se) are calculated using the 95% bootstrapped CI (2000 permutations).

Figure X.3.3 SUB2: HFA Responses to Alternation Deviants and Standards

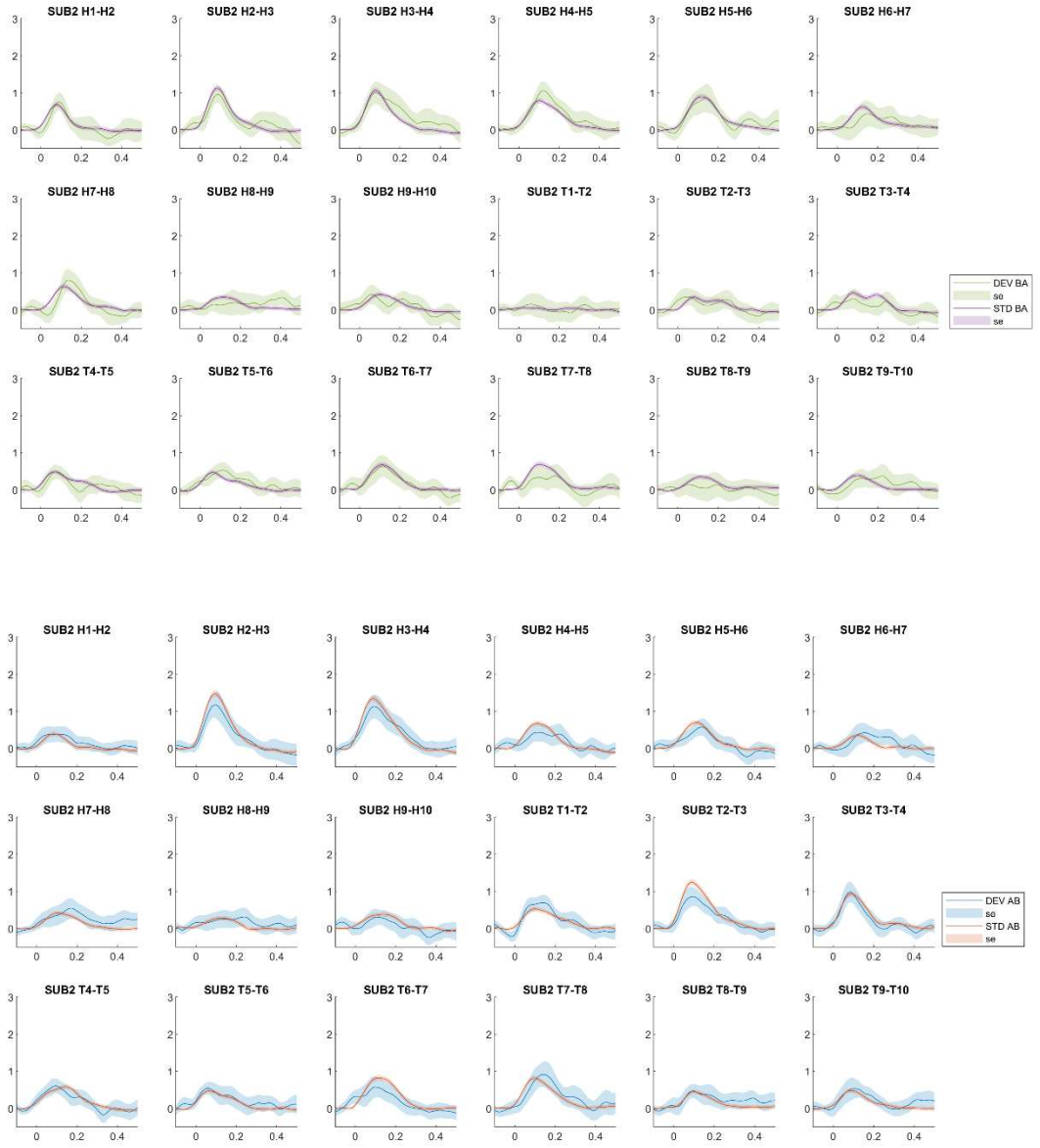

Note. HFA to Alternation Deviants (DEV AB/DEV BA) and standard condition (STD AB/STD BA) in SUB2 from channels implanted in the TPJ (channels with the prefix H) and the auditory cortex (channels with the prefix T). The y-axis represents the magnitude of the

HFA, and the x-axis represents the time in seconds with zero indicating time of stimulus onset. The standard errors of the mean (se) are calculated using the 95% bootstrapped CI (2000 permutations).

Figure X.3.4 SUB2: HFA Responses to Repetition Deviants and Standards

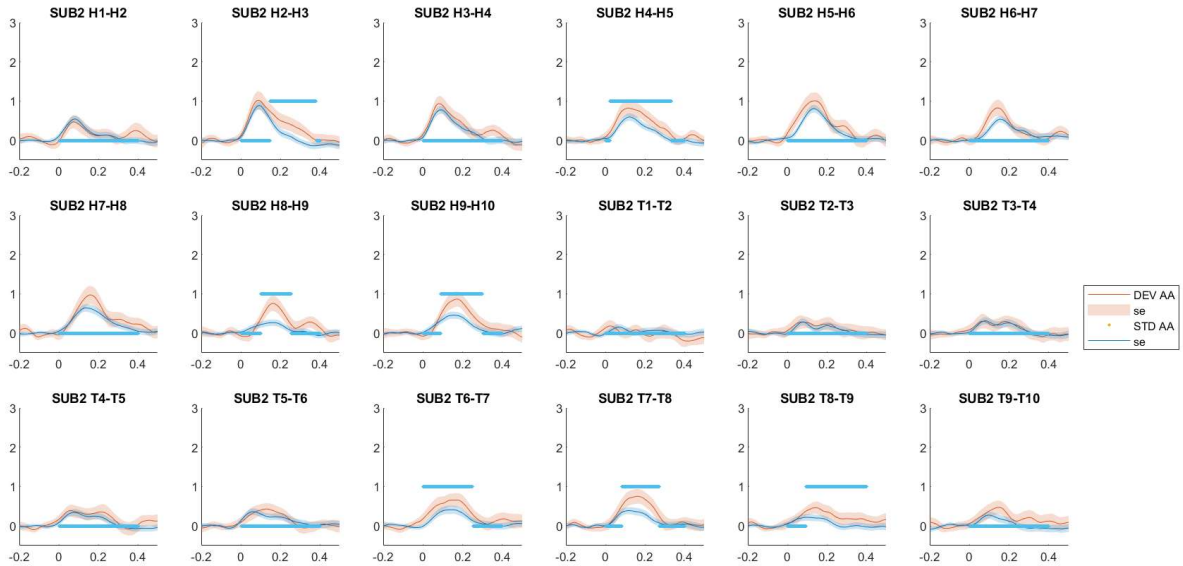

Note. HFA to Alternation Deviants (DEV AA) and standard condition (STD AA) in SUB2 from channels implanted in the TPJ (channels with the prefix H) and the auditory cortex (channels with the prefix T). The blue bar represents the time samples at which the permutation tests yielded clusters in which the HFA to Repetition Deviants were significantly stronger compared to the control condition. The y-axis represents the magnitude of the HFA, and the x-axis represents the time in seconds with zero indicating time of stimulus onset. The standard errors of the mean (se) are calculated using the 95% bootstrapped CI (2000 permutations).

Figure X.3.5 SUB3: HFA Responses to Alternation Deviants and Standards

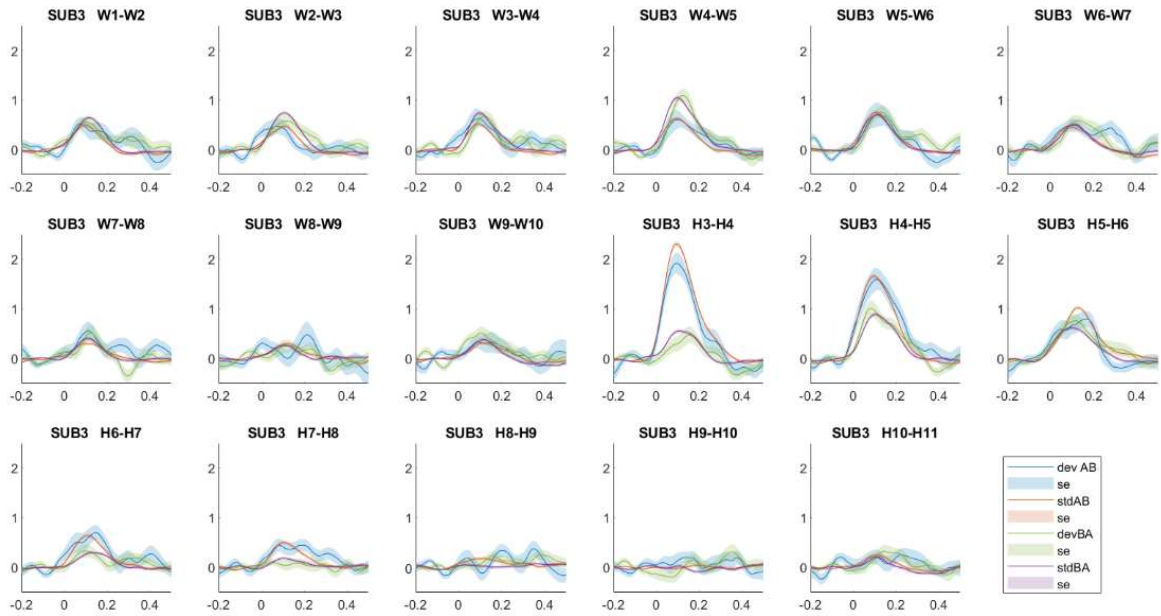

Note. HFA to Alternation Deviants (DEV AB/DEV BA) and standard condition (STD AB/STD BA) in SUB3 from channels implanted in the TPJ (channels with the prefix W) and the auditory cortex (channels with the prefix H). The y-axis represents the magnitude of the HFA, and the x-axis represents the time in seconds with zero indicating time of stimulus onset. The standard errors of the mean (se) are calculated using the 95% bootstrapped CI (2000 permutations).

Figure X.3.6 SUB3: HFA Responses to Repetition Deviants and Standards

Note. HFA to Alternation Deviants (DEV AA/DEV BA) and standard condition (STD AA/STD BB) in SUB3 from channels implanted in the TPJ (channels with the prefix W) and the auditory cortex (channels with the prefix H). The blue bar illustrates the time samples at which the permutation tests yielded clusters in which the HFAs to Repetition Deviants were significantly stronger compared to the control condition. The y-axis represents the magnitude

of the HFA, and the x-axis represents the time in seconds with zero indicating time of stimulus onset. The standard errors of the mean (se) are calculated using the 95% bootstrapped CI (2000 permutations).

Table X.1 Electrode Contact Number and Anatomical Location

Participant	Electrode label	Electrode number and anatomical location (native space)										
		1	2	3	4	5	6	7	8	9	10	11
SUB1	U	Ins	Ins/HG	HG	HG	TTS	iPT	iPT	iPT	STG	STG	-
SUB2	T	Ins	Ins	HG	HG	WM	STS	iPT	iPT	STG	STG	-
	H	pLF	pLF	pLF	pLF	pLF	sPT	sPT	SMG	SMG	SMG	-
SUB3	H	Ins	Ins/HG	HG	HG	WM	STS	STS	STS	STG	STG	STG
	W	pLF	pLF	pLF	pLF	STG	SMG	SMG	STG	STG	STG	-
		MNI coordinates (mm)										
SUB1	x	31,65	36,08	39,43	43,91	47,29	51,77	55,11	59,52	62,84	67,28	-
	y	-22,38	-22,4	-22,17	-22,39	-22,11	-22,19	-21,96	-22,45	-22,09	-21,79	-
	z	6,11	6,15	6,10	6,04	6,04	6,07	6,36	6,06	6,11	6,27	-
SUB2												
Electrode T	x	35,19	38,85	42,59	46,49	50	54,01	57,37	61,34	64,7	68,65	-
	y	-19,59	-19,19	-19,35	-19,4	-19,35	-19,34	-19,26	-19,15	-19,26	-19,33	-
	z	1,33	1,81	2,29	2,82	3,22	3,52	3,97	4,30	4,55	5,09	-
Electrode H												
	x	36.15	39.76	43.65	47.15	51.20	54.53	58.63	61.86	65.90	69.15	-
	y	-33.65	-33.68	-33.79	-33.85	-34.21	-34.02	-34.50	-34.20	-34.50	-34.66	-
	z	16.03	16.27	16.25	16.25	16.30	16.45	16.16	16.23	16.26	16.20	-
SUB3												
Electrode H												
	x	33,08	36,61	40,29	43,73	47,74	50,95	55,08	58,17	62,28	65,38	69,5
	y	-23,77	-23,56	-23,32	-23,15	-23,05	-22,97	-22,8	-22,8	-22,73	-22,42	-22,44
	z	1,07	1,02	1,12	1,00	1,10	1,08	1,21	1,27	1,34	1,41	1,50
Electrode W												
	x	37,04	40,73	44,35	47,81	51,54	55,13	58,74	62,41	66,01	69,68	-
	y	-38,60	-38,44	-38,28	-38,15	-38,10	-37,82	-37,85	-37,66	-37,57	-37,38	-
	Z	22,82	22,74	22,65	22,72	22,70	22,68	22,64	22,58	22,45	22,37	-

Note. Each cell contains the anatomical region. Abbreviations: Ins = Insula, iPT = inferior planum temporale, HG = Heschl's gyrus, pLF = posterior lateral fissure, SMG = supramarginal gyrus, STG = STG, sPT = superior planum temporale, TTS = transverse temporal sulcus, WM = white matter.